University of Stavanger

Faculty of Science and Technology

MASTER'S THESIS

Study program/ Specialization: Subsea Technology	Spring semester, 2015 Open / Restricted access
Writer: Wondwosen Belay	..... (Writer's signature)
Faculty supervisor: Prof. Jan Ignе External supervisor(s):	
Thesis title: Comparative Study On Global Motion Characterstics of Rectangular and Circular Column Semi-Sumbersibles	
Credits (ECTS):30	
Key words: - First order global motion	Pages: 109 + enclosure: 4 Stavanger, June 15/2015 Date/year

Front page for master thesis
Faculty of Science and Technology
Decision made by the Dean October 30th 2009

Abstract

A comparative study on the global motion characteristics of two semisubmersible units having similar hull arrangement, but different hull column geometry is carried out. All comparisons are considered at an operational draft. Each unit has four column ring pontoon hull. One of the units has quadratic hull column while the other unit has circular hull column. The hull of each unit has the same column center to center distance and pontoon dimension. At the considered operation draft, each of the two units is set to have similar initial stability in terms of metacentric height, similar water plane area and nearly similar displacement. Deck load arrangement is not discussed in detail but the overall mass distribution is also kept the same for the two units by employing the same radius of gyration about the global coordinates.

Both of the units that are set for comparison are considered to be unmoored and also, riser stiffness, damping and inertia effects are not included for analysis. The sesame suite of software is used for modeling of each unit, running global hydrodynamic analysis and for the post processing of the results from the analysis. The global first order motion transfer functions of the two units are compared. Statistical post processing is performed by applying sea states from a selected environmental contour line. Then, comparison between the two units is also carried out in terms of global short term maximum responses, short term minimum air gap requirement, slamming load from breaking waves and also in terms of second order horizontal mean drift loads.

Acknowledgement

I would like to express my gratitude to my supervisor Prof. Jan Igne for the useful comments, remarks and engagement through the learning process of this master thesis. Furthermore, I would like to thank my family and friends for supporting me throughout the entire process.

Contents

1. Introduction

1.1 Motivation

As offshore development activities expanded their horizon from shallow water to deep water and harsh environments, applying the concept of fixed marine facilities was no more feasible economically and installation wise. The concept of applying a semisubmersible marine vessel has then been started to serve different offshore purposes such as drilling rigs, crane vessels and oil production platforms.

During preliminary technical studies regarding offshore platform concept selection, engineers will give priority to the functional requirement of a platform. Top deck area size and equipments needed to perform the tasks defined in the functional requirement of a platform typically determine the topside weight of a platform. The following procedure is to determine the total buoyancy or displacement required from a hull to support the calculated top side weight. A hull geometry accounting for the required displacement is then proposed. Once hull geometry is defined, a preliminary stage hydrodynamic analysis will be performed to see if the proposed hull geometry has satisfactory motion and stability characteristics. The process is iterative and different geometries are considered until a satisfactory result is obtained. Once a favorable result is observed for proposed hull geometry, detail design can take place involving more accurate weight estimates, mooring and structural details.

This work is carried out to represent a preliminary stage hydrodynamic analysis, performed on two different types of proposed semisubmersible hull geometries that have nearly similar displacements. The hydrodynamic analysis carried out for each of the two proposed geometries is only based on the given geometric parameters and no iteration has been made varying the geometries.

Objective

The aim of this work is to compare a preliminary stage hydrodynamic analysis results performed on two different semisubmersible hull geometries that have nearly similar displacements, at a proposed operational draft. The hydrodynamic results will be compared based on global motion responses, air gap response and slamming load from breaking waves, at the proposed operational draft.

A four legged rectangular column and a four legged circular column semisubmersible hull units, both having a ring pontoon configuration, are the considered geometries. The two hull geometries have similar water plane area and static freeboard at an operational draft. The column center to center distance of the two geometries is also similar.

Stability analysis and detail mass distribution description are not part of the scope of this work ,but realistic metacentric height(GM) and mass distribution in terms of radius of gyration are necessary values to carry out hydrodynamic analysis. Hence, proposed values in the task outline of this work will be applied to accomplish the hydrodynamic analysis.

A semisubmersible unit can respond to wind, current and wave loads. But the most significant loads for the hulls of column stabilized units are normally those induced by waves (DNV-RP-C103,2012). Hence only water wave loads will be considered for this work. Following the suggestion by DNV's recommended practice (DNV-RP-F205, 2010), a linear radiation/diffraction analysis is found sufficient to determine the global hydrodynamic water wave excitation loads.

Since the hydrodynamic analysis that will be performed will be a linear/first order analysis, the velocity potential that will be used to describe the flow around each semisubmersible unit will be assumed to be proportional to the wave amplitude and the average wetted area of each unit up to mean water line will be considered.

The results of linear hydrodynamic analysis will be first order global excitation load transfer functions, first order global motion transfer functions, potential wave damping, added mass, and second order global mean drift excitation load transfer functions, all give in a regular wave frequency domain . The term "global" here refers to results that are calculated at the center of gravity of each semisubmersible unit.

The global motion responses will be compared in terms of first order global motion transfer functions or response amplitude operators (RAOs) for six degrees of freedom. The six degrees of freedom considered are three translations (surge, sway, heave) and three rotations (roll, pitch, yaw).

Given a regular wave with certain amplitude and frequency, the generated RAOs can be used to determine the responses of the units. However, real waves in a sea are not regular waves comprised of only a single amplitude and frequency, but rather can be thought of as a superposition of several waves with different amplitude and frequency. This superposition gives what are known as irregular waves and they best describe a real sea state. A sea state is a general condition of the free surface of the sea at a certain location and moment, characterized by statistics, consisting of significant wave height , average zero up crossing period and wave power spectrum.

To determine how the semisubmersible units will respond in real waves, each RAO will be combined with selected sea states expressed in terms of a wave spectrum, to give short term response spectrum,

assuming linear relation between wave amplitude and each unit's response. Based on the response spectrum, short term responses can be estimated using short term response statistics. The estimated short term responses will then compared for each degree of freedom.

The other subject of interest is the air gap response comparison for the two semisubmersible units. For few selected locations, air gap responses will be calculated based on linear radiation/diffraction analysis to determine the diffracted wave field and linearized platform motion, as per the proposal by DNV's recommended practice (DNV-RP-C205,2010). From the linear analysis, motion transfer function of relative water wave crest elevation with respect platform deck bottom will be obtained in frequency domain. The motion transfer function of the relative water wave crest elevation will be combined with selected sea states, to give short term relative motion response spectrum. From the relative motion response spectrum, short term relative motion responses will be determined using short term response statistics. The short term relative motion responses will be subtracted from the static air gap, to give air gap responses. The obtained air gap responses for the two semisubmersibles units, will then be compared.

Slamming loads from breaking waves on the columns of the two units will be compared based on space average slamming pressure, which is based on DNV's recommended practice (DNV-RP-C205,2010). In the space average slamming pressure formula, the focus will be to determine the relative normal velocity between breaking water wave and the surface of columns. The impact velocity of breaking water wave will be calculated based on a selected sea state while the velocity of the platform will be calculated based on the surge velocity of the semisubmersible units.

The Sesam suit of software will be used to for modeling, analysis and post processing of results.
Sesam GeniE will be used to prepare a panel model of the semisubmersible units , which will be later used in radiation/diffraction analysis. The panel model will later be imported to Sesam HydroD, where the graphical environmental modeling is done. The hydrodynamic analysis based on linear radiation/diffraction theory is then done in frequency domain, by the Wadam software module, which is executed from Sesam HydroD. The hydrodynamic result interface file created by Wadam is then read by Postresp, which is a general interactive graphical postprocessor. Postresp will be used to graphically present the results of the first order radiation/diffraction results. Postresp will also be used to carry out all short term response statistics for global motion responses, air gap responses and wave slamming.

Sea states corresponding to ultimate limit state (ULS) design requirement, having 10^{-2} annual probability of exceedance (100 years return period), will be considered for global motion extreme response calculations , air gap extreme minimum response calculations and 10^{-2} probability breaking wave impact load calculations.

2. General description of a semisubmersible Unit

A semisubmersible vessel is supported primarily on large pontoon like structures submerged below the sea surface and the operating decks are elevated several meters above the pontoons on large steel columns. The pontoons and the columns make up the hull of a semisubmersible unit. A semisubmersible vessel obtains buoyancy and stays afloat in a marine environment due to the displaced water caused by the vessel's submerged hull.

A typical semisubmersible unit design has four circular or rectangular columns connected at the bottom by pontoons with a rectangular cross section. The configuration and geometry of a semisubmersible unit not only affects the buoyancy and stability aspects, but also has a great impact on the mobility of the unit. Once a satisfactory result has been obtained for a certain geometry and configuration in terms of buoyancy and stability, hydrodynamic analysis can be carried out to predict if the motions are acceptable for the desired operation (Thaigaragan & Chakrabarti, 2005).

In the following sub sections, matters related to mobility, stability and motion characteristics of a semisubmersible unit such as natural period and added mass will be discussed.

2.1 Mobility

For drilling semisubmersible rigs, the columns are usually connected by two parallel pontoons and the bottom pontoon connected column pairs are connected to each other by relatively small slender members called braces. As drilling semisubmersible rigs are moved from place to place more frequently than production semisubmersible platforms, using braces for the purpose of cross connection of the column pairs instead of pontoons, reduces drag resistance and fuel consumption during transit. However, for production semisubmersible units, transportation is of secondary importance as the units are usually intended to stay at a specific site for relatively longer period. Hence, the usual practice is to adopt a ring pontoon configuration for production semisubmersible units. During transit to operation

site, the semisubmersible units are not submerged into water. This is because the units can float on top of the water only using the pontoons and transportation is made easier. Transportation is achieved by using tug boats or using their own propulsion system. Once the units are transported to site, they are anchored in place using a mooring line or kept within specific position, using a dynamic positioning system.

2.2 Stability

A semisubmersible platform is designed as being column stabilized and the column primarily provide flotation stability (Speight,2015).

Stability is the ability of a system to return to its undisturbed position after an external force is removed. when a floating vessel is in static equilibrium, it is under the influence of two forces: weight (W) and buoyancy (b) (Thaigaragan & Chakrabarti,2005).While weight (W) is the product of mass and gravitational acceleration, buoyancy (b) is given by the weight of the displaced volume of water, due to the presence of the body. The weight (W) of the vessel acts through the center of gravity of the vessel (G) , while the buoyancy force (b) acts through the center of buoyancy of the vessel (B). When a vessel is in upright position there is no heeling. In this case, the line of action of weight (w) and buoyancy (b) lie on the same line, which is the geometric center line of the vessel. A vessel in upright position is shown in figure 1.

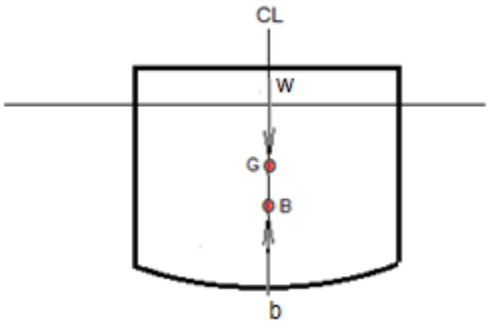

Figure 1. A vessel in upright position

When external loads from wind, current and waves are imposed on such a system, which is in static equilibrium, the external loads will cause heeling moment which causes a heeling angle (θ), on the vessel. A vessel which has been inclined by an external force is shown in figure 2.

Once a heeling angle (θ) occurs, the center of buoyancy (B), shift to (B'), to the direction of the heeling moment with the amount of heel, and the force of buoyancy acts vertically upward through (B'). The

weight of the vessel acts vertically downward through the center of gravity (G).The perpendicular distance between the lines of action of the forces (GZ) is called the righting lever. These two equal and opposite forces produce a moment or couple which may tend to right or capsize the vessel. The moment is called moment of statical stability and may be defined as the moment to return the vessel to initial position when inclined by an external force. The moment of statical stability is given by equation 1 (Barrass, 2011) .

$$RM = GZ \cdot \Delta \qquad 2.1$$

Where :

RM = moment of statical stability

GZ = righting lever

Δ = weight displacement of the vessel

At small angles of heel the force of buoyancy may be considered to act vertically upwards through a fixed point called the initial metacentre (M). This shown in figure 2, in which the vessel is inclined to small angle (θ).

From equation 2.2, the righting lever can be written as in terms of initial metacentre height (GM) and a small heeling angle, θ. (Barrass, 2011)

$$GZ = GM \cdot Sin\,\theta^o \qquad 2.2$$

Where :

GM = Metacentre height

θ = small heeling angle (in degrees)

Inserting equation 2.2 in to equation 2.1, it can be seen that for any particular displacement, at small angles of heel, the righting moment will vary directly as the initial metacentric height (GM) .

$$RM = \Delta \cdot GM \cdot Sin\,\theta^o \qquad (for\ small\ angles\ \ Sin\,\theta^o \sim \theta^o) \qquad 2.3$$

For small heeling angle (θ), the position of the metacentre determines if a vessel is stable or unstable (Thaigaragan & Chakrabarti,2005). In a vertical plane, if the metacentre lies above the point of center of gravity (G), GM will be greater than zero giving positive righting moment and the vessel will be stable. If

the metacentre lies below the point of center of gravity, the GM will be negative giving a negative righting moment. This indicates that the righting moment will cat in the direction of the heeling moment, which will leave the vessel initially unstable. Figure 2 case I illustrates stable vessel, i.e. GM > 0, while case II illustrates unstable vessel, where GM < 0.

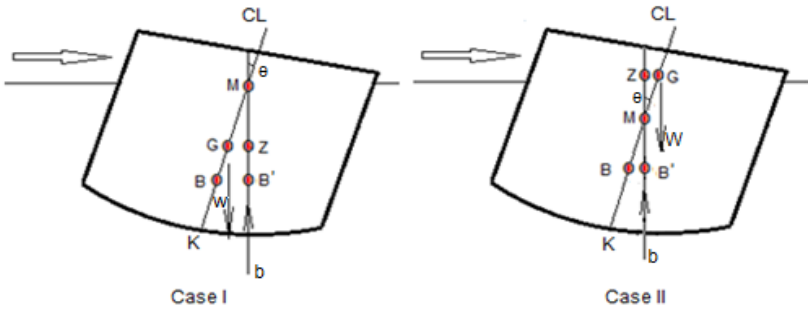

Figure 2. Stable and Unstable Vessel

Evaluating the GM from figure 2, it can be seen that;

$$GM = KB + BM - KG \qquad 2.4$$

Where :

KB = Distance from the keel (K) of the vessel to the buoyancy center

BM = Distance from center of buoyancy to metacentre (metacentric radius)

KG = Distance from the keel of a vessel to center of gravity of the vessel

The metacentric radius (BM) is given by equation 2.5 (Biran & Pulido, 2014);

$$BM = \frac{I}{\nabla} \qquad 2.5$$

Where :

I = moment of inertia of the water plane about the axis of inclination

$\nabla =$ Volume displacement

During preliminary design stage, it is a common practice to consider intact stability only at small angles of heel.(Thaigaragan & Chakrabarti,2005).

Applying the same principle to a semisubmersible unit and referring to equation 2.4, If the vertical center of gravity (KG) of a semisubmersible is known, then the initial stability (GM) is known

(Thaigaragan & Chakrabarti,2005). This implies that, given a target GM, the values of KB and BM can be determined from hydrostatic analysis, and the value of KG can be obtained. The value of KB is associated with the geometry of the submerged hull, while the value of BM as can be seen in equation 2.5, is associated to the volume displacement of the submerged hull and the moment of inertia of the water plane area, which in this case is the columns of the semisubmersible unit.

3. Units considered for comparison

	Rectangular semi Unit	Circular semi unit
Column dimension [m]	23 x23	25.5 dia.
Column Length [m]	46	46
Column corner radius [m]	3	-
Pontoon width [m]	23	23
Pontoon height [m]	11	11
Column center to center distance [m]	79.5	79.5
Draft [m]	24	24
Freeboard [m] (static air gap)	22	22

Table 3.1 Detail about units set up for comparison

4 Theoretical Background

In this chapter, the basic information about waves that is needed to evaluate hydrodynamic loads on offshore structures and responses of offshore structures is given.

4.1 Potential wave theory

Real fluid's behavior is complex, thus it is difficult to calculate the fluid's velocity, acceleration, pressure and surface elevation in exact manner. However, by idealizing the fluid and introducing assumptions, it is possible to obtain acceptable results.

In potential wave theory, sea water is assumed incompressible and inviscid. The fluid motion is irrotational. A velocity potential (φ) can then be used to describe the fluid velocity vector, V *(x,y,z,t)* ,at time (t) at the point X =(x,y,z) in Cartesian coordinate system fixed in space (Faltinsen,1990). This is shown in equation 4.1.

$$V = \nabla \varphi = i\frac{\partial \varphi}{\partial x} + j\frac{\partial \varphi}{\partial y} + k\frac{\partial \varphi}{\partial z} \qquad 4.1$$

Where (∇) is del operator and *i, j* and *k* are unit vectors along *x, y* and *z* axes, respectively. The fluid is irrotational when the vorticity vector ($\vec{\omega}$) is zero everywhere in the fluid. This is shown in equation 4.2

$$\vec{\omega} = \nabla \times V = 0 \qquad 4.2$$

Since water is assumed to be incompressible, equation 4.3 has to be satisfied.

$$\nabla \cdot V = 0 \qquad 4.3$$

It follows that the velocity potential has to satisfy the Laplace equation given by $\nabla^2 \phi$;

$$\frac{\partial^2 \varphi}{\partial x^2} + \frac{\partial^2 \varphi}{\partial y^2} + \frac{\partial^2 \varphi}{\partial z^2} = 0 \qquad (4.4)$$

By applying the relevant boundary conditions on the fluid, a velocity potential of irrotational and incompressible fluid motion that satisfies the Laplace equation can be obtained.

The pressure (P) at a chosen location can be expressed by Bernoulli's equation as shown in equation 4.5 (Faltinsen,1990), where (ϱ) is the fluid (water) density, (g) is gravitational acceleration, (Z) is location on z-axis which is positive upward and (C) is an arbitrary function of time which is constant. (C) can be set to an arbitrary convenient constant.

$$P + \varrho g z + \varrho \frac{\partial \varphi}{\partial t} + \frac{\varrho}{2} V \cdot V = C \qquad (4.5)$$

4.1.1 Boundary Conditions

In order to solve Leplace equation $\nabla^2 \phi$, boundary conditions are needed. A solution with sinusoidal waves at the surface is required. The boundary conditions will be found from physical considerations.

The boundary conditions needed to solve the Laplace equation are ;

-Bottom boundary condition

- Kinematic body surface boundary condition

-Free surface boundary condition

4.1.1.1 Bottom boundary condition

No water can flow through the bottom. A flat bottom is considered here, where (*h*) is water depth.

$$\frac{\partial \varphi}{\partial z} \Big|_{z=-h} = 0 \qquad 4.6$$

4.1.1.2 Kinematic body surface boundary condition

No fluid enters or leaves the body surface. This gives the kinematic body surface boundary condition and it is given as;

$$\frac{\partial \varphi}{\partial \mathrm{n}} = \mathrm{U} \cdot \hat{n} \quad on\ the\ body\ surface \qquad 4.7$$

(∂/∂n) denotes differentiation along the normal(n) to the body surface, where the positive normal direction is defined to be into the fluid domain. (U) can be any type of body surface velocity.(U) maybe different for different point on the body surface.

It is to be noted that, the tangential velocity component on a body surface in a potential flow problem is unspecified (Faltinsen, 1990).

4.1.1.3 Free surface boundary conditions

There are two boundary conditions on the free surface, these are;

-Kinematic free surface condition

-Dynamic free surface condition

Kinematic free surface condition

Before formulating kinematic free surface condition, the meaning of substantial derivative $\frac{\mathrm{D}F}{\mathrm{D}t}$ of a function, *F* (*x,y,z,t*) shall be introduced. This expresses, the rate of change with time of the function (*F*) if we follow a fluid particle in space (Faltinsen,1990). Mathematically, it can be expressed as;

$$\frac{\mathrm{D}F}{\mathrm{D}t} = \frac{\partial F}{\partial t} + V \cdot \nabla F \qquad 4.8$$

Where (*V*) is the fluid velocity at the point *(x,y,z)* at time (*t)* and (∇) is del operator.

Now let us define the free surface by the equation

$$z = \xi(x, y, t) \qquad 4.9$$

Where *x,y,z* are orthogonal axes in the Cartesian coordinate system and (***ξ***) is free surface elevation.

Next, the function (*F*) is defined by the following equation

$$F\ (x, y, z, t) = z - \xi(x, y, t) = 0 \qquad 4.10$$

A fluid particle on the free surface is assumed to stay on the free surface. This means it always satisfies equation 4.11 and $\frac{\mathrm{D}F}{\mathrm{D}t} = 0$. The following kinematic boundary condition then applies to the free surface

$$\frac{\partial}{\partial t}\big(z - \xi(x,y,t)\big) + \nabla\varphi \cdot \nabla\big(z - \xi(x,y,t)\big) = 0 \qquad 4.11$$

Here, the fluid velocity (*V*) in equation 4.8 is expressed by velocity potential (*φ) (refer to equation 4.1).*

Simplifying equation 4.11 we get the kinematic free surface boundary condition as:

$$\frac{\partial\xi}{\partial t} + \frac{\partial\varphi}{\partial x}\frac{\partial\xi}{\partial x} + \frac{\partial\varphi}{\partial y}\frac{\partial\xi}{\partial y} - \frac{\partial\varphi}{\partial z} = 0 \quad on\ z = \xi(x,y,t) \qquad 4.12$$

Dynamic free surface condition

As shown in equation 4.5 , the pressure (*P*) at a chosen location can be expressed by Bernoulli's equation. At the surface (*P*) is equal to atmospheric pressure (P_0) and (*Z*) is equal to free surface elevation (***ξ***). Following what has been described about (*C)* in sub chapter 4.1 and letting $C = \frac{P_0}{\varrho}$, the two terms $\frac{P}{\varrho}$ and $\frac{P_0}{\varrho}$ will cancel each other out when P = P_0 at the surface (zero relative pressure) :

$$g\xi + \frac{\partial\varphi}{\partial t}\Big|_{z=\xi} + \frac{1}{2}(V\cdot V)\Big|_{z=\xi} = 0 \qquad 4.13$$

Expressing the fluid velocity (*V)* by velocity potential (*φ)* we obtain:

$$g\xi + \frac{\partial\varphi}{\partial t}\Big|_{z=\xi} + \frac{1}{2}\left(\left(\frac{\partial\varphi}{\partial x}\right)^2 + \left(\frac{\partial\varphi}{\partial y}\right)^2 + \left(\frac{\partial\varphi}{\partial z}\right)^2\right)\Big|_{z=\xi} = 0 \qquad 4.14$$

4.2 Linear wave potential theory

Observing equations 4.12 and 4.14, it can be seen that both the kinematic and dynamic free surface conditions are non linear because they contain nonlinear terms in their expression. The free surface is also not known until the equations are solved. However, by liberalizing the non linear free surface conditions, it is possible to simplify the problem and still get sufficient information in most cases (Faltinsen, 1990).This can be achieved by applying what is called linear wave theory. Linear wave theory means that the velocity potential is proportional to the wave amplitude and is valid if the wave amplitude is small relative to a characteristic wavelength and body dimension. By Taylor expansion, it is possible to transfer the free surface conditions from the free surface $z = \xi(x,y,t)$ to the mean free surface at $z = 0$. Since the wave amplitude has already been assumed to be small, its practical to

neglect higher order terms proportional to the wave amplitude. By keeping only linear terms in the wave amplitude we get from equations 2.12 and 2.14 that;

$$\frac{\partial \xi}{\partial t} = \frac{\partial \varphi}{\partial z} \quad on\ z = 0 \qquad (Kinematic\ condition) \tag{4.13}$$

$$g\xi + \frac{\partial \varphi}{\partial t}\Big|_{z=0} = 0 \quad (Dynamic\ condition) \tag{4.15}$$

It is to be noted that the free surface elevation (***ξ***) can be calculated from equation 4.15, once after the velocity potential (*φ)* is obtained. Combining equations 4.14 and 4.15 then gives:

$$\frac{\partial^2 \varphi}{\partial t^2} + g\frac{\partial \varphi}{\partial z} = 0 \quad on \quad z = 0 \tag{4.16}$$

When the velocity potential is harmonically oscillating in time with angular frequency (ω), equation 4.16 can be written as:

$$-\omega^2 \varphi + g\frac{\partial \varphi}{\partial z} = 0 \quad on \quad z = 0 \tag{4.17}$$

4.3 Regular linear wave theory

The first requirement in the derivation of potential function is the selection of suitable analytical form including constants to be determined (Barltrop and Adams, 2013). Regular linear waves have only single wave amplitude *(**ξ**$_a$)* and angular frequency *(ω)* along with linearized free surface conditions. Potential function for regular waves propagating in positive *X* direction, satisfying the Laplace equation along with sea bottom and linearized surface boundary conditions is given for infinite and infinite water depths in equations 4.18 and 4.19 respectively.

$$\varphi = \frac{g\xi_a}{\omega}\frac{\cosh\ k\ (z+h)}{\cosh kh}\cos(\omega t - kx) \qquad (finite\ depth\ potential) \tag{4.18}$$

$$\varphi = \frac{g\xi_a}{\omega} e^{kz}\ \cos(\omega t - kx) \qquad (infinite\ depth\ potential) \tag{4.19}$$

where (*h*) is water depth, (*g*) is gravitational acceleration, (k) is wave number. Wave number is the spatial frequency of waves and is given by the formula;

$$k = \frac{2\pi}{\lambda} \tag{4.20}$$

Where *(λ)* is wave length, which is important parameter when dealing with regular waves .Wavelength is a measure of the distance between repetitions of a shape feature such as peaks, valleys, or zero-crossings. Wave length of a regular wave is indicated in figure 4.1.

The angular frequency (ω) can be used to calculate the wave period (T), which is the time it takes for two successive crests or troughs to pass a fixed point.

$$T = \frac{2\pi}{\omega} \qquad 4.21$$

As mentioned, the surface profile $\boldsymbol{\xi}(x,t)$, using two dimensional representations, can be obtained from the potential function by using boundary condition. Water wave particle velocity and acceleration can be determined from the surface profile once the surface profile is obtained.

$$\xi = \xi_a \sin(\omega t - kx) \qquad 4.22$$

Similarly, the wave particle velocity is obtained by taking the first derivative of the potential function along the horizontal direction ($u = \frac{\partial \varphi}{\partial x}$) and vertical direction ($w = \frac{\partial \varphi}{\partial z}$).

Wave water particle acceleration is obtained by taking the second derivative of the potential function along the horizontal direction ($\dot{u} = \frac{\partial^2 \varphi}{\partial x^2}$) and vertical direction ($\dot{w} = \frac{\partial^2 \varphi}{\partial z^2}$).

Connection between wave number *(k)* and angular frequency *(ω)* is given by the dispersion relation.

$$\frac{\omega^2}{g} = k \tanh kh \quad (for\ finite\ depth) \qquad 4.23$$

$$\frac{\omega^2}{g} = k \quad (for\ infinite\ depth) \qquad 4.24$$

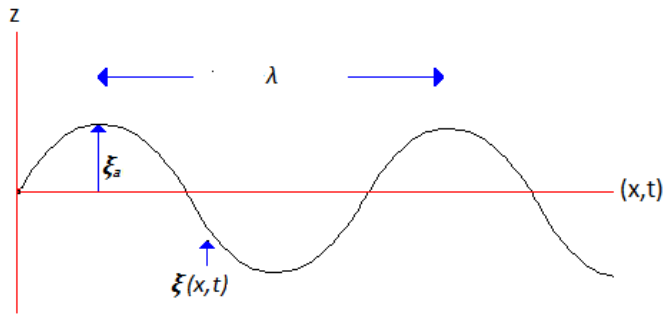

Figure 4.1 Regular wave profile

4.4 Irregular waves

Real waves in a sea are not regular waves having only a single amplitude and an angular frequency, but rather can be considered as the superposition of a number of regular wave components. In practice, linear theory is used to simulate irregular seas and to obtain statistical estimates (Faltinsen, 2005). The

wave elevation of a long crested irregular sea propagating along the positive x axis can be written as the sum of a large number of wave components. This is given as:

$$\xi = \sum_{j=1}^{N} A_j \sin(\omega_j t - k_j x + \varepsilon_j) \qquad 4.25$$

Where parameters (A_j), (ω_j), (k_j) and ($\mathcal{E}_j$) are the wave amplitude, angular frequency , wave number and random phase angle of wave component number *j,* respectively. The random phase angles ($\mathcal{E}_j$) are uniformly distributed between 0 and 2π and constant with time.

It is assumed that a sea surface elevation can be described as a stationary random process (Faltinsen,2005). A state where the sea surface elevation is in a stationary random process for certain duration of time is called a sea state. The duration of time where the sea surface elevation process is assumed to be stationary can range from half hour up to ten hours.

In a sea state, the instantaneous surface elevation $\xi(x,t)$, which is made up of *(N)* components of regular linear waves, is assumed to be Gaussian distributed with zero mean, *E=0,* and variance σ^2 is given by the equation (Faltinsen, 2005);

$$\sigma^2 = \sum_{j=1}^{N} \frac{1}{2} A_j{}^2 \qquad 4.26$$

The wave amplitude (A_j) of each component *j* in a sea state can be expressed in terms of wave spectrum *s(ω).* Wave energy density spectrum or commonly called wave spectrum *s(ω)* shows the distribution of wave energy according to the frequencies of the wave components in a sea state. Wave spectrum for a specific location can be obtained from spectrum models.

$$\frac{1}{2} A_j{}^2 = s(\omega_j)\, \Delta\omega \qquad 4.27$$

Where $(\Delta\omega)$ is a constant difference between successive frequencies. In fact, the sea surface is believed to have infinity number of regular wave components. Letting N →∞ and Δω→0, the variance of the surface elevation can be expressed in terms of 0^{th} spectral moment of the wave spectrum, which is the total area under the wave spectrum.

$$\sum_{j=1}^{N} \frac{1}{2} A_j{}^2 = \int_0^{\infty} s(\omega) d\omega \qquad 4.28$$

4.5 The panel method

The panel method is one of the most common numerical techniques based on three dimensional potential theory that predicts linear wave induced motions and loads on large volume structures

(Faltinsen,1990). There exist several commercial computer programs which apply this method for first and second order load response analysis.

When using these software solutions, the basic step is to describe the geometry of the structures with panels. Most software solutions apply flat panels for representation of the geometry of structures. However, curved panels are also applicable in some programs. A Preprocessor is used to generate the panel geometry. Local coordinates at the corner of each panel describe all panels on the structures geometry. For flat panels typically, large number of panels must be applied on the structures complex surface so that the structure's geometry is not misrepresented. As the aim should be to represent the structures surface with finite elements, the smaller the size of the flat panels, the larger their number will be to represent the structures surface, and then better accuracy is obtained.

The usual practice to cross check if the discretization (representation with finite elements) of the structure's surface is done correctly is to do a mesh convergence test, and see how the results converge by using a smaller size panels. Normally, small size panels better represent a structure's surface and better results are obtained. The down side of using large number of panels is large computer memory requirement and the analysis will take much longer time to be completed.

After discretization of the structures surface with flat plates, it will be imported into a processor software. First order forces acting on the structure will be computed having the structure in its equilibrium position. The panels describing the geometry of the structure must cover the submerged surface of the structure until water mean level. Usually, larger number of panels is necessary towards the mean water level (Chakrabarti, 2005).

The main assumptions in the panel model for linear global load and response analysis are;

- The flow is assumed to be potential flow (free of separation and lifting effects)
- Free surface and body boundary conditions are linearized
- Oscillation amplitudes of the fluid and the body are small relative to cross sectional dimensions of the body

For the diffraction problem, a velocity potential comprising the incident wave potential and the diffracted wave potential on the panel surface is known. Then the pressure on the structures surface is obtained from the linear term of Bernoulli's equation. Integrating this pressure distribution over the structures surface yields global excitation forces and moments in six degrees of freedom.

Similarly from the radiation problem, a 6 x 6 global added mass coefficient matrix and 6 x 6 global wave potential damping coefficient matrix. Further, a 6 x 6 global restoring coefficient matrix will be obtained from hydrostatic analysis.

The above values along with the input structural mass matrix or mass model will be used to solve the equation of motion which will give first order motions in six degree of freedom.

In addition to the above outputs, the first order radiation/diffraction software computes the following results for large arbitrary shaped structures:

- free surface profile of wave at the structure's surface
- steady drift force by the momentum principle
- steady drift force by direct pressure integration principle
- Interaction of large neighboring structures and resulting motions of floating structures (if multi body modeling is adopted).

4.6 Regular linear wave Forces

Typically, floating structures may respond to wave forces with motion on three different time scales namely wave frequency motions (WF), low frequency motions (LF) and high frequency motions (HF) (DNV-RP-F205,). The largest wave loads on offshore structures take place at the same frequencies as the waves causing (WF) motions. In this sub chapter, linear wave loads resulting in (WF) motion of structures will be discussed.

The forces on a submerged offshore structure in waves arise from the dynamic pressure distribution on its surface.

$$F = \iint P\,\hat{n}\,ds \qquad 4.29$$

Where $\hat{n}$ is a normal to the wetted body surface and *(S)* refers to an integration variable along the submerged (wet) body surface.

The dynamic pressure (*P*) can be calculated, once a velocity potential (φ) is obtained as shown in equation 4.5. For linear theory, the velocity potential (φ) and the dynamic pressure (*P*) can be decomposed to ;

- Incident wave potential (φ_I)

- Diffracted wave potential (φ_D)
- Radiated wave potential (φ_R)

Based on body size and geometry, the velocity potential (φ) of wave field around a structure can be given as ;

$$\varphi = \varphi_I + \varphi_D + \varphi_R \qquad 4.30$$

In addition to the boundary conditions that have to be satisfied by the incident wave potential, radiation/diffraction potential components have to satisfy :

$$\frac{\partial \varphi_D}{\partial n} = -\frac{\partial \varphi_I}{\partial n} \quad on\ the\ body\ surface \text{ at mean position}$$
$$\frac{\partial \varphi_R}{\partial n} = U \cdot \hat{n} \quad on\ the\ body\ surfaceat\ at\ mean\ positioon \qquad 4.31$$

4.6.1 Froude Krylov force on structures

As incident wave propagates towards a submerged offshore structure, the wave field of propagation can be represented by incident wave velocity potential (φ_I). When the characteristic structural dimension of the body is small relative to the incident wave length, the presence of the structure will not affect the incoming incident wave velocity potential (φ_I) (Chakrabarti, 2005). Hence, the pressure distribution can be obtained from the incident wave potential, by assuming the structure is not present and doesn't alter the incident wave velocity potential. However, for small structures where the characteristic dimension is very small compared to the incident wave length, it is not practical to compute the pressure distribution around the structure from the incident wave velocity potential (φ_I) ,as the incident wave velocity potential around the structure is complex due to formation of vortices in the vicinity of the structure. Because of the complexity, it is not easy to define the pressure distribution on the structure from the incident wave potential. This means the force on the structures from the incident wave is not computed directly from the pressure distribution, as the pressure distribution is not easy to define for small structures. The practical solution to calculate the force due to incident waves in slender structures is to use Morison's empirical formula.

4.6.2 Wave diffraction force on structures

When the characteristic length of an offshore structure is large relative to the incident wave length, then the flow around the surface of the structure remains attached to the structure's surface (Chakrabarti, 2005). This applies to large offshore structures such as semisubmersibles, tension leg platforms and several other large offshore units. Because the flow remains attached to the structure, flow separation that can cause vortices in the vicinity of the structure is neglected, and the wave field can be described by potential flow. However, in this case, the incident wave potential experiences scattering (diffraction), from the surface of the structure. This diffraction effect then alters the incident wave potential over large area in its surrounding .This scattering (diffraction) effect needs to be accounted for, while calculating the pressure field.

Initially, what would be known is the incident wave potential (φ_I). Having the incident wave potential, several numerical methods can be employed to describe the wave potential flow in the vicinity of large offshore structures. As mentioned, one such method is the panel method. In the panel method, the wave potential flow around the structures is described by incident wave potential with diffraction potential effect included (Faltinsen, 1990). The pressure distribution is then expressed by the linearized Bernoulli's equation as follows;

$$\frac{\partial \varphi_I}{\partial t} + \frac{\partial \varphi_D}{\partial t} = \frac{-P}{\varrho} \qquad 4.32$$

Notice that only the dynamic component of the Bernoulli's is presented above. This dynamic pressure distribution when integrated along the wet surface of the structure gives an excitation wave force on the structure, which creates harmonic oscillation effect on the body.

4.6.3 Added mass and damping coefficients

The added mass and damping loads are steady state hydrodynamic forces and moments due to forced harmonic rigid body motions (Faltinsen, 1990).In this case, no incident waves are considered, however the forced motion of a structure generates outgoing waves. These radiated/outgoing waves caused by the motion of the structure can be described by a radiation wave potential. An oscillating pressure field is then introduced because of the radiation wave potential. When this oscillating pressure field is integrated along the wetted surface of the structure, it gives a radiation force on the structure by the radiated waves.

For six degree of freedom (heave, pitch, roll, surge, sway and yaw), the radiated waves from the structure give rise to six radiation potentials, then producing six pressure fields on the structures surface

(Chakrabarti, 2005).When considering a radiated force F_{ik}, in (*j)* degree of freedom caused by structural forced oscillatory motion in (*k)* degree of freedom, each radiation force in (*j)* degree of freedom can be caused by six modes of motion (*k) for (K = 1,...,6).*

As an example, a radiation force F_{11} and F_{12} are radiation forces in surge direction *(j =1)* caused by surge *(K = 1)* and sway*(K = 2)* motions respectively. Hence, a six by six force matrix will be the total result.

As mentioned, the radiation force is caused by the motion of an oscillating structure. Hence, there is a relation between the force component and the oscillating body's motion. The force component that is in phase with the velocity of the structure acts as a damping term and is called wave potential damping matrix. The wave potential damping is responsible for energy dissipation of the oscillation. The component of the force that is in phase with the structure's acceleration behaves like an inertial term and is named as the added mass matrix. The added mass arises because of the mass of water accelerated when the structure oscillates (moves) through the water. This can be seen in equation 4.32.

$$\iint -\varrho\left(\frac{\partial \varphi_R}{\partial t}\right)\hat{n}\, ds = F_{jk} = -A_{jk}\frac{d^2\eta_k}{dt^2} - B_{jk}\frac{d\eta_k}{dt} \qquad 4.32$$

Where (A_{jk}) is the added mass matrix for *j* degree of freedom and in *k* degree of freedom oscillatory motion inducing it, (B_{jk}) is wave potential damping matrix for *j* degree of freedom and in *k* degree of freedom oscillatory motion inducing it and (η_k) is the oscillatory motion in *k* degree of freedom.

As can be seen from the equation above, the radiation problem gives a six by six matrix for added mass and a six by six matrix for wave potential damping. Each component in the matrices is oscillatory frequency dependent.

For the cases to be considered in this work, the semisubmersible units are symmetric with respect to XY plane and XZ plane. Then the frequency dependent added mass and potential damping matrices are symmetric along the diagonal, for both the semisubmersible units, because forward motion and current are not considered. This means $A_{jk} = A_{kj}$ and $B_{jk}=B_{kj}$. Also, due to the units' symmetry, the surge-surge elements of the frequency dependent added mass and potential damping matrices, A_{11} and B_{11}, are identical to the sway-sway elements, A_{22} and B_{22}. Similarly, the roll-roll elements of the frequency dependent added mass and potential damping matrices, m_{44} and d_{44}, are identical to pitch-pitch elements, A_{55} and BSS_{55}.

4.7 Restoring forces

For freely floating offshore structures, dynamic restoring force/moment is caused by the change in buoyancy force on the body and is related to the motion of the body. Dynamic restoring forces can be written as (Faltinsen, 1990) ;

$$F_j^R = -C_{jk}\,\eta_k \qquad 4.33$$

Where (F_j^R)is the restoring force in *j* degree of freedom, (c_{jk}) in a restoring coefficient in *j* degree of freedom due to motion of the structure in *k* degree of freedom and η_k is motion of the structure in k degree of freedom.

As an example, if a floating vessel which is in static stability experiences a small roll angle (θ) due to an inclining moment, the buoyancy center shifts from the stationary point to a new location, giving rise to a righting moment (RM) to resist the inclining moment and prevent the vessel (see chapter 2). This restoring moment, given by equation 2.3, is a roll restoring moment and can be related to equation 4.33.

$$RM = \boxed{-\Delta \cdot GM}\,\boxed{\theta^o} \approx F_4{}^R = \boxed{-C_{44}}\,\boxed{\eta_4} \qquad 4.34$$

Where (η_4) is the roll angle and is represented by (θ^o).Negative sign indicates that righting moment is in opposite direction to inclining moment. Then the restoring coefficient is equated to ;

$$C_{44} = \Delta \cdot GM \qquad 4.35$$

In heave direction, the change in buoyancy would be the restoring force ($F_3{}^R$). The change in buoyancy is given by

$$F_3{}^R = \boxed{-\varrho g A_{wp}}\,\boxed{h} \approx \boxed{-C_{33}}\,\boxed{\eta_3} \qquad 4.36$$

Where (η_3) represents the structural heave (h). Then the heave restoring coefficient would be

$$C_{33} = \varrho g A_{wp} \qquad 4.37$$

In general there is a 6 x 6 restoring matrix coefficient (c_{jk}) for (j and k = 1,...,6). No coupling effect exists between the coefficients for the units considered for this project.

$$C_{jk}=\begin{bmatrix} 0 & 0 & 0 & 0 & 0 & 0 \\ 0 & 0 & 0 & 0 & 0 & 0 \\ 0 & 0 & C_{33} & 0 & 0 & 0 \\ 0 & 0 & 0 & C_{44} & 0 & 0 \\ 0 & 0 & 0 & 0 & C_{55} & 0 \\ 0 & 0 & 0 & 0 & 0 & 0 \end{bmatrix}$$

4.8 Mass matrix

The mass matrix consists of mass and inertia terms. For a floating unit symmetric about XZ and YZ plane and having center of gravity (0,0, Z_{cog})the mass matrix is given by:

$$M_{jk}=\begin{bmatrix} M & 0 & 0 & 0 & M_{Z_{cog}} & 0 \\ 0 & M & 0 & -M_{Z_{cog}} & 0 & 0 \\ 0 & 0 & M & 0 & 0 & 0 \\ 0 & -M_{Z_{cog}} & 0 & I_{44} & 0 & 0 \\ M_{Z_{cog}} & 0 & 0 & 0 & I_{55} & 0 \\ 0 & 0 & 0 & 0 & 0 & I_{66} \end{bmatrix}$$

Where (M) is total mass of the structure and (I) is moment of inertia .

Moment of inertia (I) about an axis is given by

$$\sum_{i=1}^{N} m_i \, r_i^{\,2} \qquad 4.38$$

Where m_i is a point mass in the body configuration, $r_i^{\,2}$ is the distance from the axis of rotation to the local center of gravity of the point mass and (N) is the number of point masses in the body configuration.

For analysis purpose, the body mass distribution can be conveniently set by giving a radius of gyration (R). Radius of gyration refers to the distribution of the components of an object around its axis.

$$R^2 = \frac{I}{M} \qquad 4.39$$

4.9 Equation of motion of floating structures in frequency domain

A structure freely floating or held by a soft mooring line will be free to move in all the six degrees of freedom i.e. in surge, sway, heave, roll, pitch and yaw degrees of freedom. In order to determine the motion of the structure in each of the mentioned degrees of freedom, it is possible to compute the dynamic equation of equilibrium (equation of motion) in frequency domain.

According to Newton's second law of motion, a mass system (M) will accelerate in the direction of the net force, if the vector sum of forces acting on it is different from zero.

Relating Newton's second law of motion to a freely floating offshore structure with a mass (M), if the net force acting on the structure is different from zero, then the structure will accelerate.

The system can be expressed by d'Alembert's principle as follows:

$$F_{(E)j}(t) + F_{(R)j}(t) + F_{(s)j}(t) = M\,\ddot{\eta}_k(t) \qquad 4.41$$

Where $F_{(E)j}$ is wave excitation force in mode (j), $F_{(R)j}$ is wave radiation force in mode (j), $F_{(s)j}$ is hydrostatic restoring force in mode (j) and $\ddot{\eta}_k$ is structural acceleration in mode (K) .Mode in this case refers to degree of freedom.

Referring to section 4.6, it was mentioned that :

- the incident plus diffraction potential gives rise to an excitation force on structures $F_{(E)j}$
- the radiation potential gives added mass (A_{jk}) in mode (j) due to motion in mode (k)
  also wave potential (B_{jk}) in mode (j) due to motion in mode (k),
- while from hydrostatics, hydrostatic restoring matrix (C_{jk}) in mode (j) due to motion in mode (k)

Putting each component in equation form :

From the diffraction problem :

$$F_{(E)j}(t) = Re\left\{f_{(E)j}\, e^{i\omega t}\right\} = f_{(E)j}(\cos\omega t) \qquad 4.42$$

Note that the excitation force can be written in a complex number notation. But in this case only the real part is implied. $f_{(E)j}$ in the above equation refers to complex amplitude of exciting force in mode (j).

From the radiation problem :

$$F_R(t) = -A_{jk}\ \ddot{\eta}_k(t) - B_{jk}\ \dot{\eta}_k(t) \qquad 4.43$$

From hydrostatics:

$$F_S(t) = -C_{jk}\ \eta_k(t) \qquad 4.44$$

Where η_k and $\dot{\eta}_k$ are displacement and velocity of the structure in mode (k) respectively.

Then the total hydrodynamic and hydrostatic forces will be:

$$f_{(E)j}(\cos\omega t)\ -\ \left[A_{jk}\ \ddot{\eta}_k(t) + B_{jk}\ \dot{\eta}_k(t) + C_{jk}\ \eta_k(t)\right] =\ M\ \ddot{\eta}_k(t) \qquad 4.45$$

Rearranging will give :

$$\left[M + A_{jk}\right]\ddot{\eta}_k(t) + B_{jk}\ \dot{\eta}_k(t) + C_{jk}\ \eta_k(t) =\ f_{(E)j}(\cos\omega t) \qquad 4.46$$

A freely floating has six degrees of freedom, then the equation of dynamic motion for six degrees of freedom (k = 6) becomes:

$$\sum_{k=1}^{6}\left[M + A_{jk}\right]\ddot{\eta}_k(t) + B_{jk}\ \dot{\eta}_k(t) + C_{jk}\ \eta_k(t) =\ f_{(E)j}(\cos\omega t) \qquad for\ j = 1, \dots, 6$$

4.10 Linear global motion transfer function

In order to come up with a solution for the harmonic loading shown by the equation of motion in the previous chapter, the frequency response method will be considered.

However, in order to use the frequency response method, the solution has to be written in the complex form. In section 4.9 it was shown that the excitation force can be written in a complex number notation. Also writing the response in the complex form will give :

$$\eta_k(t) = \bar{\eta}_k e^{i\omega t} \qquad 4.47$$

Where $\bar{\eta}$ is the complex response amplitude.

Inserting equation 4.47 into the equation of motion yields:

$$\left[-\omega^2\left(M + A_{jk}\right) + i\omega B_{jk} + C_{jk}\right]\bar{\eta}_k e^{i\omega t} =\ f_{(E)j}e^{i\omega t} \qquad 4.48$$

Dividing both sides by the term $e^{i\omega t}$ gives

$$\left[-\omega^2\left(M + A_{jk}\right) + i\omega B_{jk} + C_{jk}\right]\bar{\eta}_k = f_{(E)j} \qquad 4.49$$

Rearranging will give

$$\bar{\eta}_k = \frac{1}{\left[-\omega^2\left(M+A_{jk}\right)+i\omega B_{jk}+C_{jk}\right]} f_{(E)j} \qquad 4.50$$

The term that relates the complex amplitude response and the complex excitation force amplitude is termed as the frequency response function H(ω).

$$\bar{\eta}_k = H(\omega) f_{(E)j} \qquad 4.51$$

The frequency response function has the form:

$$\left[-\omega^2\left(M + A_{jk}\right) + i\omega B_{jk} + C_{jk}\right]^{-1} = (\omega) \qquad 4.52$$

The frequency response function for a system describes the relationship between input and out put of a system as a function of frequency, where the input is usually force. The frequency response function gives the magnitude of the out put per unit of input and relative phase between output and input , as a function of frequency (Scheffer and Girdhar, 2004). When the damping term B ≠ 0, the frequency response function is complex, bearing information about the phase differences between the maximal amplitudes of $\bar{\eta}_k$ and $f_{(E)j}$.

It is common to consider the absolute value of the frequency response function when the phase difference between the excitation force and the response is not relevant. The resulting function is called the mechanical transfer function given by

$$|H(\omega)| = \frac{1}{C_{jk}\sqrt{[(1-\beta^2)^2 + (2\lambda\beta)^2]}} \qquad 4.53$$

Where(β) and (λ) are relative frequency and relative damping respectively and are given by the formulae:

$$\beta = \frac{\omega}{\omega_o} \qquad 4.54$$

$$\lambda = \frac{B_{jk}}{2(M+m)_{jk}\omega_0} = \frac{B_{jk}}{B_{crit}} \qquad 4.55$$

where $\omega_o$is the natural frequency of the structure.

The denominator term in equation 4.55 is called critical damping (B_{crit}). Shortly, the critical damping can be defined as damping just sufficient to prevent oscillations. It is related to a state where the roots of the characteristic equation of free damped motion coincide.

What has been shown above in equation 4.51 is a global structural response per wave excitation force. Global here means that the location where the response is considered is at the center of gravity (COG) of the structure. In case a response per wave amplitude (ξ_a) is needed, it is possible to divide both sides of equation 4.50 by wave amplitude (ξ_a). The result will give the linear global motion transfer function $X_k(\omega)$ in mode *(k),* which is commonly called the global response amplitude operator (RAO). This is because in linear wave theory, wave excitation force is taken to be linearly proportional with wave amplitude and response of the structure

$$X_k(\omega) = \frac{\bar{\eta}_k}{\xi_a} = \frac{f_{(E)j}/\xi_a}{[-\omega^2(M+A_{jk})+i\omega B_{jk}+C_{jk}]} \qquad 4.56$$

The linear global motion transfer function is complex, which means it has information about the phase difference between excitation wave amplitude and structural response. If the phase difference between the two is irrelevant, it is practical to take the absolute value of the linear global motion transfer function. Since there are six degrees of freedom, there will be six global linear motion transfer functions, one for each degree of freedom. Each RAO is specified for each degree of freedom (k), angular frequency (ω) and wave approach direction at the center of gravity (COG).

$$|X_k(\omega)| = \left|\frac{\bar{\eta}_k}{\xi_a}\right| = \left|\frac{f_{(E)j}/\xi_a}{H(\omega)}\right| = \frac{f_{(E)j}/\xi_a}{C_{jk}\sqrt{[(1-\beta^2)^2+(2\lambda\beta)^2]}} \quad for\ k = 1,\dots,6 \qquad 4.57$$

Further, the complex global motion transfer functions of the basic motions in the six degrees of freedom may be combined to describe motions in the x, y and z directions, at arbitrary locations on the structure.

4.11 Viscous damping

Until this point, it has been addressed that the linear radiation/diffraction yields hydrodynamic coefficients which are: excitation force from diffraction problem, added mass and wave potential damping matrices from radiation problem and stiffness matrix from hydrostatics. It was also seen how these coefficients from linear radiation/diffraction are combined in the dynamic equation of motion to give the linear motion transfer function.

One of the basic assumptions in linear radiation/ diffraction analysis to determine loads on structures and their motion as listed in section 4.6 is that, the flow around big structures is considered to be potential flow, free of flow separation and viscous effects. Because of this, the damping coefficient from linear radiation/diffraction analysis arises only from wave potential damping, which is the result of radiating/outgoing waves generated by oscillating structures.

Actual viscous fluid has non linear skin friction and non linear vortex shedding contribution to the damping term in the dynamic equation of motion (Fossen,2011). These contributions are usually deemed as small for large structures and are neglected.

As freely floating structures are oscillating at lower frequencies, the ability of the structures to generate radiating/outgoing waves also decreases. Due to this, the potential damping term in the dynamic equation of motion also decreases appreciably. This becomes a concern when structures are oscillating at (low frequencies) their natural frequency. Recalling equation 4.57, from section 4.10, when the structure is oscillating at resonant frequency, the relative frequency (β) will be one. The motion of the structure is then controlled by the relative damping (λ). The relative damping is in turn determined by the ratio of the actual damping (B_{jk}) and critical damping (B_{crit}) as shown in equation 4.55. If there is very small actual damping contribution from wave potential damping, which usually is the case for structures oscillating at their natural frequency, the value of the relative damping will be significantly small. This sets the response amplitude to have a very large vale, which is usually unrealistic. Ignoring the effect of the viscous contribution to the damping, when structures are oscillating near and at their natural frequency, then results in over estimation of structural response. Therefore, a good prediction of viscous contribution to the damping must be included to obtain realistic structural response.

One way to include the viscous effect on damping is to use both panel model and Morison model to describe the structural geometry in a hydrodynamic analysis. This is commonly called a dual model. The panel model captures the radiation/diffraction coefficients in the hydrodynamic analysis while the Morison model captures the viscous coefficient. Another option is to introduce the actual damping in terms of critical damping ratio which is the relative damping (λ).

4.12 Global Response Analysis: statistical method

What has been discussed so far is about the theoretical background for obtaining the linear global motion transfer functions, from linear radiation/diffraction theory in frequency domain. These linear global motion transfer functions give the associated response amplitude of the structure, for a

considered regular wave amplitude, frequency and wave approach direction at the center of gravity (COG) of the structure.

However, real waves in a sea are irregular having infinity number of frequencies, amplitudes and phase angles and can be considered as a superposition of many regular wave components. In order to see how the structure would responds in irregular waves, stochastic methods are considered the good methods for simulating the irregular nature of waves (DNV-RP-C103,2010). Stochastic methods apply the statistical distribution of waves for the calculation of short term and long term responses. Frequency domain analysis is the most suitable for global motion response analysis of column stabilized units by applying stochastic methods.

The basic steps for stochastic analysis of global motion responses are:

1) Obtain linear global motion transfer function (RAO)
2) Combine the RAO with a wave spectrum(sea state) characterized by significant wave height (Hs) and zero crossing period (Tz) which then gives response spectrum
3) Obtain extreme response using a 3-hr extreme value distribution by applying a desired facile level($\tilde{\alpha}$).
4) Repeat steps 2 and 3 for different wave spectra(sea states) of interest

Note that a result obtained from the above stochastic analysis would yield short term response for a considered stationary environmental condition, accounting the variability of the response in the short term. However environmental conditions in a real sea are variable in the long run too. This means, to determine the structure's long term response accounting both the variability of the response for a given environment and the variability of the environment in the long run, full long term response analysis should be carried out. Full long term analysis means, calculating the short term response using several sea states that might happen in the future and observing the structures short term response. A large number of sea states might need to be used to investigate the short term response, so that statistical accuracy is obtained. For this reason, full long term analysis is a demanding task, especially if the response process is non linear. Another option is to do short term response analysis by considering sea states from an environmental contour line.

4.12.1 Wave spectrum

As mentioned, real sea can be thought of as a superposition of infinity number of regular waves propagating with different frequencies, amplitudes and random phase angles. It is also noted in section 4, that the wave surface elevation process is believed to follow a steady Gaussian distribution with zero mean. This steady state surface elevation process is termed as a sea state and it can last from half an hour to few hours, depending on the location considered. If North Sea environment is considered, the sea state duration is usually taken as 3 hours.

The distribution of wave energy according to the frequencies of the wave components in a sea state is then indicated using a wave spectrum s(ω). The wave spectrum s(ω) is usually characterized by a significant wave height (Hs) and a spectral peak period (Tp). Significant wave height (Hs) is associated to the mean of the highest third of the waves in a sea state described by the wave spectrum. While spectral peak period (Tp) is the period associated to the highest energy in the wave spectrum.

The other issue is that, real waves making up a wave surface are usually of a three dimensional nature, meaning they propagate from different directions. In the resulting three dimensional pattern, waves are often called short crested, because of their appearance (Babanin,2011). Since the total energy in a wave spectrum of a sea state is from the contributions of the directional waves. Directional wave spectrum $s(\omega, \theta)$ is expressed as :

$$s(\omega, \theta) = s(\omega)\, f(\theta) \qquad 4.58$$

Where s(ω) is unidirectional wave spectrum with energy distribution depending on (ω), while the function $f(\theta)$ represents the directional distribution of energy in the waves. Compared to short crested waves with directional distribution of energy, unidirectional waves are generally considered to give conservative results (E. Frostick, J. McLelland, T.G. Mercer, 2011).

Considering North sea environmental conditions, it is a good approach to consider the Torsethaugen wave energy distribution model for a random combination of (Hs) and (Tp) (Torsethaugen, 1996). The Torsethaugen spectrum is typically obtained by superposing two JONSWAP spectra, one associated to the energy distribution in wind generated waves (wind seas) and the other associated to the energy distribution of swells. This spectral model then has two peaks in the spectra model; one for the wind sea system and the other for the swell system. Each sea system is defined by five parameters. For further reading about the parameters, (Torsethaugen, 1996) may be referred. However, by means of regression and curve fitting, they are all parameterized into single Hs and Tp pair that describes the whole spectrum.

In this spectrum model, the locally fully developed sea concept is used to divide Hs-Tp space in two different types (Torsethaugen, 1996) :

a) Wind dominated sea Tp < Hs
b) Swell dominated sea Tp > Hs

Where (T_{pf}) is the spectral peak period for fully developed sea at a considered location and is given by

it is determined by maximum fetch depending on the topography or low pressures in the area. (T_{pf}) gives the relation between Hs and Tp of the considered location and it is given by:

$$T_{pf} = a_f H_s^{\frac{1}{3}} \qquad 4.59$$

Where (a_f) is a parameter slightly dependent of fetch length of the water, which a given wind has blown. It assumes a value of 6.6 if long fetch exists and a value of 5.5 for shorter fetch lengths.

This project is dealing with the global motion characteristics of semisubmersible units. Considering heave motion especially, the typical resonant response lies around frequencies where the spectral energy is governed by swells. In order to capture the effect of swells, a Torsethaugen spectral model is adopted for the Hs-Tp combinations to be used.

4.12.2 Response spectrum

In linear analysis, the wave surface elevation is assumed to follow a steady Gaussian distribution (normal distribution) with a zero mean, within in a considered sea state. The surface elevation is the cause of the response and the two processes are not independent. For this reason, it is possible to relate the stationary Gaussian wave surface elevation process with the stationary response process. This indicates that it is possible to obtain a response spectrum by combining the incident wave spectrum with the motion transfer function amplitude (A.Paco et.al, 2012).

Also in linear theory, is possible to obtain results in irregular waves by adding results from regular waves. If the surface elevation can be represented by equation 4.25(see equation 4.25), then the total response in k degree of freedom due to the irregular waves can be written as:

$$\sum_{j=1}^{N} \left|X_k(\omega_j)\right| \; A_j \; \sin\left(\omega_j t - k_j x + \varepsilon_j\right) \qquad 4.60$$

The variance of the total response is then given as :

$$\sigma_r{}^2 = \sum_{j=1}^{N} \frac{1}{2} \bar{\eta}_k{}^2 = \sum_{j=1}^{N} \frac{1}{2} \left|X_k(\omega_j)\right|^2 A_j{}^2 \qquad 4.61$$

Where $\bar{\eta}_k$ and $|X_k(\omega_j)|$ are response and RAO in (k) degree of freedom respectively .

Then the individual response $\bar{\eta}_k$ can be written interms of the wave spectrum using similarities from equation 4.27 (see equation 4.27):

$$\frac{1}{2}\bar{\eta}_k{}^2 = \frac{1}{2}|X_k(\omega_j)|^2 A_j{}^2 = s(\omega_j)\,\Delta\omega\,|X_k(\omega_j)|^2 \qquad 4.62$$

Then letting N →∞ and Δω→0, the variance of the total response can be expressed in terms of 0^{th} spectral moment of the response spectrum, which is the area under the response spectrum (see equation 4.66).

$$\sigma_r{}^2 = \int_0^\infty s(\omega)\,|X_k(\omega)|^2\,d\omega \qquad 4.63$$

If the above value is the variance of the response spectra, the response spectra $s_{\bar{\eta}_k}(\omega)$ is then given by (from statistic rule of normal distribution) :

$$s_{\bar{\eta}_k}(\omega_j) = s(\omega_j)\,|X_k(\omega_j)|^2 \qquad 4.64$$

Once the response spectra is obtained, it can be used to obtain the significant response and further an short term responses for the desired short term probability of exceedance may be obtained, using statistical methods which will be shown in the next section.

The significant response $2\cdot\bar{\eta}_{k,S}$ (double amplitude) for the response variable $\bar{\eta}_k$, is defined as the mean of the one-third largest responses in the response spectrum. This is related to the zero moment

$$2\cdot\bar{\eta}_{k,S} = 4\sqrt{m_o} \qquad 4.65$$

The B's order Spectral moments can be obtained by

$$m_B = \int_0^\infty \omega^B\, s_{\bar{\eta}_k}(\omega)\,d\omega \qquad 4.66$$

The mean zero up crossing period then can be obtained from

$$T_{z,k} = 2\pi\sqrt{\frac{m_o}{m_2}} \qquad 4.67$$

4.12.3 Short term extreme response and response statistics

In the previous section it was shown how a response spectrum would be obtained in linear analysis. It was also mentioned the response process follows a Gaussian distribution with a zero mean in a considered sea state. For a Gaussian distributed process, the extreme values are considered to follow Rice distribution.

$$F_s(x) = \Phi\left(\frac{x}{\varepsilon\sigma_x}\right) - \sqrt{1-\varepsilon^2}\,\Phi\left(\frac{\sqrt{1-\varepsilon^2}}{\varepsilon}\frac{x}{\sigma_x}\right)e^{\frac{-1}{2}\left(\frac{x}{\sigma_x}\right)^2} \qquad 4.68$$

Where in this case x is the response, ϕ( ) is normal probability integral, σ_x is the response standard deviation which is the root of the response variance and Ɛ is a spectral width parameter.

Ɛ is then given as a function of zero, second and fourth spectral moments as:

$$\varepsilon = \left[1 - \frac{M_2^2}{M_0 M_4}\right]^{\frac{1}{2}} \qquad 4.68$$

In cases where Ɛ= 0, the Rice distribution reduced to Rayleigh distribution which is given by :

$$F_s(x) = 1 - e^{-\left(\frac{x^2}{2\sigma_x^2}\right)} \qquad 4.69$$

The most probable largest response X_{max} occurring within a time interval of (N_c) response maxima is approximately given by :

$$\sigma_s = \sqrt{2}\sigma_x[\ln(\sqrt{1-\varepsilon^2}N_c)]^{1/2} \qquad 4.70$$

Where (N_c) is response maxima.

In the case of narrow banded spectrum i.e. $\varepsilon = 0$, ($N_s = N_c$), where (Ns) represents the number of zero up crossings in the short term sea state.

The most probable largest response is given by :

$$\sigma_s = \sqrt{2}\sigma_x\sqrt{\ln N_s} \qquad 4.71$$

Where (Ns) represents the number of zero up crossings in the short term sea state.

The maximum short term response corresponding to ($\bar{\alpha}$) fractile Resp(max) is then given by (DNV-RP-C103):

$$\text{Resp(max)} = \sigma_s\sqrt{-0.5\ln\left(1-\bar{\alpha}^{\frac{1}{N_s}}\right)} \qquad 4.72$$

Where (N_S) can be determined from the duration of short term sea state (D_S) and the mean zero up crossing response period (T_x):

$$N_s = \frac{D_s}{T_x} \qquad 4.73$$

4.12.4 Environmental contour line method

As mentioned, to obtain the long term response of a structure is to carry out full long term analysis considering various sea states. But this process is time consuming as there are many sea states to be considered. Especially for strongly non linear problems, the full long term analysis is extremely complex. Hence the environmental contour line approach is considered a useful tool to reduce the number of sea states to be tested (S. Haver and S.R. Winterstein,2009). Even though carrying out full long term analysis is not as strenuous task to carry out for a linear response, as it is for non linear response, using an environmental contour method for linear response simplifies the task to a great deal as well.

In an environmental contour plane, all combinations of sea states defined in terms of significant wave height (Hs) and spectral peak period (Tp) corresponding to an annual probability of exceedance (q) are located along a contour line (J.Jia,2014). Figure 4.2 shows a contour line plane for a field at North sea.

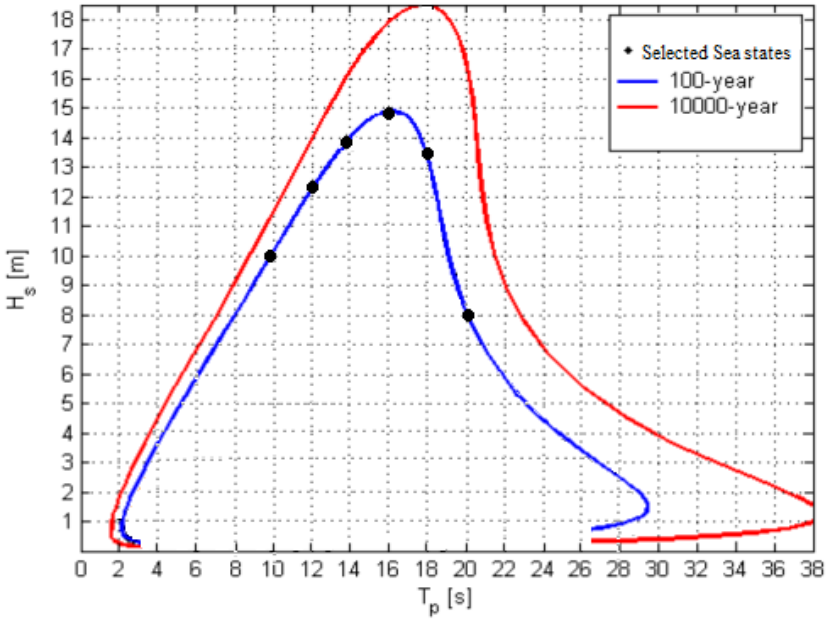

Figure 4.2 Environmental contour line plane for a field in North Sea

[souce: J.Eik and E.Nygaard "statfjord late life metocean design basis" Statoil]

When short term response is analyzed using sea states from an environmental contour line, it means the result also covers the long term variability, and is taken as the short term response in the long run.

The steps in carrying out short term response analysis using an environmental contour line method are:

1. Select probability of exceedance (q) the short term response is desired to have in the long run
2. Select an environmental contour line with the corresponding probability of exceedance (q) from an environmental contour plane. This contour line consists of all combinations of Hs and Tp for the desired value of (q).
3. The (q) probability of selected response is estimated by the value of a 3h extreme value distribution (typically a Rayleigh distribution for narrow banded response spectrum) that is exceeded by probability 1- ($\bar{\alpha}$).

For design load/responses of structures at operational conditions, the ultimate limit state governs and design should consider 100 year return period (q = 10^{-2}) loads/responses (DNV-RP-C103). To accomplish this, if 100 year (q = 10^{-2}) contour lines are to be applied for calculating a maximum short term response, NORSOK standard N003 recommends a fractile value ($\bar{\alpha}$)=0.85-0.9. (NORSOK-NOO3, 2007).

The environmental contour line shown in the figure above

5. Air gap response

One important aspect in the design of floating offshore structures is the provision of sufficient initial air gap (a_o). Initial air gap refers to the clearance between mean water level and bottom of platform deck. The reason for this is that during wave action, the initial air gap determines the instantaneous air gap $a(t)$ which is the clearance between wave crest and bottom of an offshore platform deck. In harsh environments, if the floating offshore structure is not designed with sufficient initial air gap, the wave crest rises considerably and causes wave impact load on the deck. This happens when the wave crest rises with a value $\xi(x, y, t)$, making the instantaneous air gap $a(t)$ attain a negative value. The impact from wave crest hitting a platform is enormous and is considered to have a global effect. However, on this project the slamming load from possible wave crest hitting on a platform deck is not quantified as the discussion will only be regarding air gap clearance. Equation 5.1 show the relation between initial air gap, instantaneous air gap and net wave surface elevation (DNV-RP-C205,2010).

$$a(t) = a_o - \xi(x, y, t) \qquad 5.1$$

Where *x* and *y* are horizontal locations from center of gravity (COG) to a considered location on platform deck bottom and *t* is time.

In order to avoid water wave impact on platform deck from happening, accurate prediction of instantaneous wave surface/crest elevation $\xi(x, y, t)$ must be carried and sufficient initial air gap must be provided so that an adequate instantaneous air gap $a(t)$is maintained in the long run. However, the provision initial air gap has to be economically optimal, as unnecessarily increased initial air gap normally results in high cost.

5.1 Air gap response : simplified method

A simplified method to investigate air gap is to carry out a linear radiation/diffraction analysis in frequency domain, to determine the diffracted wave field and the linearized platform motion. (DNV-RP-C205,2010). Considering a linear regular incident wave with frequency(ω), propagating from a specific direction towards a platform, the air gap response $a(\omega)$ which is the clearance between wave crest and bottom of platform deck, is given by :

$$a(\omega) = a_o - \xi_{rel}(x, y, \omega) \qquad 5.2$$

Where a_o is the initial air gap, and $\xi_{rel}(x,y,\omega)$ is the relative wave surface elevation between wave surface elevation $\xi(x,y,\omega)$ and linearized platform vertical displacement $\delta(x,y,\omega)$ for a selected location (P) on platform bottom defined by coordinates (x,y) from the COG of the platform.

If the air gap response $a(\omega)$ in equation 5.2 happens to be negative, it may result in wave impact on platform deck. For a proposed initial air gap (a_o), the decisive parameter to determine an air gap response is then the relative wave surface elevation $\xi_{rel}(x,y,\omega)$.

The Norwegian standard recommends an air gap margin of 1,5 m on the 10^{-2} wave event, is recommended for fulfilling the ULS criteria.(NORSOK-NOO3, 2007)

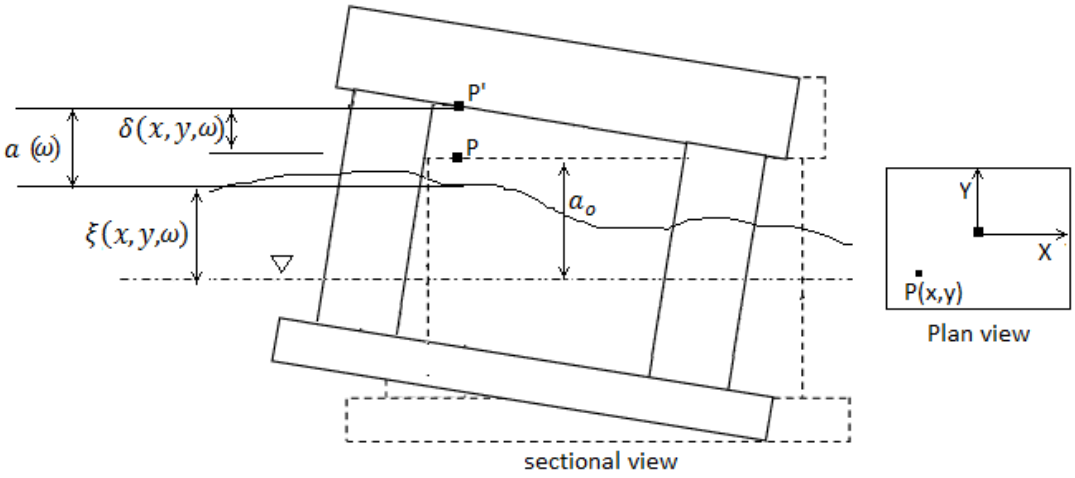

Figure 5.1 Parameters for air gap response

5.1.1 Surface elevation

As a regular incident wave is propagating towards an offshore structure, the wave surface elevation $\xi(x,y,\omega)$ is considered to be both globally and locally affected due to the structures presence. The global effect is due to radiation/diffraction effect of the structure and is termed as upwelling. The local influence is due to run-up and other strongly non linear effects. As the name implies, the local effects are confined in a region close to vertical surface of the surface piercing structure (DNV-RP-C205).

Due to the global effects, the wave surface elevation $\xi(x,y,\omega)$ in linear radiation/diffraction analysis consists of contributions from first order incident wave (I), radiated waves (R) and diffracted waves (D). Hence, wave surface elevation including the effect of radiation/diffraction for a specified location can be

obtained using linear radiation/diffraction analysis software in terms of linear complex motion transfer function in terms of RAO, $\xi(x, y, \omega)^{RAO}$.

For structures comprised of slender members such as a jacket platform, radiation effect is zero and diffraction effect is also to a limited amount. However, for large volume floating structures like a semisubmersible unit, both radiation and diffraction effects are huge. These effects give magnified wave surface elevation.

Wave surface elevation very close to vertical water surface penetrating surfaces is dominated by a local run up effect. Generally, radiation/diffraction analysis, whether first order or second order analysis, does not give a reliable result at locations where a run-up effect prevails. For this reason, the simplified method shall not be used very close to vertical columns. A good practice to investigate air gap very close to vertical surfaces would be to employ a model test.

5.1.2 Platform vertical displacement

The vertical displacement of a floating platform is given as:

$$\delta(x, y, \omega) = \eta_3(\omega) - x \sin[\eta_5(\omega)] + y \sin[\eta_4(\omega)] \qquad 5.3$$

Where:

$\eta_3(\omega)$= platform heave translational motion (positive upward)

$\eta_4(\omega)$= platform roll rotational motion (positive in positive x axis direction)

$\eta_5(\omega)$= Platform pitch rotational motion (positive in positive y axis direction)

Recalling what has been discussed in section 4, from first order linear radiation/diffraction analysis, linear global motion transfer RAOs are calculated. The global complex motion transfer RAO's for heave, roll and pitch are $X_3(\omega), X_4(\omega) and\ X_5(\omega)$ respectively. The translational heave and rotational (roll/pitch) motions in equation 5.3 can be represented by the calculated complex RAOs. Complex here refers to the phase lead/lag information between the wave elevation amplitude and the response amplitude is included in the RAOs. This will give the vertical platform displacement RAO at the selected location, for each frequency and wave propagation direction considered.

$$\delta(x, y, \omega)^{RAO} = X_3(\omega) - x \sin X_4(\omega) + y \sin X_5(\omega) \qquad 5.4$$

5.1.3 Relative wave surface elevation

The relative wave surface elevation $\xi_{rel}(x, y, \omega)$ is computed from the diffracted wave surface elevation $\xi(x, y, \omega)$ and the platform's vertical displacement $\delta(x, y, \omega)$ at a chosen location (P). This is given by:

$$\xi_{rel}(x, y, \omega) = \propto \cdot \xi(x, y, \omega) - \delta(x, y, \omega) \qquad 5.5$$

The parameters in equations 5.2 and 5.3 are presented in figure 5.1, for the case of a semisubmersible floater. In addition, the purpose of the asymmetry factor ($\propto$) used in equation 5.3 is to modify the incident regular wave's surface elevation crests and troughs. In linear wave theory, waves are assumed to be perfectly sinusoidal. However, real water waves have longer crest and shallower troughs. Including the asymmetry factor ($\propto$) is for the better representation of real waves. It is common practice to apply asymmetry factor ($\propto = 1.2$) for standard floater units such as tension leg platforms and semisubmersibles (DNV-RP-C205).

If wave surface elevation linear motion transfer function $\xi(x, y, \omega)^{RAO}$ and platform vertical displacement linear motion transfer function $\delta(x, y, \omega)^{RAO}$ are used in equation 5.5, then relative wave surface elevation will then be considered as a linear motion transfer function $\xi_{rel}(x, y, \omega)^{RAO}$ for the relative wave surface elevation. This RAO is applicable only to the considered location, frequency and wave approach direction.

$$\xi_{rel}(x, y, \omega)^{RAO} = \propto \cdot \xi(x, y, \omega)^{RAO} - \delta(x, y, \omega)^{RAO} \qquad 5.6$$

Once a RAO is generated for certain locations of interest, response spectrum can be generated considering irregular waves in terms of wave spectrum of selected sea states from an environmental contour line. Eventually, extreme minimum air gap response corresponding to the maximum relative wave surface elevation can be obtained using the same statistical methods.

5.2 Short term minimum air gap

In linear analysis, the wave surface elevation is assumed to follow a steady Gaussian distribution (normal distribution) with a zero mean, within in a considered sea state. For air gap, the surface elevation is the cause of the vertical platform displacement and the two processes are not independent (DNV-RP-C205). For this reason, it is possible to relate the stationary Gaussian wave surface elevation process with the stationary Gaussian relative wave surface process.

The relative wave surface elevation RAO, $\xi_{rel}(x, y, \omega)^{RAO}$ is then considered as a linear motion transfer function and shall be combined with a wave spectrum, given by sea states from (q= 10^{-2}) environmental

contour line, to give the relative wave surface elevation response spectrum. Then using the relative surface elevation response spectrum and a 3-hr extreme value distribution (typically a Rayleigh distribution for narrow banded spectrum) by applying a desired facile level(ᾱ= 0.9). The result will give short term maximum wave surface elevation.

The short term minimum air gap can then be computed by deducting the maximums wave surface elevation from the static air gap.

$$min[a(\omega)] = a_o - [\xi_{rel}(x, y, \omega)]^{max} \qquad 5.7$$

6. Slamming Load From Breaking Waves on Platform Column

When propagating waves break, they impose impact loads at the vertical face of offshore structures which usually have higher magnitude than loads from non breaking waves. This impact load is usually termed as wave breaking slamming load. Slamming loads usually have localized effects. For instance, slamming loads on the face of free surface penetrating structures such as columns of platforms can be mentioned. For this reason, the design of offshore structures should take slamming loads from breaking waves into account.

In order to design offshore structures that withstand loads form wave breaking, the primary step would be to estimate the expected loads from wave breaking. If the impacts loads are undermined, the result would be unfavorable. If loads to be used for design purposes are over estimated, then the design solution is not economical. The estimation of impact loads is however not an easy task. This is due to the randomness in both the wave breaking process and the variation of impact pressure, even when considering a single form of wave breaking process.

6.1 Slamming load

When a water wave breaks, the kinematics that used to describe it before breaking would no more be applicable to describe the wave anymore. At this time, the pressure may rise to more than ten times the

hydrostatic pressure corresponding to the wave height, though its duration will be very short (Y. Goda, 2010).The duration of a breaking wave's impact load is very short and its magnitude is highly sensitive to geometry of the wave front and wall, the deep water steepness of the incident wave, the beach slope and the degree of air entrainment in the water (K. Mconnell. et.al, 2004). Due to its complexity and

random nature, it is difficult to come up with analytical solution to impact pressure. On the other hand , efforts to use experimental methods for prediction of impact loads have not been successful because of the dynamic responses of measurement systems, when exposed to impact loads and measured force distortion occurs (Zhou et al. ,1991).

Chan et.al. (1990) conducted a set of systematic and controlled experiments on vertical cylinder that can represent a column of an offshore structure. The purpose was to investigate the variability of plunging wave pressure on a vertical cylinder. During the experiment, plunging wave breaking was simulated by generating frequency and amplitude modulated wave packet, programmed to break at a desired location in a 30m long wave flume and impact pressure on the cylinder was measured using eight pressure transducers placed on the upstream face of the cylinder along a vertical profile. In the 115 repeated experiments conducted, it was reported that the general impact pressure was impulsive in nature and the peak pressure is prone to huge variability. The impact pressure characteristics (such as the peak pressure and pressure oscillations) varied depending on the relative wave breaking location to the cylinder and the wave breaking kinematics. Then they disregarded the results from breaking waves associated to significant shift in the wave breaking location. It is difficult to make sure that all wave breakings occur at the same location run after run but they used implicit method to filter out results belonging to a more or less identical wave breaking location. They claimed doing so would be helpful for the assessment of impact pressure variability due to wave breaking kinematics only. Given the general nature of the impulsive pressure, they came up with a probabilistic distribution for the extreme cases of impact. The authors concluded with a physical interpretation of the experiment indicating that, in case a statistical method is adopted to determine the impact pressure due to breaking waves on structures, it is necessary to merge the statistics of wave breaking process and the probability of an impact pressure resulting from the considered form of wave breaking.

Zhou et al. (1991) carried out a similar type of experiment which also concluded that the peak pressure is prone to high variability in location and wave breaking kinematics.

6.2 Slamming load prediction : Based on DNV's recommended practice

The recommended practice by DNV gives a space average slamming pressure (P_s) for a given (q) probability of annual exceedance, over a strip of area (A) on a platform column, that is exposed to slamming pressure by the following equation [DNV-RP-C205,2010]:

$$P_s = \frac{1}{2}\varrho C_s v^2 \qquad 6.1$$

Where (ϱ) is sea water density, (C_s) is space average slamming coefficient and (v) is the relative horizontal velocity between water and surface.

The annual probabilities of exceedance that slamming loads will be computed for this project are (q = 10^{-2}) and (q = 10^{-4}). If accidental ultimate limit state (ULS) design is considered, slamming loads from wave breaking, with annual probability of exceedance (q = 10^{-2}) or 100 year return period should be applied for the design of offshore structures. On the other hand, If accidental limit state (ALS) design is considered, slamming loads from wave breaking, with annual probability of exceedance (q = 10^{-4}) or 10,000 year return period should be applied for the design of offshore structures. Since the required loads for design purposes in both cases are majorly contributed by the breaking waves, it is similar to saying breaking waves with annual probability of exceedance (q = 10^{-2}) and (q = 10^{-4}) need to be employed respectively for the ULS and ALS design purposes. The Norwegian standard (NORSOK-NOO3, 2007) can be referred to, for the different combination of environments that can be applied in order to meet the limit state requirements.

For this project, comparison is carried out for the two considered semisubmersible units, based on annual probability of exceedance (q = 10^{-2}) and (q = 10^{-4}) wave slamming loads against platform columns.

These (q) probabilities will be taken from the contour map in section 4, figure 4.2.

6.2.1 Slamming coefficient

Considering the space average slamming coefficient(C_s), the recommended value of (2π) which normally applies to flat plates will be applied to both units.

6.2.2 Relative velocity

The relative horizontal velocity (v) between water and surface i.e. platform in this case, for (q) probability of annual exceedance is given by :

$$v = u + \dot{\eta}_1 \qquad 6.2$$

Where (u) is the breaking wave horizontal water particle velocity and ($\dot{\eta}_1$) is platform surge velocity for the employed (q) probability of annual exceedance.

6.2.2 .1 Platform surge velocity

The basic assumption in this case will be that the platform surge velocity ($\dot{\eta}_1$)will follow linear nature. Motion due to second order effects will not be considered.

It was already shown in section 4, how motion transfer functions can be obtained from linear analysis. The surge velocity $RAO_{Vel.sur}$ is then obtained by multiplying the surge displacement $RAO_{Mot.sur}$ by the angular frequency squared (ω^2) of the sinusoidal wave, which is associated with the peak period ($T_p{}^{(q)}$) of the selected worst (q) probability sea state.

$$(\omega) = \frac{2\pi}{T^{(q)}} \qquad 6.3$$

Then using the sinusoidal wave frequency (ω) and surge displacement $RAO_{Mot.sur}$, the surge velocity $RAO_{Vel.sur}$ is given

$$RAO_{Vel.sur} = RAO_{Mot.sur}\ \omega^2 \qquad 6.4$$

Then the surge velocity spectrum $S(\omega)_{Vel.sur}$ will be calculated by multiplying the surge velocity $RAO_{Vel.sur}$ by a wave spectrum S(ω), having sea state parameters corresponding to (q) probability of exceedance.

$$S(\omega)_{Vel.sur} = RAO_{Vel.sur}{}^2 \mathrm{S}(\omega) \qquad 6.5$$

Since water surface elevation process is Gaussian process with mean zero, then the surge velocity response is also assumed to be Gaussian process with zero mean. Then the variance for surge velocity ($\sigma_{\mathrm{sur.vel}}{}^2$) is then can be calculated by :

$$\sigma_{\mathrm{sur.vel}}{}^2 = \int_0^\infty S(\omega)_{Vel.sur}\, d\omega \qquad 6.6$$

Assuming that 68% of the time, the platform would be moving with a surge velocity that is likely to fall with a band of one standard deviation, the surge velocity would be given as (K.Haver and A.Suyuthi, 2009).

$$(\dot{\eta}_1) = \pm\sigma_{\mathrm{sur.vel}} \qquad 6.7$$

6.2.2 .2 Breaking wave impact velocity

According to DNV, (q) probability breaking wave impact velocity ($u^{(q)}$) can be estimated by :

$$\left(u^{(q)}\right) = 1.2\ C_B{}^{(q)} \qquad 6.8$$

Where $C_B{}^{(q)}$ is the phase speed of the worst (q) probability breaking wave.

According to DNV, the most probable largest breaking wave height $(H_B{}^{(q)})$ for the worst (q) probability significant wave height $(H_s{}^{(q)})$ is given by :

$$H_B{}^{(q)} = 1.4\ (H^{(q)}) \qquad 6.9$$

The worst (q) probability significant wave height $(H_s{}^{(q)})$ and its associated peak period $\left(T_p{}^{(q)}\right)$are read from an environmental contour line.

For this work, the environmental contour line map in section 4 is used.

Based on equation 6.9, it is possible to utilize breaking steepness criteria for deep water waves to get a relation between (q) probability significant wave height $H_B{}^{(q)}$ and $L_B{}^{(q)}$. Breaking wave criteria is given by:

$$\frac{H_B{}^{(q)}}{L_B{}^{(q)}} = 0.143 \qquad 6.10$$

Even though the wave under consideration is not harmonic wave, best it can be done is to assume it as a harmonic wave. By doing so, it is possible to find a relation for wave length and period using the dispersion relation. The dispersion relation is given by (H. Holthuijsen,2007):

$$T_B{}^{(q)} = \sqrt{\frac{2\pi}{g} L_B{}^{(q)}} \qquad 6.11$$

Where (g) is gravitational acceleration and $(L_B{}^{(q)})$ is breaking wave length.

Further the phase speed of a harmonic wave can be given by :

$$C_B{}^{(q)} = \frac{L_B{}^{(q)}}{T_B{}^{(q)}} \qquad 6.12$$

From equation 6.11, period of breaking wave breaking wave $(T^{(q)})$ can be calculated. Then from equation 6.12, phase velocity $C_B{}^{(q)}$ of the breaking wave can be calculated. Using the values, (q) probability impact load can be estimated.

	q	$(H_s{}^{(q)})$	$(T_p{}^{(q)})$	$H_B{}^{(q)}$	$L_B{}^{(q)}$

		[m]	[s]	[m]	[m]
Rectangular column Semi	10^{-2}	14.9	16	20.86	145.9
	10^{-4}	18.5	18	25.9	181.1
Circular column Semi	10^{-2}	14.9	16	20.86	145.9
	10^{-4}	18.5	18	25.9	181.1

Table 6.1 Extreme sea states and breaking wave characterstics

7 Second order loads and motions

As discussed in section 4, the first order diffraction theory computes the loads (forces and moments) on a structure in its equilibrium position. As the structure is considered to stay in its equilibrium position, body boundary condition is set at the structure's surface while in equilibrium position. The dynamic pressure given by Bernoulli's equation and water particle kinematic are linearized. The free surface condition for both the dynamic pressure and water particle kinematics is set at the mean water level.. However, in reality the structure moves and changes its equilibrium position due to wave excitation loads. The mean water level also moves continuously, varying the submerged part of the structure. Considering these two effects along with the second order velocity term in the Bernoulli's equation up to the second order introduces mean (non oscillating) and oscillating second order loads. Second order here refers to terms proportional to the second power of wave amplitude.

The mean drift force/moment is time averaged force over one cycle. According to (Chakrabarti, 2005),the second order terms introduce four individual contributions from the above effects and are described as:

1. **Free surface term:** The water free surface where the structure is floating in changes instantaneously changing the submerged part of the structure about the still water line. The structure also experiences angular motion continuously, and it has the same effect as the instantaneously

changing water surface. The inclusion of these two terms as the relative elevation produces a higher order load on the structure

2. **Velocity squared term in the Bernoulli's equation** : The first order excitation load considers only the linear pressure term in the Bernoulli's equation. But when the velocity squared term of the complete equation is considered, it introduces a higher order load on the floating structure

3. **Body motion term**: the first order excitation load on the structure is computed in its equilibrium position. However, the structures moves from its equilibrium position due to first order excitation load. This newly assumed position of the structure changes the pressure distribution on its surface. Including the first order pressure distribution along with the pressure distribution of the displaced position introduces a second order load on the structure.

4. Rotation term: first order excitation load is calculated along the axis of the structure in its equilibrium position. However, when the structure is displaced from its equilibrium position it undergoes angular motion as mentioned. This angular motion changes the direction of the loads that are computed in its equilibrium position. When the load is resolved from the rotated direction, second order loads result.

A simple example to show that mean and oscillating second order loads exist is to consider the velocity squared term in the Bernoulli's equation. The two dimensional version is shown here. (The complete Bernoulli's equation can be referred to equation 4.14)

$$\frac{1}{2}\varrho\left(\left(\frac{\partial\varphi}{\partial x}\right)^2+\left(\frac{\partial\varphi}{\partial z}\right)^2\right)\approx\frac{1}{2}\varrho(u^2+w^2) \qquad 7.1$$

Where *(u)* and *(w)* are horizontal and vertical regular linear wave water particle velocities respectively, in two dimensional representations.

Considering a linear regular wave with surface elevation $\xi = \xi_a \cos(\omega t - kx)$ propagating in the positive X-axis direction in deep water, the horizontal and vertical water particle velocity components *(u) and (w)* at a fixed location on X-axis is given by :

$$u = u_0 \cos(\omega t) \qquad 7.2$$

$$w = w_0 \sin(\omega t) \qquad 7.3$$

Where (u_o) and (w_o) are horizontal and vertical velocity amplitudes,(ω) is angular frequency and *(t)* is time.

Writing the square of the horizontal and vertical velocities respectively will give:

$$u^2 = {u_0}^2 \cos^2(\omega t) = \frac{1}{2}{u_0}^2(1 + \cos 2\omega t) \qquad 7.4$$

$$w^2 = {w_0}^2 \sin^2(\omega t) = \frac{1}{2}{w_0}^2(1 - \cos 2\omega t) \qquad 7.5$$

Then inserting the above values in equation 7.1 yields

$$\frac{1}{2}\varrho(u^2 + w^2) \approx \frac{1}{2}\varrho\left[\boxed{\frac{{u_0}^2}{2} + \frac{{w_0}^2}{2}} + \boxed{\frac{{u_0}^2}{2}(\cos 2\omega t) - \frac{{w_0}^2}{2}(\cos 2\omega t)}\right] \qquad 7.6$$

In the above equation, the first two non-oscillating pressure terms correspond to mean drift load while the rest oscillating pressure term are related to oscillating second order double frequency load. As it can be seen the frequency of the third and fourth terms are double the frequency of the wave. The velocity squared term of the Bernoulli's equation is only one cause of the mean and the double frequency loads. Similarly, there are other additional drift load components arising form the other three contributions listed above.

In addition to this, when waves have multiple frequencies as is the case for random waves, the presence of non-oscillating mean drift load and oscillating second order load may also be shown by a simple derivation using the velocity squared term in the Bernoulli's equation. Choosing two random wave components of a wave group with angular frequencies ω_1 and ω_2, the horizontal and vertical water wave particle velocity can be presented by linear summation of the horizontal velocities of the two wave components respectively as :

$$u = u_1 \cos(\omega_1 t) + u_2 \cos(\omega_2 t) \qquad 7.7$$

$$w = w_1 \cos(\omega_1 t) + w_2 \cos(\omega_2 t) \qquad 7.8$$

Where (u_1) and (w_1) are the horizontal and vertical wave particle velocity amplitudes of the first wave component respectively, while (u_2) and (w_2) are the horizontal and vertical wave particle velocity amplitudes of the second wave component respectively.

Then inserting these values in equation 7.1 and expanding yields:

$$\frac{1}{2}\varrho(u^2+w^2) \approx$$

$$\frac{1}{2}\varrho\left[\boxed{\frac{{u_1}^2}{2}+\frac{{u_2}^2}{2}+\frac{{w_1}^2}{2}+\frac{{w_2}^2}{2}}+\boxed{({u_1}^2-{w_1}^2)\cos 2\omega_1 t+({u_2}^2-{w_2}^2)\cos 2\omega_2 t}+\right.$$

$$\left.\boxed{(u_1u_2-w_1w_2)\cos(\omega_1+\omega_2)t}+\boxed{(u_1u_2+w_1w_2)\cos(\omega_1-\omega_2)t}\right] \qquad 7.9$$

When there are multiple when components, mean and oscillating double frequency forces/moments act on the structure, due to the terms in the first and second box of equation 7.9, as mentioned for the case of regular waves. In addition, the terms in the third and fourth box of equation 7.9 correspond to oscillating sum ($\omega_1+\omega_2$) and difference ($\omega_1-\omega_2$) frequency second order drift loads, respectively. As can be seen, these loads are introduced due to the interaction between the pair of frequencies in the random waves. The velocity squared term in the Bernoulli's equation is only one contribution for the mean and oscillating second order wave drift load components on a structure. The rest three contributions which were also listed for regular waves, have their own role towards other additional mean and oscillating second order wave drift loads. In addition, the second order velocity potential ($\varphi_{(2)}$) based on two distinct frequencies in a random wave group contributes to high frequency (sum frequency) and slowly varying (difference frequency) second order drift forces/moments. (Chakrabarti, 2005).

However, the second order velocity potential ($\varphi_{(2)}$) does not contribute to mean drift forces.To show that the second order velocity potential does not contribute to mean drift loads, it is good to consider a second order velocity potential ($\varphi_{(2)}$), which is proportional to the square of regular incident wave amplitude $(\boldsymbol{\xi}_a)^2$ and can be expressed by time dependence given by :

$$\varphi_{(2)} = a + b\cos(2\omega t + \mathcal{E}) \qquad 7.10$$

Where (a) and (b) are time independent parameters and ($\mathcal{E}$) is a random phase.

The pressure associated to the second order velocity potential can be given by Bernoulli's equation:

$$-\varrho\frac{\partial\varphi_{(2)}}{\partial t} = \varrho 2\omega b\sin(2\omega t + \mathcal{E}) \qquad 7.11$$

As can be seen from equation 7.11, the mean value of this oscillating pressure part is zero. This indicates that the second order potential does not contribute to mean drift loads. The information that we are looking for regarding mean drift loads can be found from first order velocity potential (φ) and body motions in regular waves. Then results in irregular (random) waves can be found by summing results from regular waves (Faltinsen, 1990).

7.1 Second order loads on floating structures

As mentioned, in frequency domain, second order wave excitation loads can be seen separately as second order mean drift loads, second order oscillating difference frequency drift loads and second order oscillating sum frequency drift loads.

For the analysis of oscillating difference and sum frequency drift loads, bi-chromatic diffraction theory also including second order velocity potential ($\varphi_{(2)}$) effects need to be employed, using software that apply numerical methods. Bi-chromatic refers to the calculation of oscillating drift forces for a pair of frequencies *(ω_i ,ω_j),* where *(i, j = 1,N),* chosen from the frequency distribution of a random wave with *(N)* components (Chakrabarti, 2005). This analysis gives a quadratic transfer function (QTF) similar to the one in table 7.1, for each pair of frequencies *(ω_i ,ω_j).* The QTF vales in table are arbitrary and are given as an example. In this table the frequencies are presented in the vertical and horizontal axes. Each value in the table represents a QTF. Each QTF refers to the magnitude of the drift force per wave amplitude square($\xi_a{}^2$), in the direction of the considered drift load. For instance, a surge drift force is considered in table 7.1.

$\boldsymbol{\omega_j}$(rad/sec) → $\boldsymbol{\omega_i}$ rad/sec)↓	0.364	0.454	0.556	0.627	0.743
0.364	10	220	180	310	160
0.454		10	80	280	100
0.556			40	230	140
0.627				30	70
0.743					20

7.1 Quadratic transfer function of for oscillating surge drift load (KN/m^2) due to paired wave frequencies

Considering random waves with several combination of frequency pairs *(ω_i ,ω_j),* such a QTF table will be very bulky, since there are normally several frequency components in a random wave group. However, these oscillating drift loads (both difference and sum frequency loads) are usually of concern only when the natural frequency is around the difference or sum of each pair of frequencies considered. The reason for this is that, as the load caused by the sum or difference of the frequency pairs is oscillating, it will excite the structure at its natural frequency and resonance can take place, if the oscillation frequency of the exciting load and the natural frequency of the structure match. Therefore, it is sufficient to choose frequency pairs (at difference or sum frequency) that result in an oscillating load close to the natural frequency of the structure.

On the other hand, the main diagonal elements in table 7.1 where $(\omega_i = \omega_j)$ represent QTFs for second order mean drift forces for the corresponding frequency. However, it is not entirely necessary to perform a bi-chromatic diffraction method including second order potentials and look into the diagonal elements, to find the QTFs for the mean drift forces. The diagonal elements can be calculated from first order velocity potential alone, using linear diffraction theory. Hence there is no need to calculate the second order velocity potential. This makes sense, as it is already shown in equation 7.11 that the second order velocity potential does not result in mean drift load.

For the two considered semisubmersible units in this project, the horizontal (surge,sway) mean drift forces and yaw mean drift moment will be investigated for a regular wave train in frequency domain, by using the numerical software package WADAM. The result gives horizontal (surge and sway) mean drift force QTFs and a yaw mean drift moment QTF for each unit. Hence, second order difference and sum frequency drift loads are not further studied in this project.

7.1.1 Second order mean drift loads

The mean drift loads (forces/moments) are calculated from the first order velocity potential (φ) and motions. The horizontal components (surge, sway) and the moment about the vertical axis (yaw) can be calculated in a robust manner by far field method also called the momentum method (DNV-RP-F205, 2010). Using direct pressure integration method also known as the near field method ,it is also possible to calculate second order mean drift loads by integrating the second order mean wave pressure (calculated from first order velocity potential) over the wetted surface of the structure. This is a very demanding method which requires enormous body geometry discretization. This method is usually applied for the computation of vertical mean drift forces due to the limitations the momentum method has in computing the vertical mean drift loads. The second order pressure distribution on the body surface is also not given by the momentum method. Whereas, using the direct integration method, the second order wave pressure is directly integrated over the wetted surface of the hull correctly up to the second order on the wave amplitude. This means the drift forces in all six degrees of freedom can be computed using this method. (Faltinsen,1990) in his book described the major differences between the two methods. Hence, further reading regarding the major differences and assumptions using the two methods can be referred to it.

Following the suggestion by (DNV,2010), the momentum method is applied for the calculation of horizontal mean drift loads in this project. In the next sub section, the concept behind the derivation of the momentum (far field) method to determine the horizontal mean drift loads is discussed.

7.1.1.1 The far field method

The far field method, also known as the method of conservation of momentum was first applied by (Mauro, 1960). Mauro applied the theory of conservation of momentum M(t) in the fluid, through a control volume bounded by an inclosing surface(S) , to give the solution of mean horizontal drift forces on two dimensional and three dimensional bodies when the bodies are positioned in a propagating regular incident wave by assuming deep water condition.

The momentum inside the closed surface (S) can be expressed as

$$M(t) = \iiint_{\Omega} \varrho \boldsymbol{V} d\tau \qquad 7.12$$

Where (Ω) is the control volume , $\boldsymbol{V}=(V_1,V_2,V_3)$ is the fluid velocity and $(d\tau)$ is a symbol for volume integration . Note that the enclosing surface (S) does not have to follow the fluid motion.

Then by applying the time derivative of M(t), noting both volume and velocity may change with time:

$$\frac{dM}{dt} = \varrho \iiint_{\Omega} \frac{\partial \boldsymbol{V}}{\partial t} d\tau + \varrho \iint_{s} \boldsymbol{V} U_n \, ds \qquad 7.13$$

Where (U_n) is the normal component of the velocity on the surface (S) and the positive normal direction is defined to be out of the fluid.

The volume integral in equation 7.13 can be expressed in Euler's equation considering incompressible fluid :

$$\frac{\partial \boldsymbol{V}}{\partial t} + \boldsymbol{V} \cdot \nabla = -\nabla \left(\frac{P}{\varrho} + gz \right) \qquad 7.14$$

Using the generalized gauss theorem and vector algebra the volume integral can be written in terms of surface integral. Then rewriting equation 7.13 considering the term in equation 7.14 and surface integral:

$$\frac{dM}{dt} = -\varrho \iint_{s} \left[\left(\frac{P}{\varrho} + gz \right) \mathbf{n} + \boldsymbol{V}(V_n - U_n) \right] ds \qquad 7.15$$

Where $(V_n = \frac{\partial \varphi}{\partial n})$ is the normal component of the fluid velocity at the surface (S) and (**n**) is surface normal to (S).

Then letting the closed surface (S) consist of body surface (S_B), a non moving vertical circular cylindrical surface (S_∞) away from the body, the free surface (S_F) and the sea bottom (S_o) inside (S_∞) . It has to be

noted that (S_∞) doesn't necessarily mean it is has to be far away from the body. Then writing the boundary conditions :

$U_n = V_n$ on S_B and S_F

$U_n = 0$ on S_∞ and S_o

The force on the body **F**=(F_1,F_2,F_3) on is given by $\int_{S_B} P\mathbf{n}\, ds$. The pressure (P) in equation 7.14 is defined to be the difference between fluid pressure and atmospheric pressure. This implies that, on the free surface (S_F), (P=0). The term $\int_S gz\mathbf{n}\ ds$ gives no horizontal component. By time averaging equation 7.15 over one period of oscillation and having $\frac{dM}{dt} = 0$

$$\overline{F_i} = \overline{-\iint_{S_\infty} [P\mathbf{n}_i + \varrho \boldsymbol{V_i} V_n] ds} \qquad i = 1,2 \qquad 7.16$$

Where $\overline{F_i}$ (the bar above means time average) is mean drift force only in the horizontal direction *(i=1,2)* but not for the vertical direction . This is because if the conservation of momentum is used to calculate the vertical mean force, the ϱgz term can not be removed from the integrand, because it has a vertical force component. To include this component, the integral has to be performed over the free surface , unlike the case of the horizontal mean drift forces, where the integral is performed over the vertical cylindrical surface (S_∞) as seen in equation 7.16.

Newman derived a similar formula for the yaw mean drift moment (Faltinsen,1990). He first used the fluid angular momentum

$$\boldsymbol{K}(t) = \varrho \iiint_\Omega\ (r \times \boldsymbol{V}) d\tau \qquad 7.17$$

Where (r) is the position vector relative to the orientation of the coordinate system (x,y,z), which is fixed in space. The derivation is similar to that shown for equation 7.15. If fluid velocity (V_6) is defined from $r \times \boldsymbol{V}$ *= (V_4,V_5,V_6)* and (n_6) is defined from $r \times \mathbf{n}$=(n_4 ,n_5 ,n_6), then equation 7.16 is also valid for the yaw moment (*i=6)*.

Mauro's derivation of horizontal mean drift forces on a two dimensional body in incident regular deep water waves takes after equation 7.16.The assumption for the derivation of the horizontal mean drift forces include:

- The body may be fixed or floating (oscillating at its mean position)
- The body has no constant speed

- There is no current

Three velocity potentials exist in this case. These are;

I) Incident wave potential

II) Reflected wave potential (describing diffracted and radiated waves)

III) Transmitted wave potential (describing incident wave and radiated waves)

The incident wave potential includes the incident wave amplitude (ξ_a) in its expression. While the regular incident wave is propagating towards the body, due to the body's presence, there will be reflected waves. Reflected waves are linked to diffraction and radiation waves (Karimirad,2014). The reflected waves are described by reflected wave potential having reflected waves' amplitude (A_R) in its expression. Transmitted waves are the combination of incident wave and radiated waves. Transmitted wave potential in its expression contains transmitted waves' amplitude (A_T).

Then the outcome of derivation for the horizontal mean drift force $\overline{F_i}$ has the form:

$$\overline{F_i} = \frac{\varrho g}{4}\left[{\xi_a}^2 + {A_R}^2 - {A_T}^2\right] \qquad i = 1 \; or \; 2 \qquad 7.18$$

If XZ plane is chosen for the two dimensional representation, (i=1). If YZ plane is chosen for the two dimensional representation, (i=2).

Following the above formula, Mauro assumes the average energy flux is zero through the body surface (S_B). This is given by :

$${\xi_a}^2 = {A_R}^2 + {A_T}^2 \qquad 7.19$$

Therefore, equation 7.18 can be re-written in the form :

$$\overline{F_i} = \frac{\varrho g}{2} {A_R}^2 \qquad 7.20$$

According to the above formula, the wave drift force will always act in the wave propagation direction. It can also be seen from the formula that the mean drift forces are directly related to the body's ability to cause waves due to diffraction and radiation. For waves with relatively long wave lengths compared to the body's characteristic dimension, the body will not disturb the wave field. This indicates that the reflected wave amplitude (A_R) becomes very small.

On the other hand, when wavelengths are very short, the incident waves are completely reflected from the surface piercing body with vertical hull surface in the wave zone.(Faltinsen, 1990).This makes ${\xi_a}^2 = {A_R}^2$. As it is indicated in equation 7.19, the reflected wave amplitude (A_R) can never be large than the incident wave amplitude (ξ_a).This indicates that the maximum mean drift force can never be larger than the value given by equation 7.21.

$$\overline{F_{i,max}} = \frac{\varrho g}{2} {\xi_a}^2 \qquad 7.21$$

Regarding the body's ability to cause reflected waves due to radiation effect (associated to the body's motion), large body motion associated to resonance effect, for example heave resonance is likely to increase the magnitude of the reflected wave amplitude (A_R), causing higher horizontal drift force around the body's resonant frequency.

(Mauro, 1960) has also derived a formula similar to equation 7.20,for drift forces on a three dimensional structure in incident regular waves, with no current present. This is given by

$$\overline{F_1} = \frac{\varrho g}{4} \int_0^{2\pi} A^2(\theta)(\cos\beta - \cos\theta) d\theta \qquad 7.22$$

$$\overline{F_2} = \frac{\varrho g}{4} \int_0^{2\pi} A^2(\theta)(\sin\beta - \sin\theta) d\theta \qquad 7.23$$

Where β is the wave propagation direction relative to the x-axis and $A(\theta)/r^{\frac{1}{2}}$ is the wave amplitude generated by the body far away at large horizontal radial distance $r = (x^2 + y^2)^{\frac{1}{2}}$ from the body. These waves are the sum of radiation waves and diffraction waves generated by the body subjected to incident waves. The angle (θ) is defined as $= r\cos\theta$, $y = r\sin\theta$.

Equations 7.22 and 7.23 are evident that mean drift forces in three dimensional cases too are dependent on the body's ability to generate waves. For instance, if the wave propagation direction to the x-axis is zero, i.e. $\beta = 0$, the drift force will have the same direction as the wave propagation direction. But this is not necessarily the case for the general wave propagation directions. Depending on the wave propagation direction, the horizontal drift force assumes the values indicated in equations 7.22 and 7.23.

Equations 7.20, 7.22 and 7.33 are derived by assuming the conservation of energy. In many cases where energy is not conserved, for instance the roll resonant response of a structure, where viscous force dominates to a large extent, these equations are not expected to give satisfactory results.

7.1.1.2 Mean drift load quadratic transfer functions

Once the second order mean drift load values are computed considering regular incident waves in frequency domain, quadratic transfer functions (QTFs) can be generated by normalizing the mean drift load values calculated at each frequency by the square of the regular incident wave amplitude as shown in equation 7.24.

$$QTF = \frac{\bar{F}_i(\omega_j;\beta)}{{\xi_a}^2} \qquad i = 1,2,6 \qquad 7.24$$

Here $\bar{F}_i(\omega_j;\beta)$ is the mean drift load in the i^{th} direction, which is specified as surge, sway and yaw for the results of the near field method. (ω_j) is regular incident wave frequency, (β) is wave propagation direction and $({\xi_a}^2)$ is normalizing incident wave amplitude squared.

7.1.1.3 Mean drift loads in regular waves

Recalling equation 7.9 where the mean drift force contributions in the velocity squared term of the Bernoulli's equation are from a hypothetical wave group containing only two wave components, it was shown that each component's mean drift force contribution can be summed together to give the total mean drift force. This implies that mean drift force contributions from components of a real sea state can be added linearly.

$$\overline{F_{i,total}} = \sum_{j=1}^{N} \frac{\bar{F}_i(\omega_j;\beta)}{{\xi_a}^2} {A_j}^2 \qquad i = 1,2,6 \qquad 7.25$$

Where first term in the right side is the QTF of mean drift force as described in the previous section and (A_j) is the amplitude of the j^{th} wave component in the sea state.

7.2 Second order horizontal motions due to mean drift forces

Mean and oscillating (difference and sum frequency) loads are responsible for the second order motions, that a floating structure undergoes. The mean drift load is important when considering the second order motions of a floating structure which has small stiffness in certain degrees of freedom,

such as the second order surge and sway motions of a centenary moored semisubmersible. Typically, due to the small stiffness of the centenary mooring, even a small mean drift force in the horizontal direction displaces the semisubmersible to a large extent. The semisubmersible then assumes a displaced position due to the horizontal mean drift force which in turn makes its riser attain an operationally limiting increased initial angle (Chakrabarti, 2005).

Second order mean drift horizontal motions can be computed once the second order mean horizontal drift forces are obtained. This is done by accounting stiffness of the structures in the horizontal degrees of freedom. Horizontal degree of freedom stiffness in structures is contributed by mooring lines for moored structures. If mooring line stiffness detail is not available, which is usually the case for preliminary design stages by which analysis carried out without mooring effect, the mean drift horizontal load/moment magnitude shall still be a good indication of expected drift offsets.

8. Analysis tools

The SESAM suite of software is used for modeling the two units, running hydrodynamic analysis and carrying out statistical post processing of the hydrodynamic analysis results in this project. Sesam Genie is used for the modeling and meshing of each unit, Sesam HydroD is for the graphic environmental setup and the hydrodynamic analysis based on linear radiation/diffraction theory is then computed in frequency domain, by the Wadam software module, which is executed from Sesam HydroD. The graphical presentation and statistical post-processing of the hydrodynamic analysis results is carried out using the graphical post processor Postresp. Short description about each software tool is presented in this section.

8.1 Sesam GeniE

GeniE is used for engineering analyses of both fixed and floating structures (Sesam GeniE UM, 2011). GeniE may be used as a stand-alone tool using a direct analysis approach (all modeled in one and same finite element model) where the user can:

- Model structure, equipments, environment and other loads
- Calculate hydrodynamic loads and run static structural analyses including non -linear pile soil analysis
- Visualize and post process results
- Perform code checking based on recognized standards

GeniE may also be used to create hydrodynamic models (panel, Morrison, dual or composite model) of fixed or floating structures, so that it can be used for stability or hydrodynamic analysis in HydroD.
After creating a hydrodynamic model, meshing can also be carried out in Genie. The meshing of the hydro- model can be automatic or user defined. The meshed hydro-model will then be saved and exported to HydroD, as a finite element model file (T*.FEM file) for further stability or hydrodynamic analysis.

8.2 Sesam HydroD

HydroD is an interactive application for computation of hydrostatic and stability, wave loads and motion response (hydrodynamic analysis) for ships and offshore structures (Sesam HydroD UM, 2011). HydroD is an integral part of the Sesam system. Finite element model (T*.FEM) generated in the Sesam program GeniE is used as an input to HydroD, as a hydro-model. The model is read and wave loads and motions are computed by WADAM or WASIM which are modules in the Sesam suite of software. These modules are executed from Sesam HydroD. For vessels with forward speed, the WASIM module is used for analysis, while for vessels without forward speed, WADAM is used for analysis. Further, global response result interface files produced by HydroD (G*.SIF/SIN/SIU) can be read into e.g. Postresp for statistical post processing.

After starting HydroD, a user can choose one of the three wizards available depending on the purpose of the analysis. These three wizards are stability wizard, WADAM wizard and WASIM wizard. These wizards guide the user through the necessary steps to set up a specific analysis, and are highly recommended for both new and experienced users. The wizards can be accessed through toolbar buttons and menu items.

HydroD uses two different coordinate systems. The input coordinate system, which all models and input data refer to and the global coordinate system, which is at the still water line and response results coming from WADAM refer to.

For the hydrodynamic analysis of vessels with no forward speed, the WADAM wizard shall be chosen. Going through the WADAM wizards in HydroD, the finite element model (T*.FEM) can be imported as a hydro-model. Through this wizard wave frequency steps for calculation, wave direction, water depth, flotation position (including trim option), initial stability parameter, mass model , off body points (points on water surface water surface to capture free surface elevation) and other relevant parameters necessary for hydrodynamic analysis can be specified. After environmental and loading condition setting

is done in HydroD, users will be directed to a WADAM run interface. A WADAM run contains all the information required to execute WADAM.

WADAM computes hydrodynamic loads on hydro models using 3D radiation-diffraction theory. WADAM merges linear wave theory and sink-source method to describe the potential wave flow around structures. Both time and frequency domain can be used for hydrodynamic analysis in WADAM. But typically, frequency domain is deemed sufficient and is widely adopted for analysis.

The definition of models in WADAM includes three main model types: (I) a hydro-model that is set in HydroD is used by WADAM to calculate hydrodynamic loads (II) the structural model where hydrodynamic and hydrostatic loads are rep-resented as finite element loads (if load transfer to structure is desired) (III) a mass model which is relevant to floating structures only, maybe defined as finite elements with mass property, as a mass matrix or by direct input of center of gravity and mass distribution in terms of radius of gyration and product of inertia.

For large offshore structures by which potential flow dominates, the hydro-model is represented by a panel model. For slender structures, a Morison model is employed for hydrodynamic load calculation using Morison's equation. A combination of a panel and a Morison model can also be used when potential theory and Morison's equation are applied to different parts of the hydro model. Further, dual model is used when both potential theory and Morison's equation shall be applied to the same part of the hydro model.

For this work, a panel model is used to define the hydrodynamic model. Based on the panel model, first order global hydrodynamic analysis is carried out. The result gives, first order global excitation load transfer functions, potential wave damping, added mass, first order global motion transfer functions (RAOs) in rigid body degrees of freedom and second order mean drift excitation load transfer functions, in frequency domain.

8.3 Postresp

Postresp is a general interactive graphic postprocessor for post processing of general responses given as transfer functions in the frequency domain, or post processing of time series in the time domain. The transfer functions in the frequency domain part are usually generated by one of the hydrodynamic programs in the Sesam suite (i.e. WADAM, WASIM etc.) but they may as well be transfer functions for any kind of response (Postresp UM, 2007).

Postresp is a part of the Sesam program suite but can also be used to postprocess frequency dependent results from other external programs writing their results on a standard Sesam Results Interface File.

Among the features of Postresp include:

- Graphical presentation of hydrodynamic results such as motion and load transfer functions
- Create specific point and response variable
- Create wave spectrum
- Combine wave spectrum with linear transfer function of motion or load to give response spectrum
- Statical postprocessing of short term responses using Rayleigh or Rice distribution

9. Analysis arrangement

In this section, a brief description is given about the models used and the environmental setup for analysis is discussed.

9.1 The panel model

The hydro dynamic models for both the rectangular column and the circular column semisubmersible units have been prepared as a panel model. As already discussed in section 4, for large structures like semisubmersibles, where potential flow dominates, the panel model captures the hydrodynamic loading from the environment by employing the 3D radiation/diffraction theory. Since the semisubmersible units considered for comparison do not have slender members, no Morrison model has been considered.

The panel model was created using Sesam GeniE, using plate/shell members. Following the suggestion by DNV, only a quarter of the hydrodynamic model was prepared in the positive X and Y coordinates. A special feature in Sesam HydroD later applies symmetry to the model, both in XZ and YZ plane which gives the complete model during analysis. Following this procedure saves considerable CPU and PC memory (Sesam Genie UM, 2011).

9.2 The mass model

The mass models for both the rectangular column and the circular column semisubmersible units have been defined in HydroD, based on the imported panel models' geometry and additional inputs of operational draft, longitudinal and transversal metacentric height (GM) and radius of gyration about X, Y

and Z axes (about input coordinate system). Stability analysis is not considered in this work. However, hydrostatic data is necessary to obtain realistic loading condition that is to be used in the hydrodynamic analysis.

As for stability analysis, detailed mass distribution of each unit has not been addressed in this project. However, a reasonable mass distribution in terms of radius of gyration is also necessary to define the mass model. For this reason, the operational draft, minimum GM and radius of gyration are all adopted based on proposals from the outline of this work.

After the meshed panel model is imported into HydroD, a loading condition has been specified in terms of flotation position. Based on the displaced volume of water at the specified flotation position, HydroD calculates the total mass of each unit. Also, radius of gyration about X, Y and Z axes have been defined to complete the mass model in HydorD.

The mass obtained from the displaced water represents the total mass, including self weight and top deck load of the system at operational draft. Location for mass center has been specified about the input coordinate system at, a position that gives the minimum proposed GM value with respect to the Z axis.

	Rectangular column unit	**Circular column unit**
Operational Draft [m]	24	24
Minimum GM at operation [m]	4	4
Radius of Gyration abot X-axis K_{XX} [m]	40	40
Radius of Gyration abot Y-axis K_{YY} [m]	40	40
Radius of Gyration abot Z-axis K_{ZZ} [m]	50	50

Table 9.1 Mass Model and Loading condition

9.3 Wave Heading Interval

The analysis in WADAM is performed based on user specified wave heading setting that is set in HydroD. For this work, 15^0 wave heading interval is chosen for the analysis performed. The range of the wave head directions considered is from 0^0 wave approach angle up to 345^0 wave approach angle.

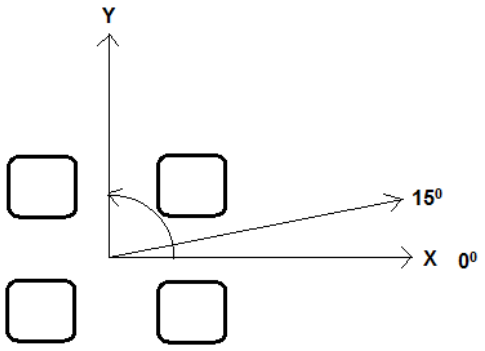

Figure. 9.1 Wave Headings for motion and load transfer functions

9.4 Period Interval

The motion transfer functions are calculated based on 0.5 of a second period interval. WADAM has a limit of 60 set of periods (frequencies), by which analysis can be performed based on. For this reason, the first run is carried out for periods from 5-30 sec and the second run is carried out for periods 30-59sec.

9.5 Water depth and water property

Water Depth [m]	300
Water Density [Kg/m^3]	1025
Water Kinematic viscosity [m^2/s]	$1.19*10^{-6}$

Table 9.2Water depth and water property

9.6 Applied viscous Damping

Viscous simplification is employed for first order heave motion transfer function in HydroD. HydroD allows a viscous damping coefficient in terms of fraction of critical heave damping. A fraction of 3% of the total critical heave damping is applied in the heave-heave degree of freedom. This final adopted critical damping is a result based assumption. This means that, other damping fractions had also been tested, but the resonance amplitude in heave-heave degree of freedom, by using 3% fraction, more or less resembled to what is observed in other semisubmersibles. As there is uncertainty underlying for choosing this fraction, it is adopted for the purpose of analysis and comparison of the two units.

Similarly for the roll-roll and pitch-pitch degrees of freedom, a 1.5% of critical damping with respect to the rotational degrees of freedom has been applied.

9.7 Off-body points setting (diffracted water surface elevation for Air gap)

At a location where air gap is intended to be investigated, wave surface elevation RAO including the effect of radiation/diffraction at the chosen location is important (see section 5.1.1).

The location that diffracted wave surface elevation is to be computed for can be specified in HydroD, in terms of off-body point (location), representing the location for air gap investigation. An Off-body point is entered with respect to HydroD's global coordinate system, which is at the still water line (Z=0). This is the coordinate that response results coming from WADAM refer to.

During hydrodynamic analysis, WADAM computes the RAO of the diffracted wave surface elevation at the chosen off-body points. This diffracted wave surface elevation's RAO is then factored and combined with platform bottom deck motion to give the relative surface elevation RAO.

As can be seen in the figure 9.2 , ten off-body points are chosen, representing ten locations and air gap will be investigated for both the rectangular column and the circular column semisubmersible units at these ten chosen locations..

Location (1) is at the global origin. Locations (2,3,8) are oriented 0^{o} with respect to global coordinate system, towards column face. Locations (6,7,10) are oriented 90^{o} with respect to global coordinate system, towards column face. Locations (4,5,9) are oriented 45^{o} with respect to global coordinate system, towards column face.

In each orientation, the column-close locations are 5m away from the face of the respective column, while the locations next to the column-close locations (i.e. locations 3,5,7) in each orientation are 10m from the face of the respective column.

The coordinates of the off-body points representing the chosen locations with respect to global coordinate system are shown in tables 9.3 and table 9.4 for the rectangular and the circular column units respectively.

Locations	1.00	2.00	3.00	4.00	5.00	6.00	7.00	8.00	9.00	10.00
X coordinate	0.00	23.50	18.25	23.25	21.85	39.75	39.75	-56.25	-54.15	-39.75
Y coordinate	0.00	39.75	39.75	23.25	21.85	23.25	18.25	-39.75	-54.15	-56.25

Table 9.3 Rectangular column semi unit off-body points

Locations	1.00	2.00	3.00	4.00	5.00	6.00	7.00	8.00	9.00	10.00
X coordinate	0.00	21.90	16.90	26.90	23.40	39.75	39.75	-57.61	-52.60	-39.75
Y coordinate	0.00	39.75	39.75	26.90	23.40	21.90	16.90	-39.75	-52.60	-57.61

Table 9.4 Circular column semi unit off-body points

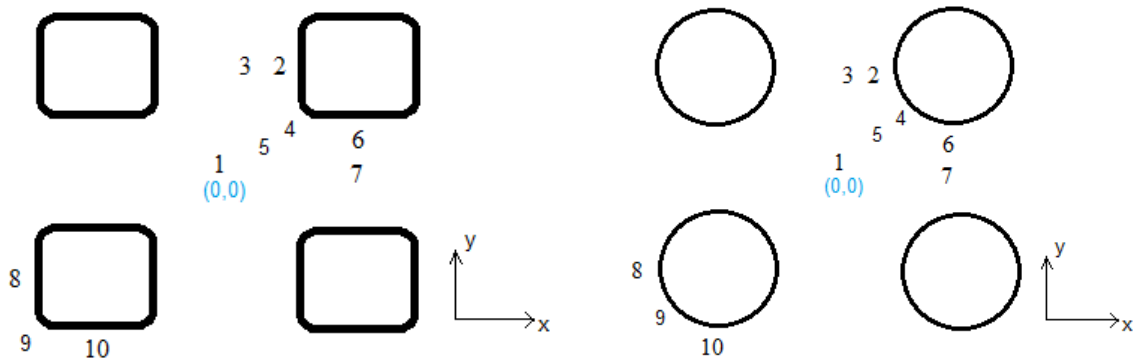

Figure 9.2 Off-body Points location for diffracted water surface RAO calculation

9.7 Mesh convergence Study

The geometric design of the hull, which is a panel model for both the rectangular column and the circular column semisubmersible units has been done in Sesam GeniE. The meshing of each panel model has also been carried out in Sesam GeniE, before being imported to HydroD. The output of the meshed geometric model was a finite element model (T*.FEM) file that is to be used for the hydrodynamic analysis, when later exported to HydroD/WADAM .The meshing in GeniE was accomplished by defining a panel mesh density that corresponds to quadrilateral elements' size that make up the complete finite element model. As discussed in section 4, meshing here refers to representation of the structure's geometry using quadrilateral finite elements, which are intended to represent the geometric panel model for hydrodynamic analysis. Typically, a finer panel mesh density or a smaller finite element size gives a more accurate result. However, as a mesh density is made finer, the computational time requirement to compute a hydrodynamic analysis in WADAM also increases. The goal should be to find out a satisfactory mesh density that balances accuracy and a reasonable computational time. The common practice to find out which mesh density balances both accuracy and computation effort is to perform a mesh convergence study convergence study.

Mesh convergence study is carried out to see the goodness of a finite element model. If the difference between two consecutive meshes is less than a fixed tolerance, a coarser mesh is normally accepted as a suitable mesh for the analysis (R.W.Lewis et.al., 2008).

The table below shows the two different element sizes used for meshing both the rectangular column semi panel model and the circular column semi panel model. The meshed panel models are applied to document the convergence of global first order motion transfer function (RAO) results.

Description	**Element Size [m]**	**Computational time Consumption [sec]**
Rectangular Column Semi	1.5 x 1.5	5706
Rectangular Column Semi	1.0 x 1.0	99142
Circular Column Semi	1.5 x 1.5	5532
Circular Column Semi	1.0 x 1.0	110757

Table 9.5 Mesh densities considered for convergence study

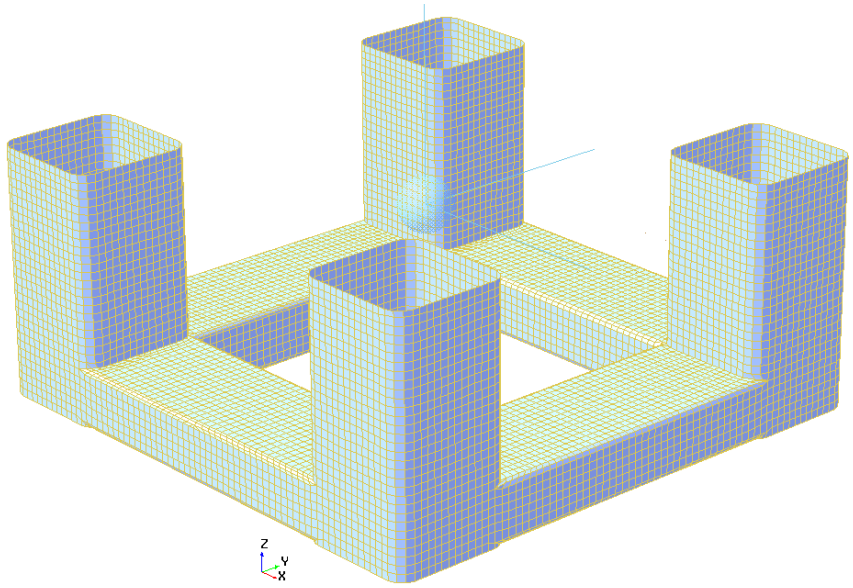

Figure 9.3 Rectangular Column Unit Panel Model with element size 1.5m x 1.5m

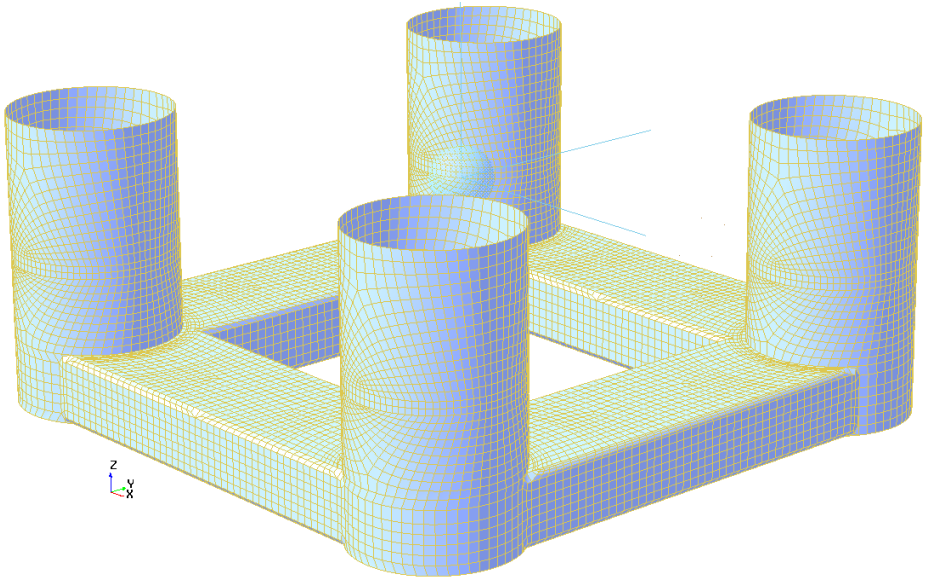

Figure 9.4 Circular Column Unit Panel Model with element size 1.5m x 1.5m

Figures 9.3 and 9.4 above show the 1.5m x 1.5m mesh density panel models for the rectangular and circular colulmn semi units respectively. The 1.0 x 1.0m mesh density panel models for both units are also included in appendix A.

Body geometry misrepresentation that occurred while using large sized finite elements for meshing, especially for the circular column semi unit panel model, left the only option of considering mesh sizes of relatively smaller element (higher densities) for a convergence study. If not as bad as the circular column, the same problem has been observed in the case of the rectangular column semi unit. Figure 9.5 shows a typical area loss observed at column surfaces, while using larger mesh elements. Even when using mesh elements' size as low as 1.5m x 1.5m, some loss of column cross sectional area had been observed in the case of the circular column. This is could eventually affect the water plane area (stiffness) when used for hydrodynamic analysis. For this reason, mesh elements with smaller size have been applied to the circular semi unit's panel model, around the still water line.

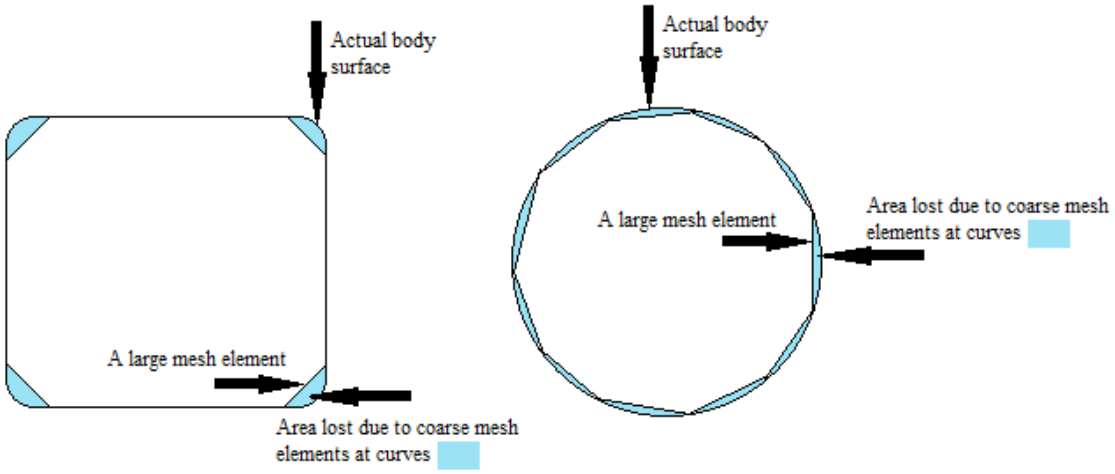

Figure 9.5 Area loss due to large mesh element at curved surfaces

The panel models representing the whole geometry of each hull are presented in here for full visualization and completeness purpose. However, only the portion of each panel i.e. from bottom pontoon until mean water level will be utilized by WADAM for the global hydrodynamic analysis.

9.7.1 First order motion transfer functions (RAOs) Convergence results

Convergence test is carried out for a wave period interval between 5sec to 30sec. Since the two semisubmersible units considered are symmetric with respect both XZ and YZ plane, only heave and pitch will be considered for motions in the vertical degree of freedom, while surge and yaw will be considered for motions in the horizontal degree of freedom. For heave, pitch and surge a wave approach of 0^o and 45^o degrees will be considered. Yaw motion has been found to be significant incident wave approach angle of 30^o , hence presentation will be based on this direction.

Rectangular column semi unit convergence results

In figures 9.6, 9.7,9.8 and 9.9, RAOs for the rectangular semi unit based on 1.5 x 1.5 m mesh density panel model and 1.0 x 1.0 m mesh density panel model are presented. For heave, pitch and surge RAO 0^o wave approach and yaw RAOs for 30^o wave approach are considered. The maximum values of the RAOs obtained by the two panel mesh densities, in each mode of motion and wave period interval considered, are used as control values to determine convergence.

Figures 8.5 shows the two heave motion RAOs obtained by using the two panel mesh densities for the wave period interval considered and for 0^o incident wave approach. The maximum values for both RAOs are found at resonance wave period, which is 24.5sec . At this wave period, the RAO given by the

coarser mesh (i.e. 1.5m x 1.5m) underestimates the maximum value given by the finer mesh (i.e. 1.0m x 1.0m) by 1%, which indicates there is a 99% convergence at this location.

The same convergence figure applies for, heave RAOs obtained by using the two panel mesh densities for the wave period interval considered and for 45^{o} incident wave approach.

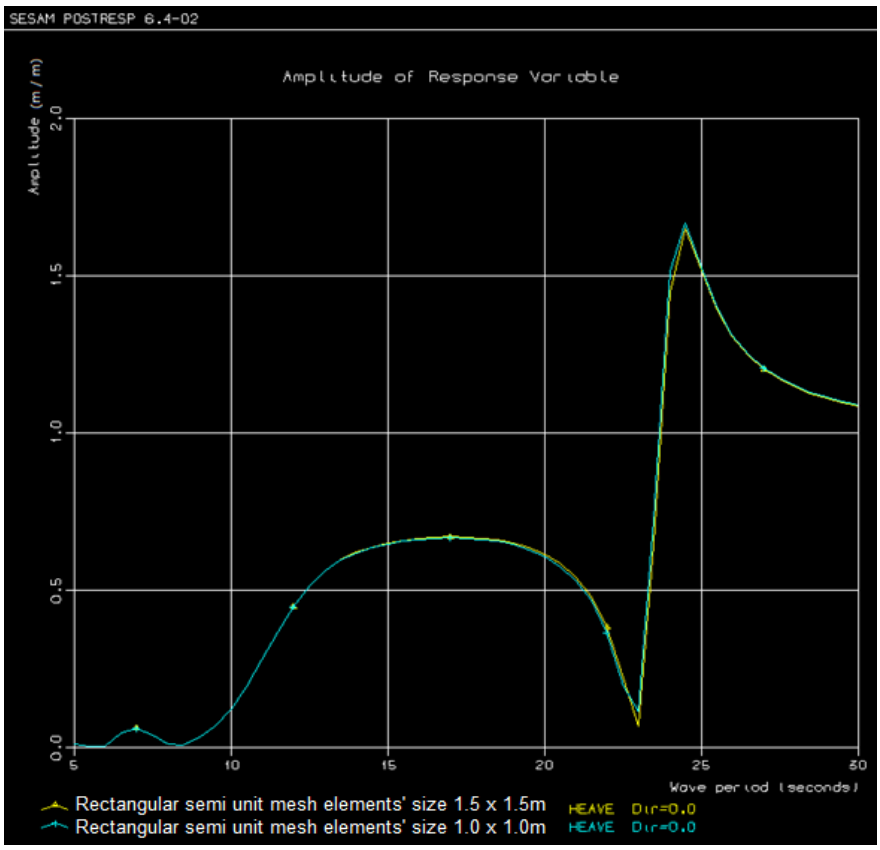

Figure 9.6 Rectangular column semi unit Heave RAO convergence, 0^{o} wave approach

Figures 9.7 shows the two pitch motion RAOs obtained by using the two panel mesh densities for the wave period interval considered and 0^{o} incident wave approach. The maximum values for both RAOs in the considered wave period interval are found at 11sec wave period . At this wave period, the higher value being the RAO given by the coarser mesh, there is a 99.79% convergence between the two values.The same applies to the pitch RAO values given by the two panel mesh densities for 45^{o} wave approach angle.

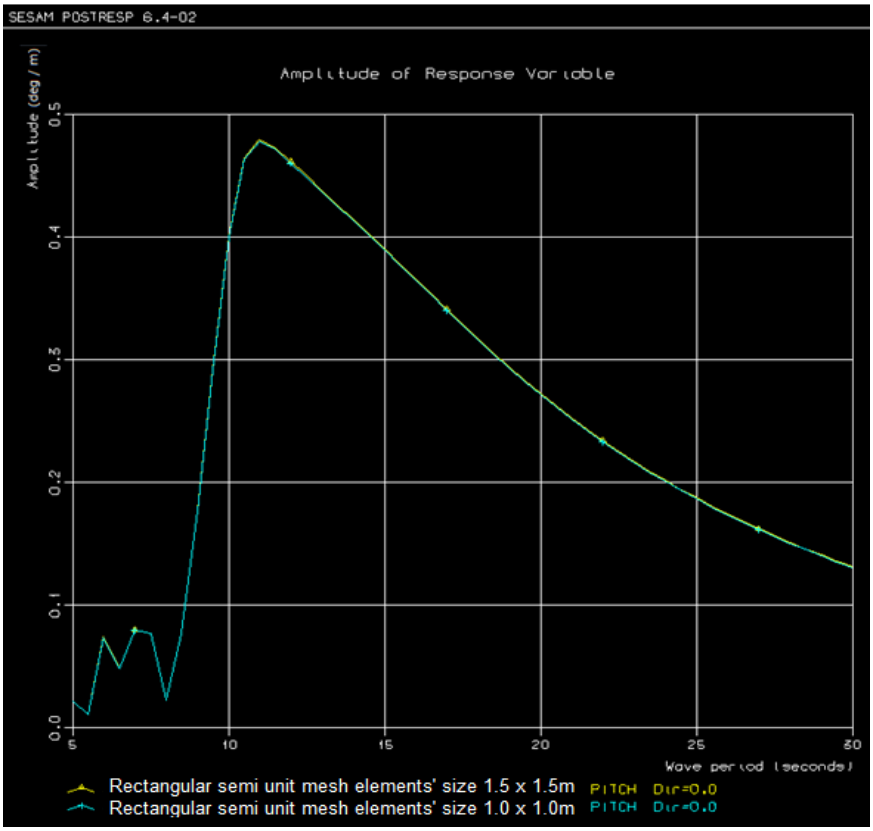

Figure 9.7 Rectangular column semi unit Pitch RAO mesh convergence, 0^{o} wave approach

Figures 9.8 shows the two surge motion RAOs obtained by using the two panel mesh densities for the wave period interval considered and 0^{o} incident wave approach. For this case there are two peak values in the wave period interval considered. The first peak is found at 8 sec wave period. At this wave period, the higher value being the RAO given by the coarser mesh, there is a 99.9% convergence. The second peak in the interval is found at 30sec wave period and for this case also, the higher value being the RAO given by the coarse mesh, there is a 99.9% convergence. The convergence ratio applies to the surge RAO values given by the two panel mesh densities for 45^{o} wave approach angle.

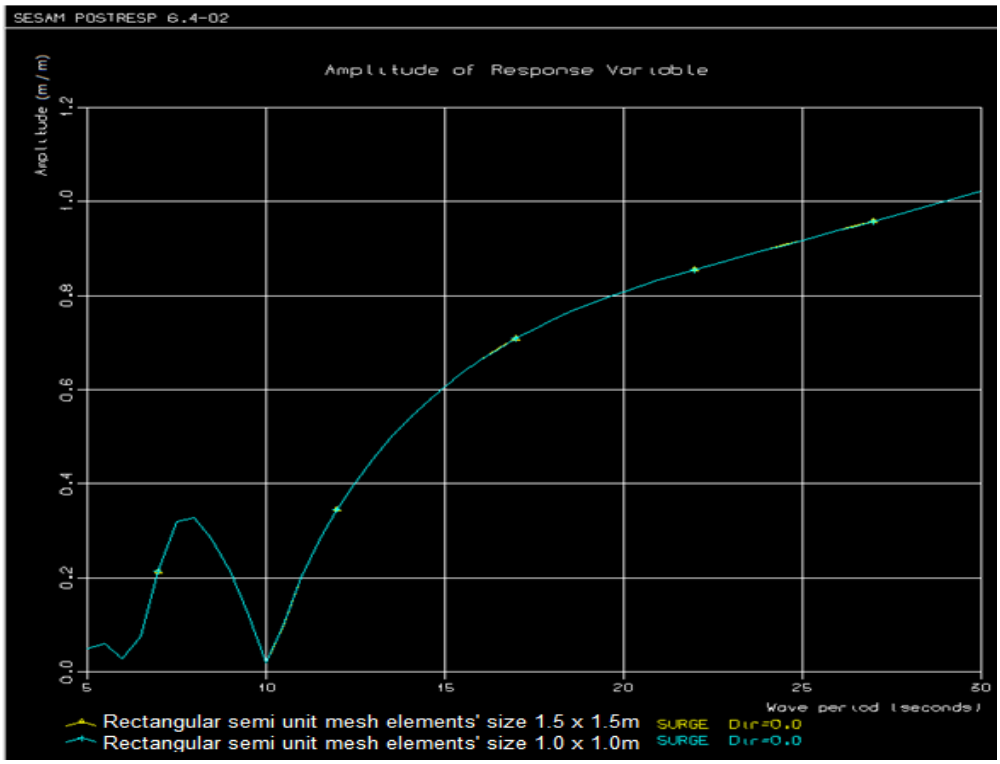

Figure 9.8 Rectangular column semi unit Surge RAO mesh convergence, 0^{o} wave approach

Figures 9.9 shows the two yaw motion RAOs obtained by using the two panel mesh densities for the wave period interval considered and 30^{o} incident wave approach. The maximum values for both RAOs in the considered wave period interval are found at 7.5sec wave period . At this wave period, the higher value being the RAO given by the coarser mesh, there is a 99.9% convergence between the two values.

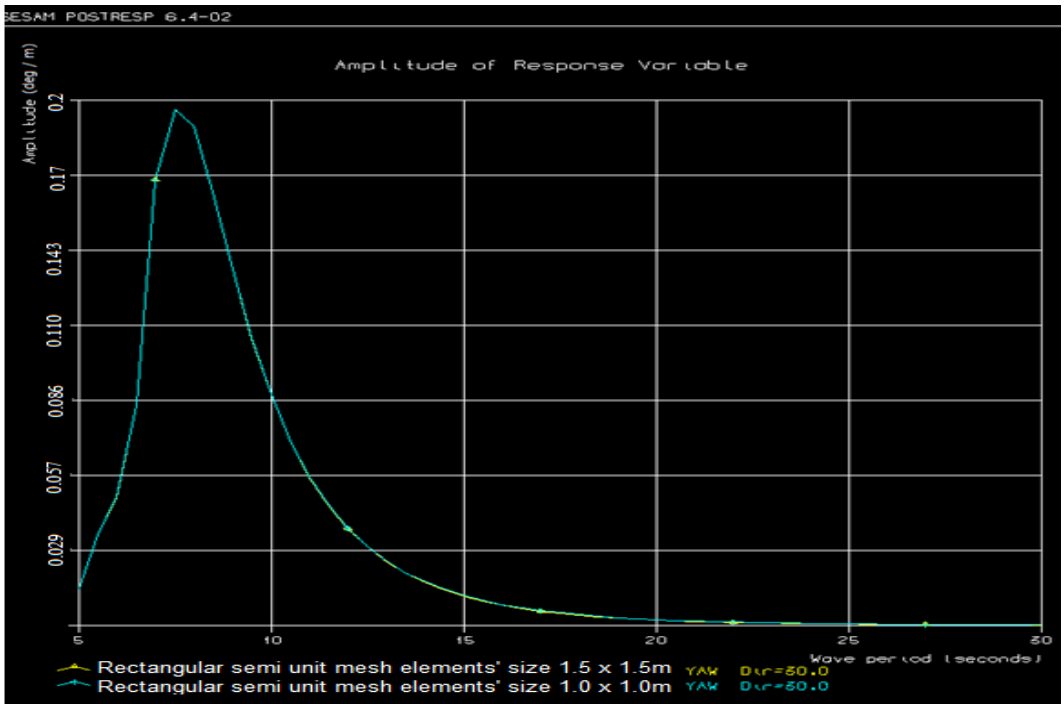

Figure 9.9 Rectangular column semi unit Yaw RAO mesh convergence, 0° wave approach

Circular column Semi Unit Convergence Results

In figures 9.10, 9.11and 9.12, motion RAOs for the circular column semi unit based on 1.5 x 1.5 m panel mesh density and 1.0 x 1.0 m panel mesh density are presented. Heave, pitch and surge RAOs for 0° wave approach and yaw RAOs for 30° wave approach are given in here. The maximum values of the RAOs obtained by the two panel mesh densities, in each mode of motion and wave period interval considered, are used as control values to determine convergence.

Figures 9.10 shows the heave and pitch motion RAOs obtained by using the two panel mesh densities, for the wave period interval considered and for 0° incident wave approach. The maximum values for the heave RAOs are found at resonance wave period, which is 24.5sec . At this wave period, the RAO given by the coarser mesh (i.e. 1.5m x 1.5m) overestimates the maximum value given by the finer mesh (i.e. 1.0m x 1.0m) by 1%, which indicates there is a 99% convergence at this location.

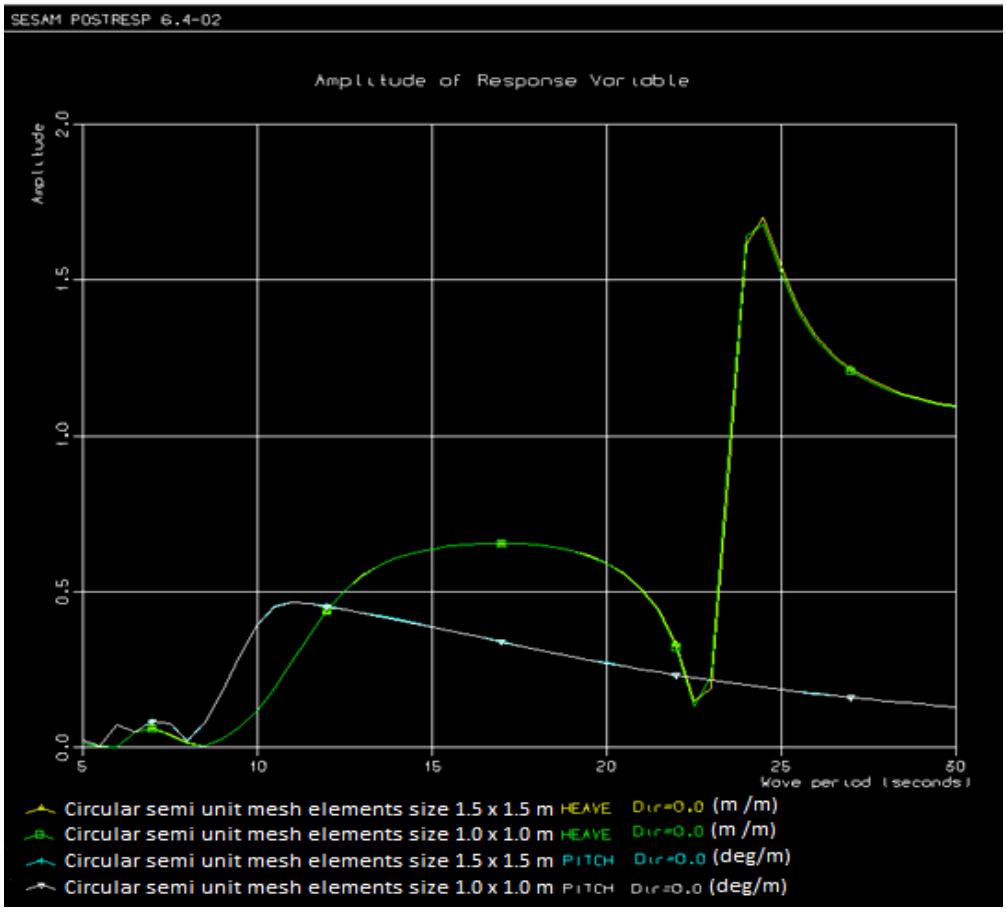

Figure 9.10 Circular column unit Heave and Pitch RAOs mesh convergence, 0° wave approach

Referring to figure 9.10 again, the two pitch motion RAOs obtained by using the two panel mesh densities for the wave period interval considered and 0^{o} incident wave approach are also presented. The maximum values for both RAOs in the considered wave period interval are found at 11sec wave period .At this wave period, the higher value being the RAO given by the coarser mesh, there is a 99.6% convergence between the two values. The same convergence ratio applies to both the heave RAO and the pitch RAO values given by the two panel mesh densities for 45^{o} wave approach angle.

Figures 9.11 shows the two surge motion RAOs obtained by using the two panel mesh densities for the wave period interval considered and 0^{o} incident wave approach. For this case there are two peak values in the wave period interval considered. The first peak is found at 8 sec wave period. At this wave period, the higher value being the RAO given by the coarser mesh, there is a 99.9% convergence. The second peak in the interval is found at 30sec wave period and for this case also, the higher value being the RAO given by the coarse mesh, there is a 100% convergence.

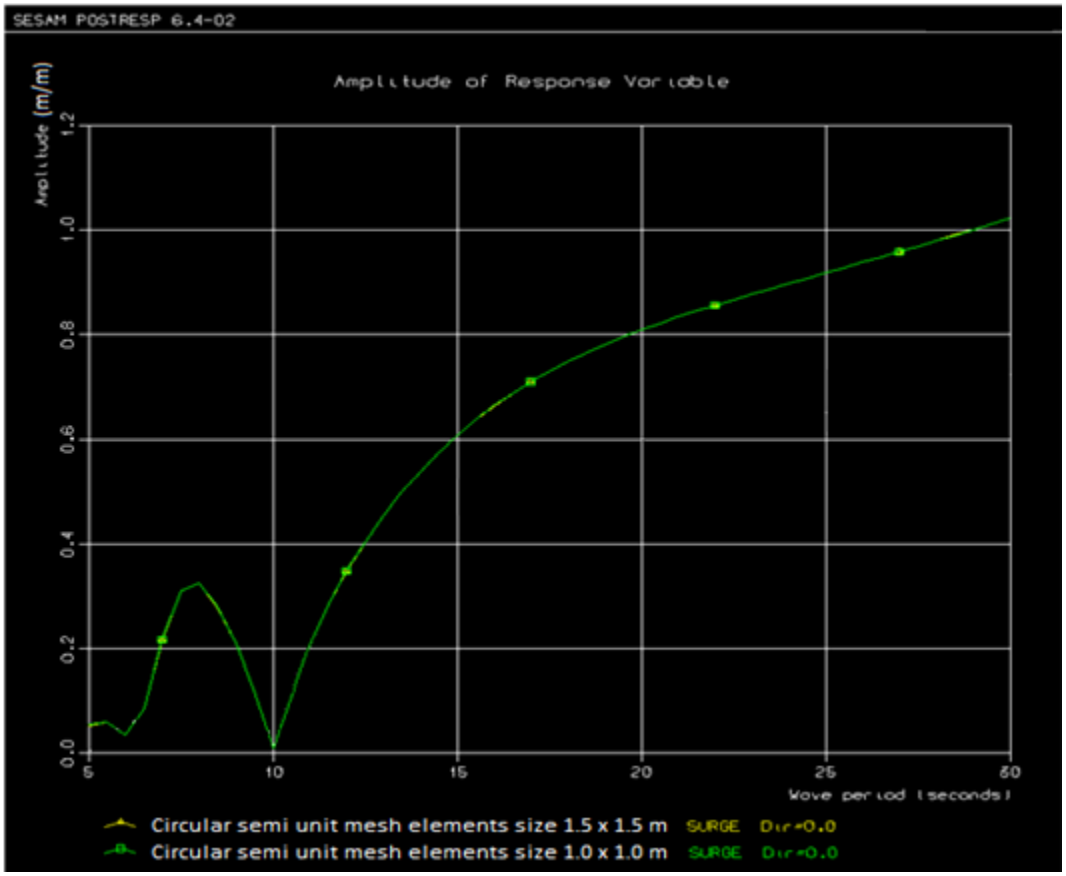

Figure 9.11 Circular column semi unit Surge RAO mesh convergence, 0^{o} wave approach

Figures 9.12 shows the two yaw motion RAOs obtained by using the two panel mesh densities for the wave period interval considered and 30^{o} incident wave approach. The maximum values for both RAOs in the considered wave period interval are found at 7.5sec wave period . At this wave period, the higher value being the RAO given by the finer mesh, there is a 99.95% convergence between the two values.

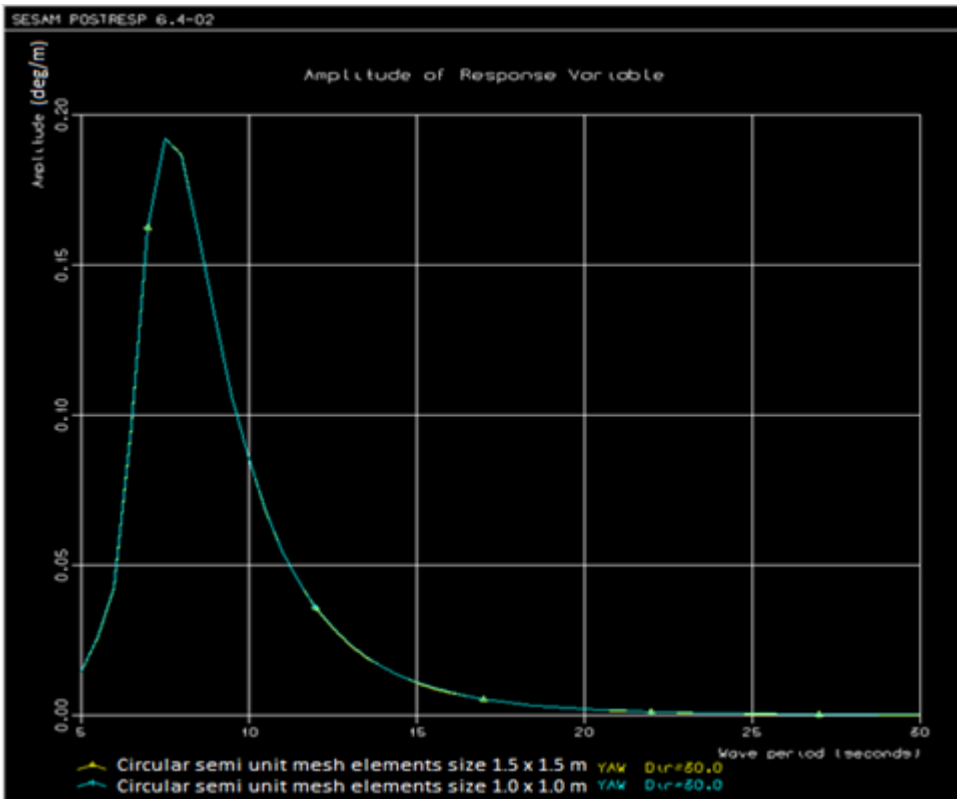

Figure 9.12 Circular semi unit Yaw RAO mesh convergence, 0^{o} wave approach

Mesh density selection

Comparing the two mesh densities both in the case of the rectangular column unit and the circular column unit, all RAOs in the considered modes of motion and wave period interval exhibit satisfactory convergence behavior not only for the control maximum values in the interval, but also for the other values as well, as the lines seem to be overlapping almost absolutely, in many of the cases.

Computational time required for the two mesh densities is presented in table 9.5. Comparing the computational time requirement for the two mesh densities, the time requirement for the denser panel mesh density is almost 20 times the requirement for the coarser panel mesh density, while the output is

reasonably comparable. For this reason, the RAOs for the two semisubmersible units will be compared based on a result obtained applying the panel mesh density of 1.5 x 1.5m.

It is assumed that the results obtained from the convergence tests, for wave period interval between 5sec-30sec, will also apply for a further wave period interval. For this reason, no convergence test is carried out for a further wave period interval that will be applied to compare the RAOs of the two units.

10. Comparison Procedures

Initially, a panel model representing the hull geometry of each unit (the rectangular and the circular column semisubmersible unit) is prepared in GeniE. Each panel model is then meshed based on the preferred mesh density. This gives the finite element model of the panel model (.FEM).

In HydroD, the (.FEM) file is imported. Then the following parameters are defined in HydroD:

- Wave periods for the hydrodynamic analysis (max 60 periods)
- Incident wave heading intervals for the hydrodynamic analysis
- Environment setting (water depth, water density and water viscosity)
- Flotation position in terms of draft depth
- Mass model; total mass is defined based on the buoyancy of the hull at flotation position, mass distribution is defined in terms of radius of gyration about X, Y and Z axes, COG(center of gravity) is defined based on minimum metacentric height (GM) requirement
- Off-body points at the chosen coordinates for air gap calculation
- Diagonal elements of critical damping ratio matrix for applied viscous simplification
- Second order mean drift force calculation based on conservation of momentum

10.1 Procedures for global motion response comparison

Postresp opens the global result interface file (G-file). Using Postresp:

- First order global motion transfer function (RAO), each in the desired degree of freedom and wave heading is displayed.
- A global RAO is selected (in a desired degree of freedom and wave heading).
- Torsethaugen spectrum is created based on a selected sea state from the ($q = 10^{-2}$) contour line, in the environmental contour plane shown in section 4.12.4, figure 4.2.
- A global motion response spectrum is created combining the selected global RAO with the created Torsethaugen spectrum
- ($q=10^{-2}$) annual probability global short term maximum response is obtained based on the created response spectrum, using a 3-hr Rayleigh distribution and a fractile ($\bar{\alpha} = 0.9$)
- Each obtained maximum global 3-hr (short term) response of ($q=10^{-2}$) annual probability of one semisubmersible unit, for a considered degree of freedom, wave heading and sea state is then compared with the respective value of the other semisubmersible unit.

The two units are symmetric with respect to XZ and YZ planes. For this reason heave and pitch are mentioned for vertical motions, while surge and yaw are mentioned for horizontal motion comparison.

10.2 Procedures for air gap comparison

Based on the global result interface file (G-file), the following procedures are followed for air gap calculation and comparison in Postresp.

- Specific point is created at a coordinate representing platform deck bottom, where air gap is to be investigated
- A motion response amplitude variable is created at this location, combining heave, roll and pitch RAOs , to obtain the motion RAO of the platform deck bottom
- The diffracted wave surface elevation RAO, which WADAM has already calculated is factored by $\propto = -1.2$, and is combined with (1xRAO) of platform deck bottom to give relative water surface elevation RAO. (Sesam Postresp recommends this sign convention for air gap calculation)
- Torsethaugen spectrum is created based on a selected sea state from the ($q = 10^{-2}$) contour line, in the environmental contour plane shown in section 4.12.4, figure 4.2.
- A relative water surface elevation spectrum is created combining the selected water surface elevation RAO with the created Torsethaugen spectrum

- ($q=10^{-2}$) annual probability maximum 3-hr (short term) relative water surface elevation is obtained based on the created response spectrum, using a 3-hr Rayleigh distribution and a fractile ($\bar{\alpha} = 0.9$)
- The obtained relative water surface elevation maximum response is subtracted from the static air gap to give the ($q=10^{-2}$) annual probability minimum short term air gap response
- Each obtained minimum short term air gap response of one semisubmersible unit, for a considered wave heading and sea state is then compared with the respective value of the other semisubmersible unit.

  The figure below describes the locations chosen for air gap investigation and the wave headings considered for each location. The black arrow stands for 0^o wave heading and numbers identifying the location printed in black correspond to locations investigated for 0^o wave heading. The red arrow stands for 45^o wave heading and numbers identifying the location printed in red correspond to locations investigated for 45^o wave heading.

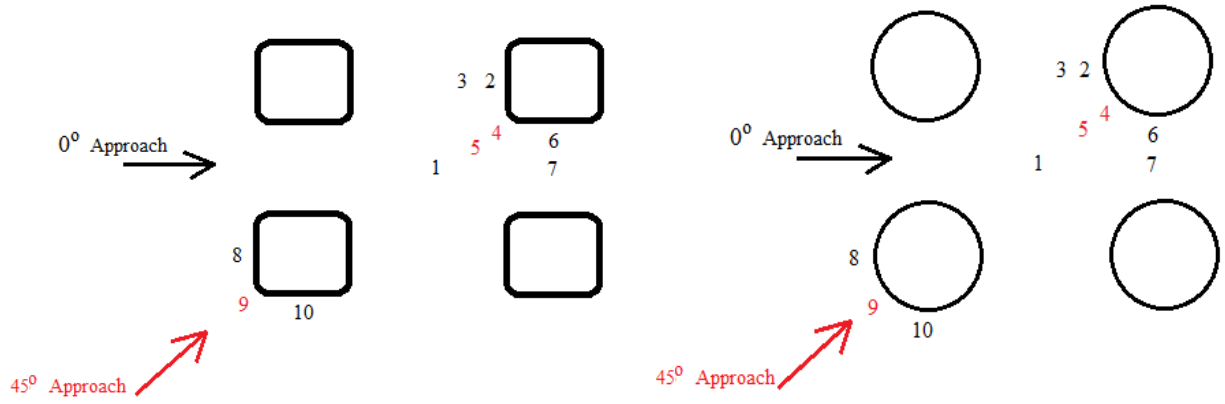

Figure 10.1 Locations and wave heading directions for air gap investigation

10.3 Procedures for slamming load comparison

Based on the global result interface file (G-file), the following procedures are followed to compute platform surge velocity in Postresp:

- A specific point is created at the origin with respect to the result coordinate system
- A surge velocity variable is created at the created point
- Torsethaugen spectrum is created based on a selected sea state from the ($q = 10^{-2}$) contour line, in the environmental contour plane shown in section 4.12.4, figure 4.2.

- A surge velocity spectrum is created by combining the surge velocity variable with the created wave spectrum, considering 0^{o} wave heading
- From the surge velocity spectrum, the standard deviation of surge motion is found as the square root of 0^{th} spectral moment.
- Phase speed of the worst ($q = 10^{-2}$) probability of breaking wave is combined with standard deviation of platform surge motion to calculate slamming impact load

10.4 Procedure for Second order horizontal mean drift forces/moment comparison

Based on the global result interface file (G-file),

- Postresp graphically presents second order horizontal mean drift forces/ moment per square of wave amplitude in wave frequency/period domain

11. Results and discussion

11.1 First order global motion transfer functions (RAOs) :Results

Results for first order global motion transfer functions are shown below.

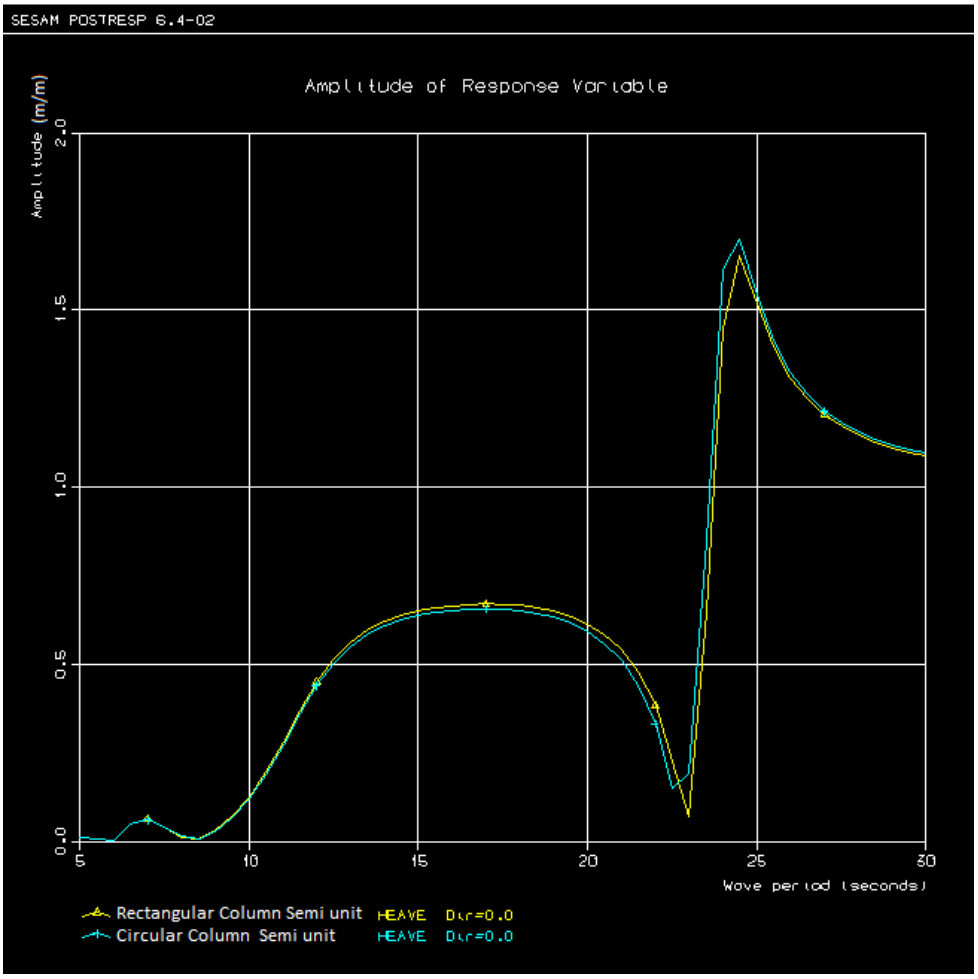

Figure 11.1 Heave motion RAO 0^{o} wave heading [5sec - 30sec]

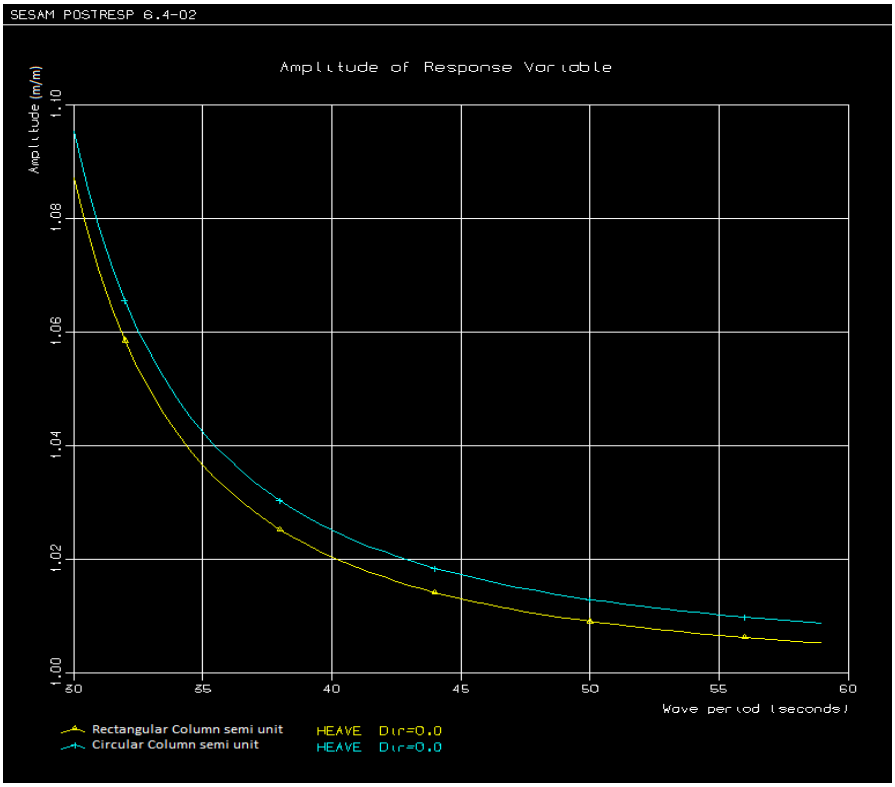

Figure 11.2 Heave motion RAO , 0^{o} wave heading [30sec - 59sec]

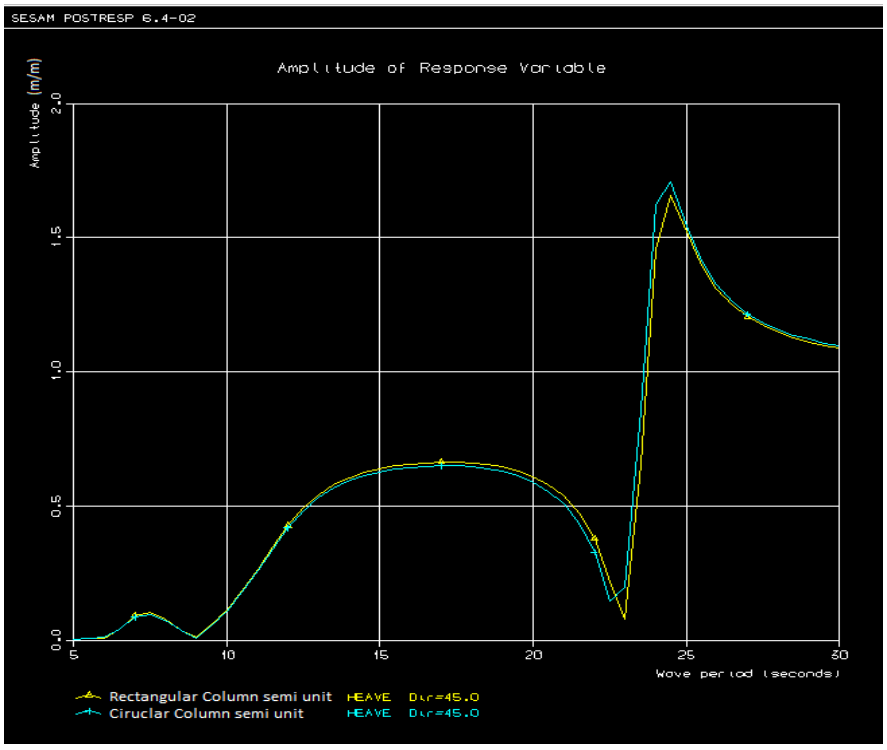

Figure 11.3 Heave motion RAO 45^{o} wave heading [5sec-30sec]

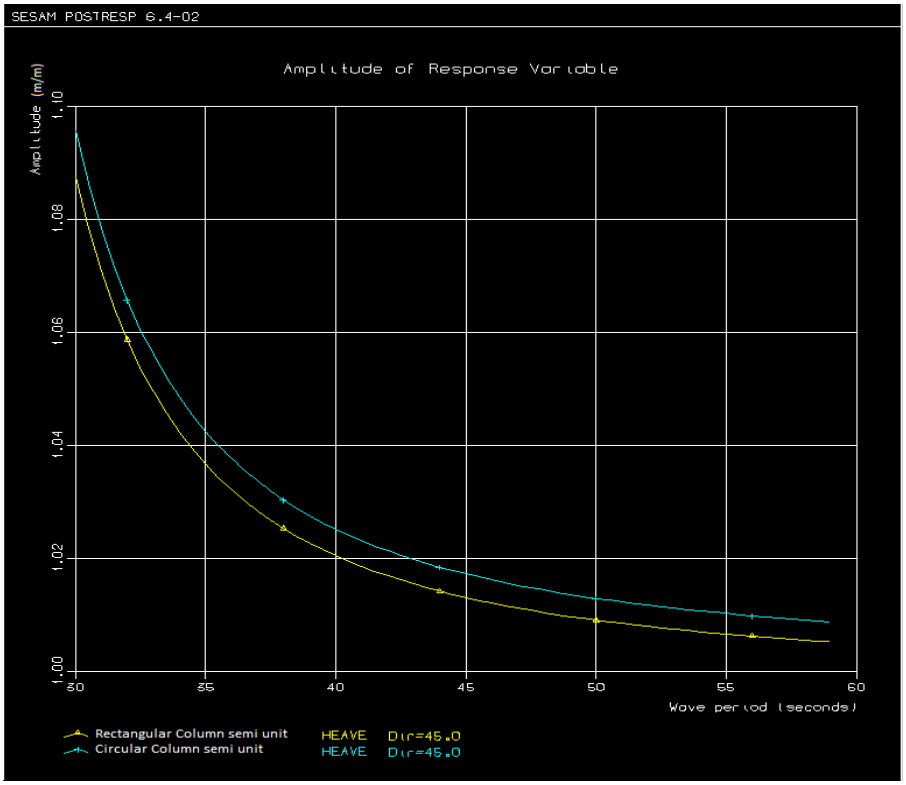

Figure 11.4 Heave motion RAO 45° wave heading [30-59sec]

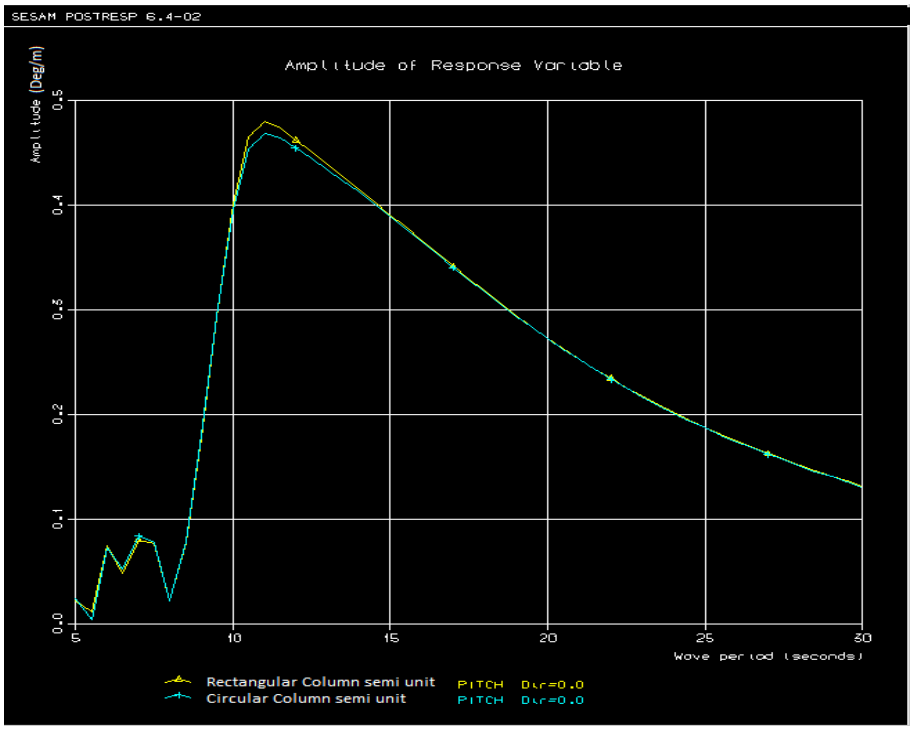

Figure 11.5 Pitch motion RAO 0° wave heading [5sec - 30sec]

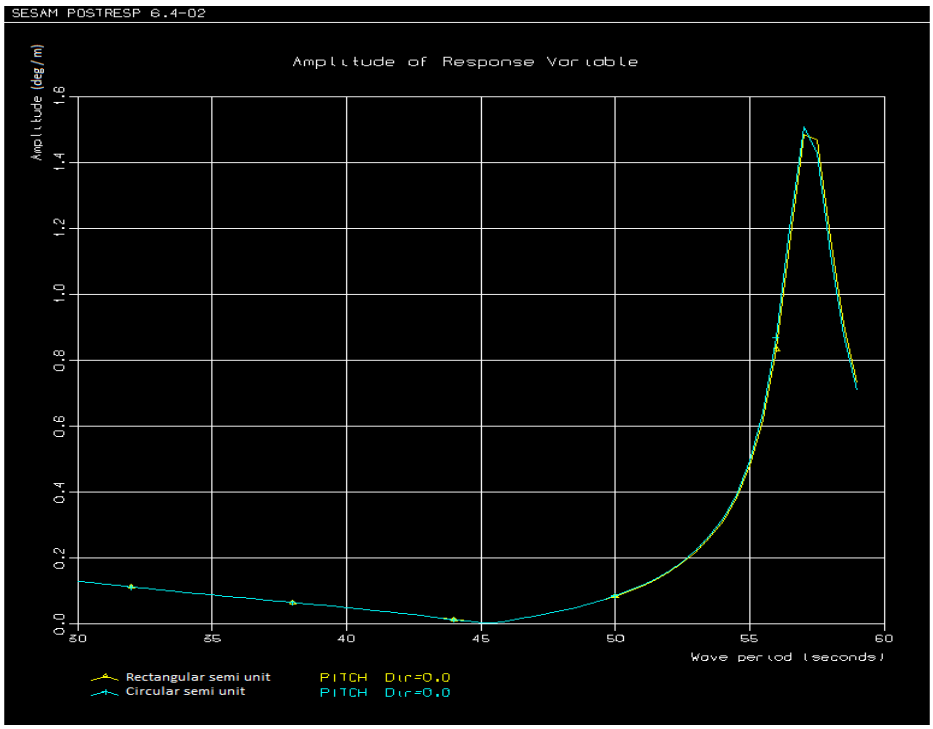

Figure 11.6 Pitch motion RAO 0^{o} wave heading [5-30sec]

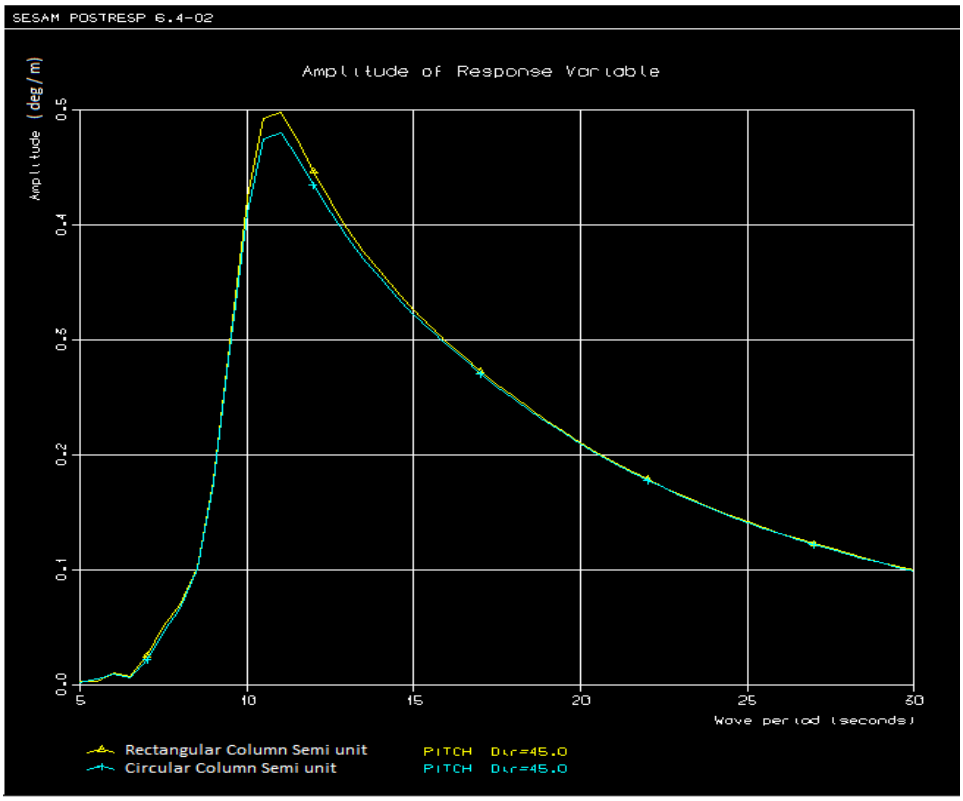

Figure 11.7 Pitch motion RAO 45^{o} wave heading [5sec - 30sec]

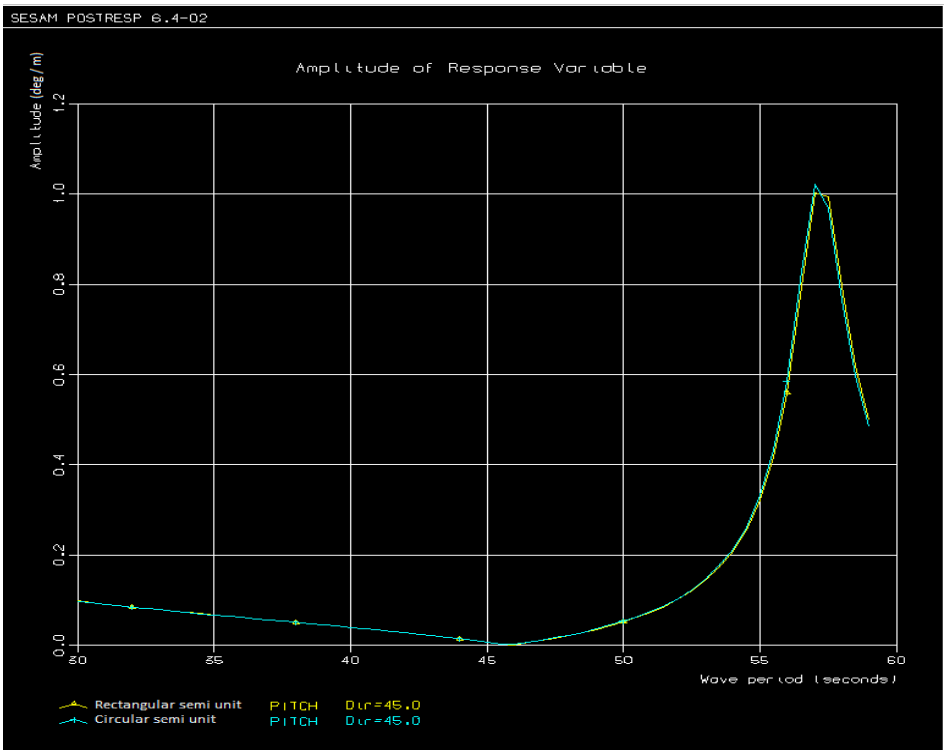

Figure 11.8 Pitch motion RAO 45° wave heading [30sec - 59sec]

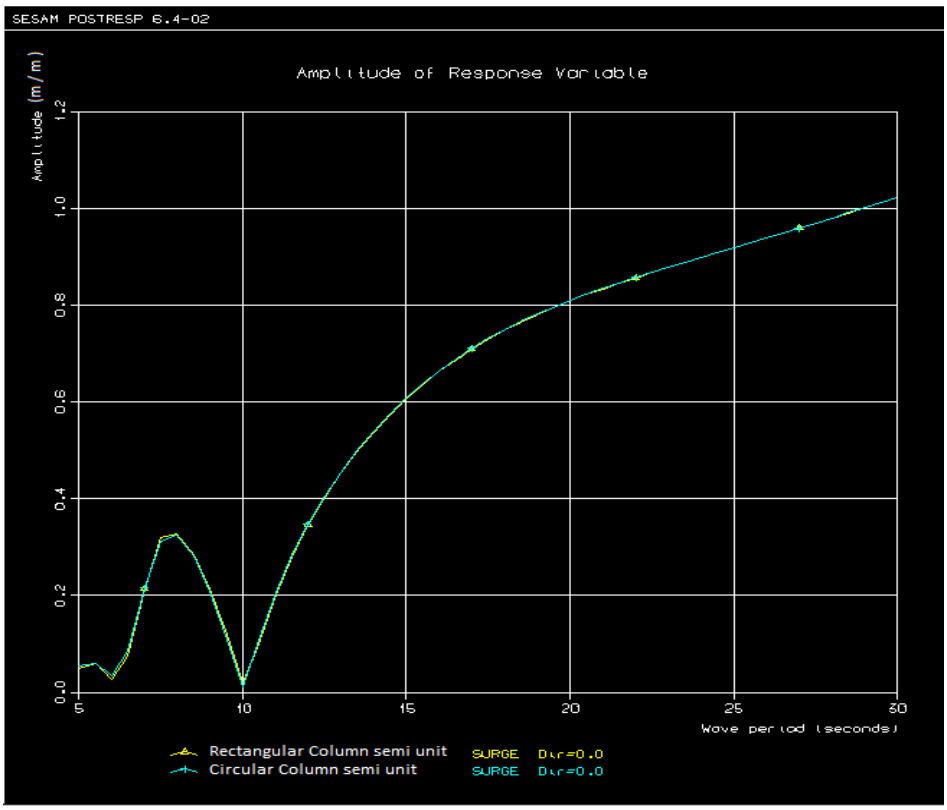

Figure 11.9 Surge motion RAO 0° wave heading [5sec - 30sec]

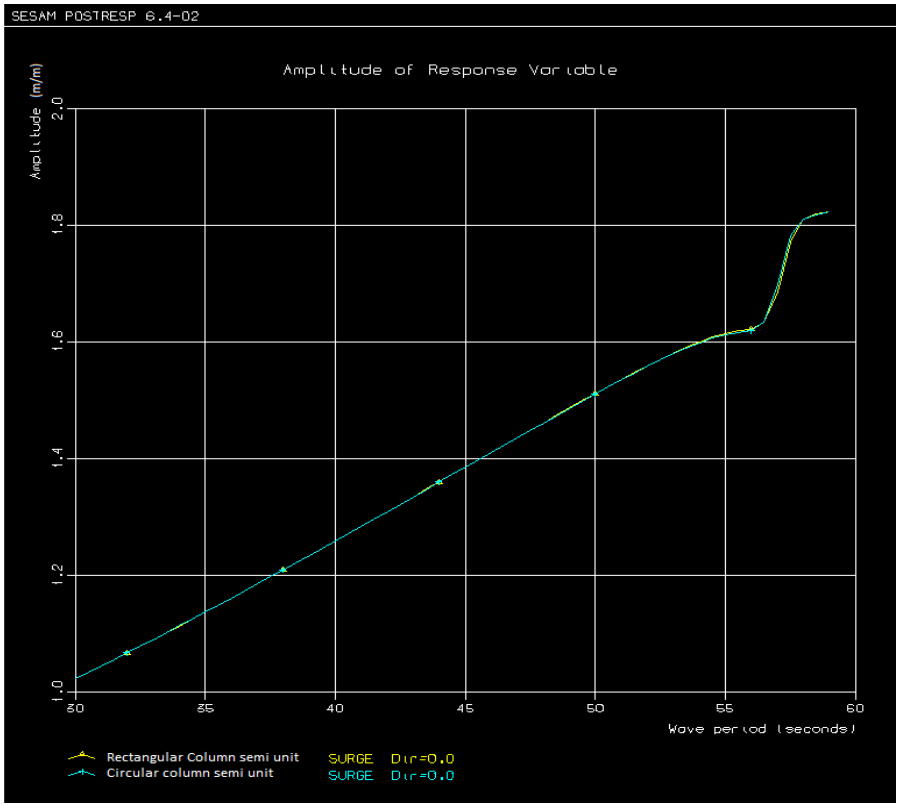

Figure 11.10 Surge motion RAO 0^{o} wave heading [30sec - 59sec]

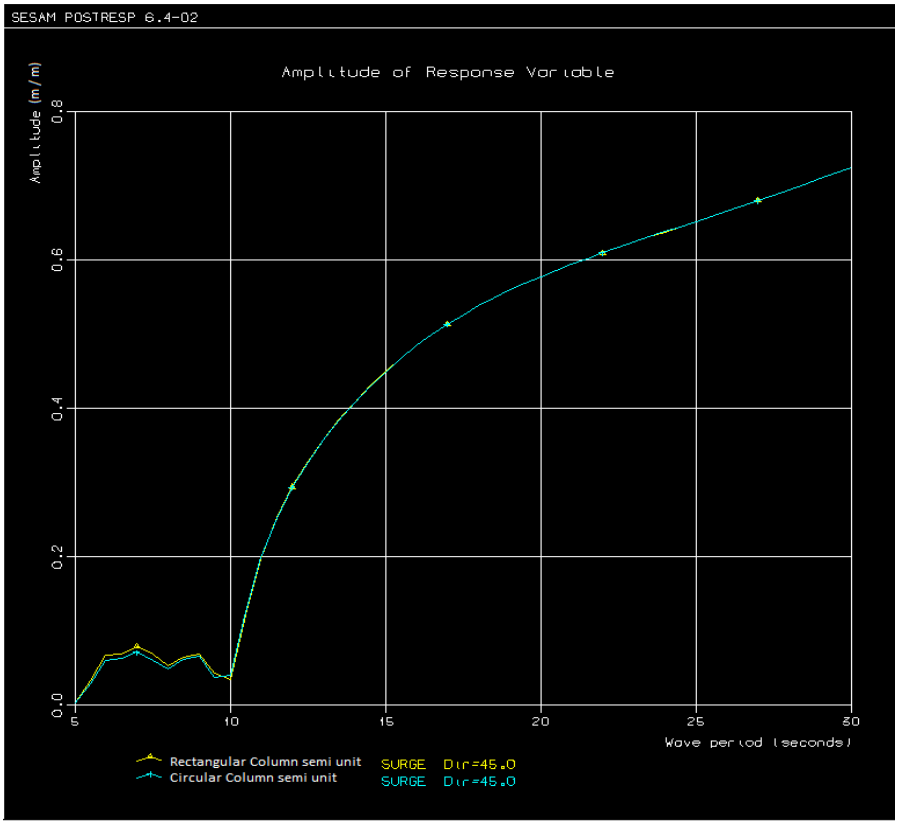

Figure 11.11 Surge motion RAO 45^{o} wave heading [5sec - 30sec]

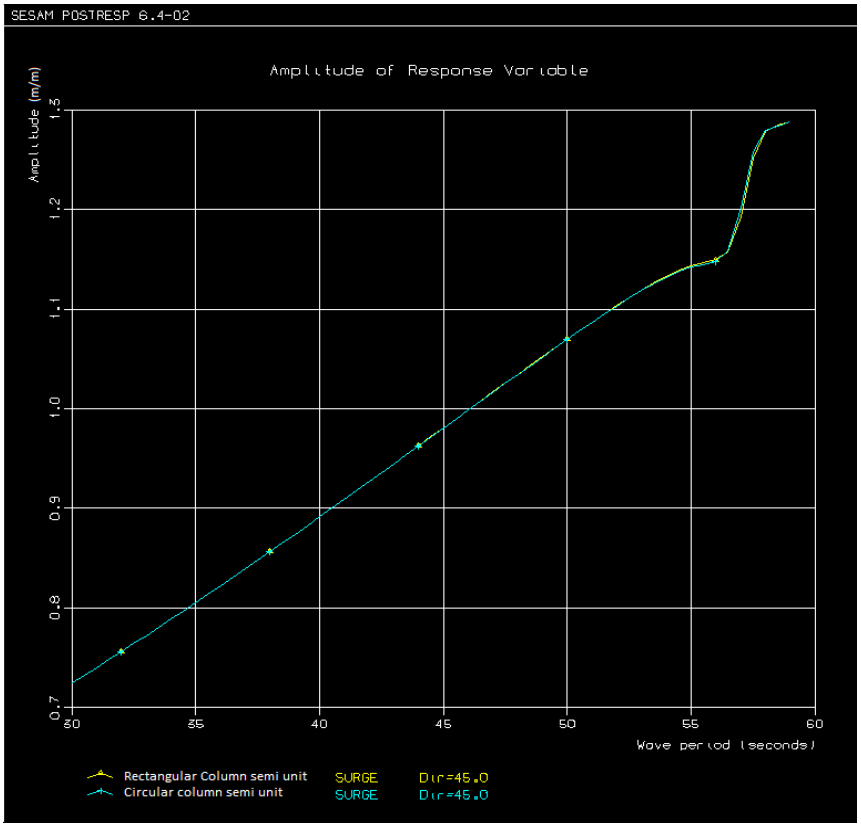

Figure 11.12 Surge motion RAO 45° wave heading [30sec - 59sec]

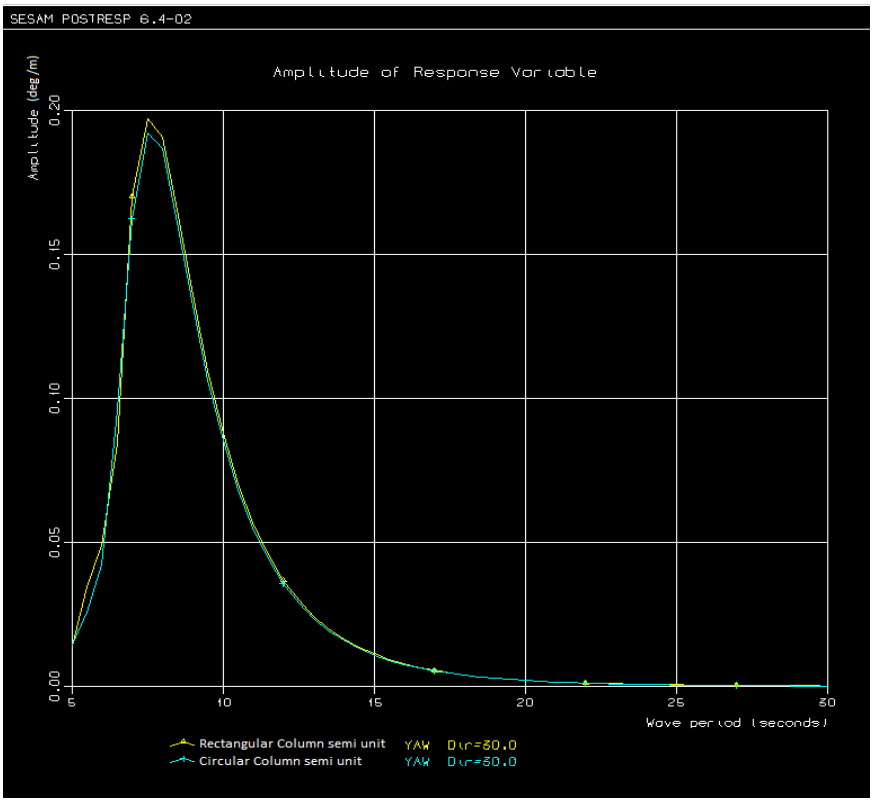

Figure 11.13 Yaw motion RAO 30° wave heading [5sec - 30sec]

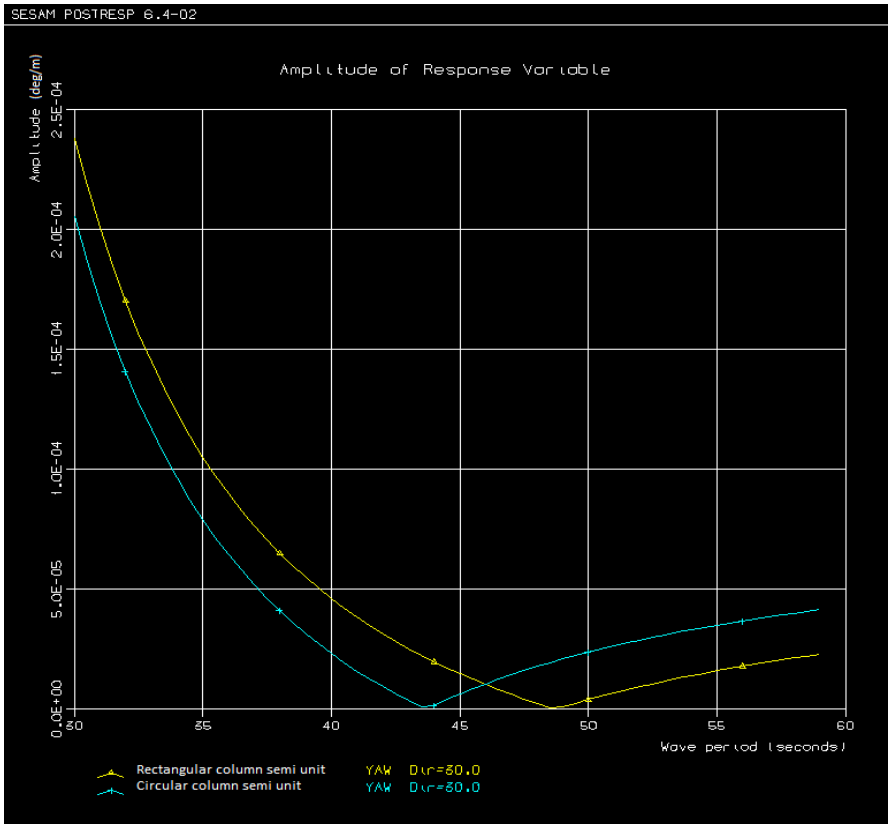

Figure 11.14 Yaw motion RAO 30^{o} wave heading [30sec - 59sec]

In figures 11.1 to figure 11.14, first order global motion transfer functions (RAOs) of the two semisubmersible units are presented.

11.2 First order global motion transfer functions (RAOs) :Discussion

Figures 11.1 and 11.2 show the heave RAOs of the two units for wave intervals 5sec-30sec and 30-59 respectively, considering 0^{o} wave heading. From the figure, it can be seen that both units have similar heave resonance period, which is 24.5sec. From 5sec to 23sec wave period interval, the rectangular column unit exhibits marginally higher RAO values, the highest RAO being 14% higher than the value of the circular column unit at wave period of 22sec.

From 23sec wave period on , the circular column unit seems to reach cancellation point, earlier and rises up quicker than the rectangular column unit's RAO. The global maximum difference between the two units' RAOs occur at a wave period of 23sec and their difference is 63%. However, at this point the RAO itself has already a small value due to hydrodynamic load cancellation effect at this wave period, since the difference it can create on the response level is taken to be insignificant. For the further

wave period interval, i.e . from 24.5sec to its continuation in figure 11.2, even though the graph obtained from Postresp makes the differences seem magnified, by looking closer one can see the difference between the RAO values is only to the second decimal level. The RAO values seem to converge and eventually attain a 99.8% match. Figures 10.3 and 10.4 show the heave RAOs of the two units for wave period intervals 5sec-30sec and 30-59 respectively, considering for 45^{o} wave heading. Apart from the small heave RAO magnitude reduction for both units, the same ratio is maintained between the two units' RAOs as the 0^{o} wave heading case.

Figures 11.5 and 11.6 show the pitch RAOs of the two units for wave period intervals 5sec-30sec and 30-59 respectively , considering 0^{o} wave heading. Generally , a 99.9 % similarity is observed for the entire wave period interval except for the vary small variations in between 10 to 13sec wave periods. But these variations are marginal and are insignificant, as their maximum difference is only 2.28%, the higher RAO value corresponding to the rectangular column unit's RAO. Similarly, looking at figure 10.6 , the pitch RAOs look well in line and are very similar. The pitch resonance wave period for both units is also similar, which is at 57 seconds. Also looking at figures 11.7 and 11.8, the pitch RAOs for the two units for, 45^{o} wave heading is shown, in this case also ,no significant difference in magnitude is observed.

In figures 10.9 and 10.10 , the surge RAOs of the two units for wave period intervals 5sec-30sec and 30-59 respectively and considering 0^{o} wave heading are shown. In this case also, no significant difference between the surge RAO values of the two units is seen. This also goes for the surge RAO's of the two units for 45^{o} wave heading as well. These RAOs are shown in figures 11.11 and 11.12. Since both units are unmoored units, there exists no resonance period in surge, due to the absence a restoring force in the lateral directions.

In figures 11.13 and 11.14 , the yaw RAOs of the two units for wave period intervals 5sec-30sec and 30-59 respectively and considering 30^{o} wave heading are shown. As can be seen, in this case also the two RAOs look almost similar. only a limited difference between the two RAO values seems to be spotted around the peak values of the two RAOs in the considered interval, which is in between 7-9sec wave periods exists. In between this wave periods, the yaw motion RAO value of the rectangular column unit has 5% more magnitude than the circular column unit's yaw motion RAO. But considering how small the magnitude of the rectangular yaw RAO itself is, the difference between the two is not something to be seen more than a marginal value. For the second interval considered, which is shown in figure 11.14, the difference between the two units' yaw RAOs narrows down to the fifth decimal place per meter of wave height considered. It can be said that there their difference is technically negligible.

11.3 Maximum global 3-hr responses (100 year return period) :Results

Selected 3-hour sea states from 100 year contour map	Spectral Peak period [s]	Significant wave height [m]	Rectangular column response (90% fractile) [m]	Circular column response (90% fractile) [m]	Circular unit's Response in terms of Rectangular units response percentage
1	10	10	3.76	3.68	97.87%
2	12	12.3	5.62	5.51	98.04%
3	14	14	7.56	7.41	98.02%
4	16	14.9	8.78	8.61	98.06%
5	18	13.5	7.76	7.62	98.20%
6	20	8	4.19	4.12	98.33%

Table 11.1 Maximum heave 3-hr responses for 0^{o} degree wave heading

Selected 3-hour sea states from 100 year contour map	Spectral Peak period [s]	Significant wave height [m]	Rectangular column response (90% fractile) [m]	Circular column response (90% fractile) [m]	Circular unit's Response in terms of Rectangular units response percentage
1	10	10	3.68	3.61	98.10%
2	12	12.3	5.47	5.38	98.35%
3	14	14	7.38	7.25	98.24%
4	16	14.9	8.63	8.46	98.03%
5	18	13.5	7.65	7.52	98.30%
6	20	8	4.13	4.06	98.31%

Table 11.2 Maximum heave 3-hr responses for 45^{o} degree wave heading

Selected 3-hour sea states from 100 year contour map	Spectral Peak period [s]	Significant wave height [m]	Rectangular column response (90% fractile) [deg]	Circular column response (90% fractile) [deg]	Circular unit's Response in terms of Rectangular units response percentage
1	10	10	3.545	3.502	98.79%
2	12	12.3	4.946	4.880	98.67%
3	14	14	5.670	5.612	98.98%
4	16	14.9	5.816	5.764	99.11%
5	18	13.5	4.942	4.899	99.13%
6	20	8	2.871	2.841	98.96%

Table 11.3 Maximum pitch 3-hr responses for 0^{o} degree wave heading

Selected 3-hour sea states from 100 year contour map	Spectral Peak period [s]	Significant wave height [m]	Rectangular column response (90% fractile) [deg]	Circular column response (90% fractile) [deg]	Circular unit's Response in terms of Rectangular units response percentage
1	10	10	3.453	3.363	97.39%
2	12	12.3	4.735	4.613	97.42%
3	14	14	5.204	5.092	97.85%
4	16	14.9	5.177	5.079	98.11%
5	18	13.5	4.427	4.340	98.03%
6	20	8	2.645	2.586	97.77%

Table 11.4 Maximum pitch 3-hr responses for 45^{o} degree wave heading

Selected 3-hour sea states from 100 year contour map	Spectral Peak period [s]	Significant wave height [m]	Rectangular column response (90% fractile) [m]	Circular column response (90% fractile) [m]	Circular unit's Response in terms of Rectangular units response percentage
1	10	10	3.93	3.93	100.00%
2	12	12.3	5.38	5.40	100.37%
3	14	14	7.12	7.14	100.28%
4	16	14.9	8.85	8.87	100.23%
5	18	13.5	8.26	8.27	100.12%
6	20	8	4.58	4.58	100.00%

Table 11.5 Maximum surge 3-hr responses for 0^{o} degree wave heading

Selected 3-hour sea states from 100 year contour map	Spectral Peak period [s]	Significant wave height [m]	Rectangular column response (90% fractile) [m]	Circular column response (90% fractile) [m]	Circular unit's Response in terms of Rectangular units response percentage
1	10	10	2.77	2.77	100.00%
2	12	12.3	4.00	3.99	99.75%
3	14	14	5.29	5.29	100.00%
4	16	14.9	6.49	6.49	100.00%
5	18	13.5	5.98	5.98	100.00%
6	20	8	3.30	3.30	100.00%

Table 11.6 Maximum surge 3-hr responses for 45^{o} degree wave heading

Selected 3-hour sea states from 100 year contour map	Spectral Peak period [s]	Significant wave height [m]	Rectangular column response (90% fractile) [deg.]	Circular column response (90% fractile) [deg.]	Circular unit's Response in terms of Rectangular units response percentage
1	10	10	1.074	1.047	97.49%
2	12	12.3	1.067	1.040	97.47%
3	14	14	1.007	0.981	97.42%
4	16	14.9	0.884	0.861	97.40%
5	18	13.5	0.925	0.902	97.51%
6	20	8	0.647	0.631	97.53%

Table 11.7 Maximum yaw 3-hr responses for 30^{o} degree wave heading

11.4 Maximum global 3-hr responses (100 year return period) :Discussion

In tables 11.1 to 11.6, results for the maximum global 3-hr (short term), 90% fractile responses considering a 100 year return period ($q = 10^{-2}$) annual probability of exceedance are presented.

Looking at table 11.1, the global maximum 3-hr, 90% fractile heave motion responses for the two semisubmersible units, for 0^{o} wave heading are presented for six selected sea states from the environmental contour line presented in section 4. Looking at the results, it is seen that the circular column units' heave responses are nearly 2% lower than the heave responses of the rectangular column units, for all the sea states considered. The marginal difference that was observed in the heave RAOs of the two units are reflected in the 100 year storm situation too. Table 10.2 shows the maximum 3-hr heave responses but for 45^{o}. In this case, the individual response levels are a only a little bit lower than the 0^{o} wave heading situation but as can be seen from the fraction percentages of each unit's responses, a more or less similar ratio is observed.

In table 11.3, the global maximum 3-hr, 90% fractile pitch motion responses of the two units are presented for 0^{o} wave heading and also for the selected different sea state. Not much variation is observed. It is also seen that the already marginal differences diminish for the case of the worst sea

state. In the case of the 3-hr maximum pitch response for 45° wave heading which is shown in table 11.4, except from the individual values being slightly lower than the 0° wave heading case, the difference between the responses of the two units is also in this case marginal, the smaller response belonging to the circular column unit. This is reasoned to the similarity of the pitch motion RAOs that have been presented in section 11.1.

In table 11.5, the global maximum 3-hr, 90% fractile surge motion responses of the two units are presented for 0° wave heading and also for the selected different sea state. For the sea states with relatively lower energy, they surge responses are surprisingly similar. But for the rest of the sea states with relatively higher energy, there is a slight difference in the responses, the higher responses in this case belonging to the circular column unit. For the 45° wave heading case, which is shown in table 10.6, in almost all the cases they surge responses of the two units exhibit similar surge response behavior.

The maximum 3-hr, 90% fractile yaw motion responses of the two units for 30° wave heading is present in table 11.7. Small differences are observed in this case also. The yaw responses of the rectangular column unit seem to be persistently nearly 2.5% higher than the circular unit's responses. But looking at the responses themselves, this small percentage for a response that has already a small magnitude might be regarded as insignificant.

11.5 100 year return period Minimum 3-hr air gap : Results

Selected 3- hour sea states from 100 year contour map	Spectral Peak period [s]	Significant wave height [m]	Rectangular column maximum relative wave surface elevation [90%]fractile	Circular column maximum relative wave crest elevation [90%]fractile [m]	Minimum Air gap Rectangular column semi [m]	Minimum Air gap Circular column semi [m]
1	10	10	10.00	10.11	12.00	11.89
2	12	12.3	12.50	12.66	9.50	9.34

3	14	14	13.47	13.65	8.53	8.35
4	16	14.9	13.31	13.52	8.69	8.48
5	18	13.5	12.17	12.37	9.83	9.63
6	20	8	7.70	7.82	14.30	14.18

Table 11.8 Air gap for Location 1, 0^o wave heading

Selected 3- hour sea states from 100 year contour map	Spectral Peak period [s]	Significant wave height [m]	Rectangular column maximum relative wave surface elevation [90%]fractile	Circular column maximum relative wave crest elevation [90%]fractile [m]	Minimum Air gap Rectangular column semi [m]	Minimum Air gap Circular column semi [m]
1	10	10	19.93	18.74	2.07	3.26
2	12	12.3	21.89	20.77	0.11	1.23
3	14	14	21.73	20.77	0.27	1.23
4	16	14.9	20.28	19.52	1.72	2.48
5	18	13.5	19.62	18.76	2.38	3.24
6	20	8	13.08	12.42	8.92	9.58

Table 11.9 Air gap for Location 2, 0^o wave heading

Selected 3- hour sea states from 100 year contour map	Spectral Peak period [s]	Significant wave height [m]	Rectangular column maximum relative wave surface elevation [90%]fractile	Circular column maximum relative wave crest elevation [90%]fractile [m]	Minimum Air gap Rectangular column semi [m]	Minimum Air gap Circular column semi [m]
1	10	10	18.80	17.78	3.20	4.22
2	12	12.3	20.93	19.97	1.07	2.03
3	14	14	20.91	20.10	1.09	1.90
4	16	14.9	19.61	18.98	2.39	3.02
5	18	13.5	18.80	18.08	3.20	3.92
6	20	8	12.42	11.87	9.58	10.13

Table 11.10 Air gap for Location 3, 0^{o} wave heading

Selected 3- hour sea states from 100 year contour map	Spectral Peak period [s]	Significant wave height [m]	Rectangular column maximum relative wave surface elevation [90%]fractile	Circular column maximum relative wave crest elevation [90%]fractile [m]	Minimum Air gap Rectangular column semi [m]	Minimum Air gap Circular column semi [m]
1	10	10	16.47	17.77	5.53	4.23
2	12	12.3	19.06	20.12	2.94	1.88
3	14	14	19.26	20.20	2.74	1.80
4	16	14.9	18.32	19.11	3.68	2.89

5	18	13.5	17.16	18.13	4.84	3.87
6	20	8	11.14	11.89	10.86	10.11

Table 11.11 Air gap for Location 4, 45^{o} wave heading

Selected 3- hour sea states from 100 year contour map	Spectral Peak period [s]	Significant wave height [m]	Rectangular column maximum relative wave surface elevation [90%]fractile	Circular column maximum relative wave crest elevation [90%]fractile [m]	Minimum Air gap Rectangular column semi [m]	Minimum Air gap Circular column semi [m]
1	10	10	14.86	15.97	7.14	6.03
2	12	12.3	17.71	18.62	4.29	3.38
3	14	14	18.07	18.90	3.93	3.10
4	16	14.9	17.33	18.04	4.67	3.96
5	18	13.5	16.01	16.84	5.99	5.16
6	20	8	10.27	10.90	11.73	11.10

Table 11.12 Air gap for Location 5, 45^{o} wave heading

Selected 3- hour sea states from 100 year contour map	Spectral Peak period [s]	Significant wave height [m]	Rectangular column maximum relative wave surface elevation [90%]fractile	Circular column maximum relative wave crest elevation [90%]fractile [m]	Minimum Air gap Rectangular column semi [m]	Minimum Air gap Circular column semi [m]
1	10	10	12.04	11.87	9.96	10.13
2	12	12.3	13.88	13.7	8.12	8.3
3	14	14	14.34	14.2	7.66	7.8
4	16	14.9	13.97	13.89	8.03	8.11
5	18	13.5	13.15	13.1	8.85	8.9
6	20	8	8.51	8.45	13.49	13.55

Table 11.13 Air gap for Location 6, 0^{o} wave heading

Selected 3-hour sea states from 100 year contour map	Spectral Peak period [s]	Significant wave height [m]	Rectangular column maximum relative wave surface elevation [90%]fractile	Circular column maximum relative wave crest elevation [90%]fractile [m]	Minimum Air gap Rectangular column semi [m]	Minimum Air gap Circular column semi [m]
1	10	10	11.52	11.56	10.48	10.44
2	12	12.3	13.54	13.55	8.46	8.45
3	14	14	14.11	14.13	7.89	7.87
4	16	14.9	13.82	13.87	8.18	8.13
5	18	13.5	12.88	12.96	9.12	9.04

6	20	8	8.24	8.29	13.77	13.71

Table 11.14 Air gap for Location 7, 0° wave heading

Selected 3-hour sea states from 100 year contour map	Spectral Peak period [s]	Significant wave height [m]	Rectangular column maximum relative wave surface elevation [90%]fractile	Circular column maximum relative wave crest elevation [90%]fractile [m]	Minimum Air gap Rectangular column semi [m]	Minimum Air gap Circular column semi [m]
1	10	10	17.1	16.06	4.9	5.94
2	12	12.3	19.8	18.93	2.2	3.07
3	14	14	19.1	18.38	2.9	3.62
4	16	14.9	17.28	16.74	4.72	5.26
5	18	13.5	16.69	16.01	5.31	5.99
6	20	8	11.33	10.76	10.67	11.24

Table 11.15 Air gap for Location 8, 0° wave heading

Selected 3- hour sea states from 100 year contour map	Spectral Peak period [s]	Significant wave height [m]	Rectangular column maximum relative wave surface elevation [90%]fractile	Circular column maximum relative wave crest elevation [90%]fractile [m]	Minimum Air gap Rectangular column semi [m]	Minimum Air gap Circular column semi [m]
1	10	10	21.06	21.07	0.94	0.93
2	12	12.3	22.30	22.24	-0.30	-0.24
3	14	14	22.17	21.99	-0.17	0.01
4	16	14.9	20.11	19.91	1.89	2.09
5	18	13.5	19.20	19.17	2.80	2.83
6	20	8	12.86	12.92	9.14	9.08

Table 11.16 Air gap for Location 9, 45^{o} wave heading

Selected 3- hour sea states from 100 year contour map	Spectral Peak period [s]	Significant wave height [m]	Rectangular column maximum relative wave surface elevation [90%]fractile	Circular column maximum relative wave crest elevation [90%]fractile [m]	Minimum Air gap Rectangular column semi [m]	Minimum Air gap Circular column semi [m]
1	10	10	12.37	11.86	9.63	10.14
2	12	12.3	13.11	12.71	8.89	9.29
3	14	14	13.04	12.70	8.96	9.30

4	16	14.9	12.29	12.07	9.71	9.93
5	18	13.5	12.24	11.97	9.76	10.03
6	20	8	8.22	8.00	13.78	14.00

Table 11.17 Air gap for Location 10, 0^o wave heading

11.6 100 year return period Minimum 3-hr air gap : Discussion

Tables 11.8 to 11.17 show the ten different locations along their respective wave headings considered for air gap investigation under the deck of the two units.

Table 11.8 shows the 100 year return period minimum 3-hr air gap at location 1 for 0^o wave heading. The minimum air gap values under the deck of the rectangular column unit show marginally higher figures for all the sea states considered. As this location is relatively far from column, the effect of diffracted water from column on the total relative wave surface elevation has been observed to be small. The other factor involved in relative water elevation is platform vertical displacement. Since the heave response of the rectangular column unit is marginally higher than the circular column unit, it floats a bit more with the waves and the relative water surface elevation between is decreased in this case.

For locations 2, whose results is presented in tables 11.9 , 0^o wave heading was considered. The result shows that for two of the six sea states considered, the minimum air gap of 1.5m requirement by NORSOK-003 is breached, in case of both units. In , spite of this the general air gap behavior of the circular column is better at this location.

For location 3, a bit larger difference is seen in terms of the minimum air gap requirement. It is seen that the rectangular column breaches this requirement, for sea states number (2) and (3), while the circular column unit has an air gap of more than 1.5 meters in all the cases.

Results for locations 4 and 5 are presented in tables 11.11 and 11.12. In both cases , the rectangular column unit shows a better air gap behavior. However, the minimum air gap requirement is not breached by any of the units for both locations 4 and 5.

Locations 6 and 7 are not critical locations, as both units exhibit almost similar type of air gap behavior at this locations. For location 6, the rectangular column unit shows marginally higher relatives surface

water elevation values for the different sea states considered, while at location 7, the relative wave surface elevation in the case of the two units has a difference only to the second level. In this situation it can be concluded that they have similar air gap behavior.

As can be seen from table 11.5, at location 8, the circular column shows better air gap behavior. Table 11.6 shows the minimum air gap at location 9, for 45^{o} wave heading. This is by far the most critical location of all the locations. For this location, the rectangular column unit attains a negative air gap for sea states (2) and (3), while the circular column shows a negative air gap value only for sea state (2).At location 9, whose results are presented in table 11.17, the circular unit shows a slightly better air gap behavior.

Totally, ten locations have been considered for air gap investigation .Three out of the ten locations i.e. locations 1, 4 and 5 strongly favored the rectangular column unit. For two of the locations, i.e. for locations 6 and 7, no significant difference has been observed. Five out of the ten locations, including the location where the most critical air gap behavior was observed, indicate that the circular column has slightly better air gap behavior.

11.5 Slamming load results and discussion

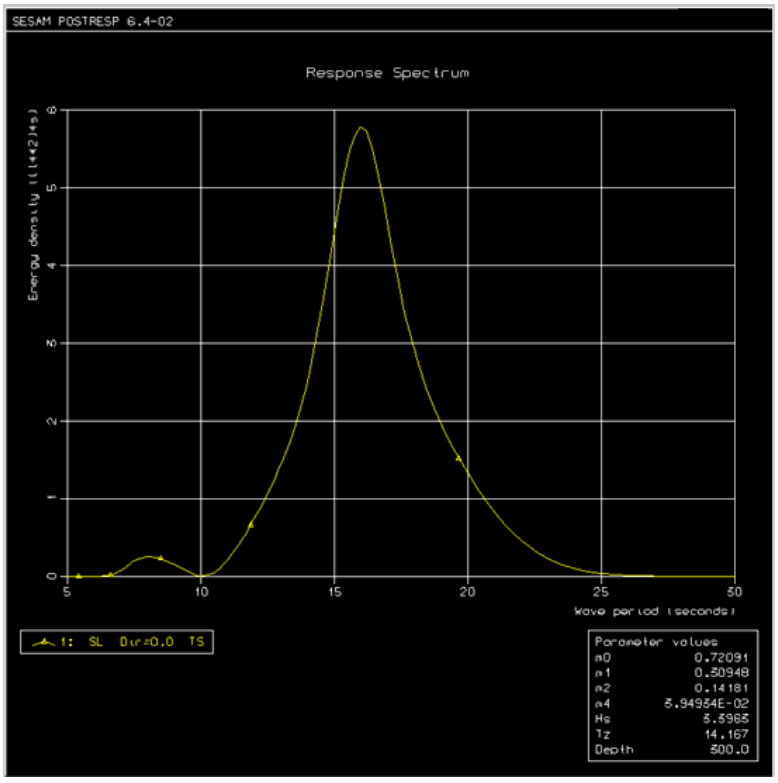

Figure 10.15 Surge velocity spectrum for rectangular column unit

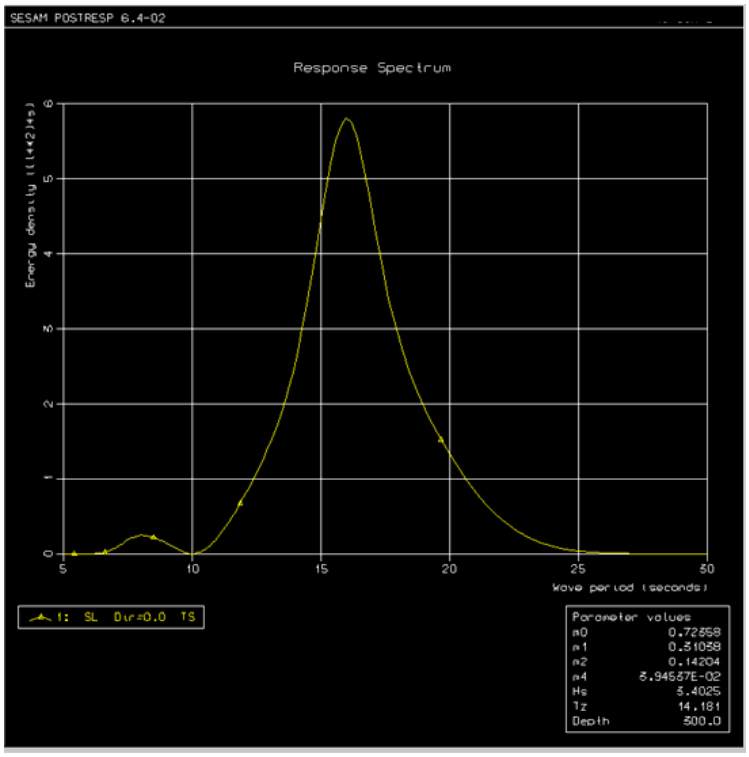

Figure 10.16 Surge velocity spectrum for circular column unit

	q	$H_B^{(q)}$ [m]	$L_B^{(q)}$ [m]	$C_B^{(q)}$ [m/s]	$\sigma_{sur.vel}$ [m/s]	$C_B^{(q)} + \sigma_{sur.vel}$ [m/s]	$C_B^{(q)} - \sigma_{sur.vel}$ [m/s]	C_B	$+P_s$ [KPa]	$-P_s$ [KPa]
Rectangular column Semi	10^{-2}	20.86	145.9	15.09	0.849	15.939	14.24	6.28	818.238	653.204
Circular column Semi	10^{-2}	20.86	145.9	15.09	0.850	15.94	14.24	6.28	818.444	653.020

Table 10.17 Extreme slamming impact

The surge velocity spectra for the two units are shown in figures 10.15 and 10.16. The standard deviation of surge velocity for the two units is calculated from the 0^{th} moment of the surge velocity spectrum of each unit. Using this result, the space average slamming load is calculated and is seen in the last two columns of table 10.17. The two results are based on the assumption that the platform might

be moving towards the breaking wave or away from the breaking wave. The obtained values are almost the same. The differences between them can be ruled out as insignificant.

11. 7 Second order mean drift horizontal forces/moment : Result and discussion

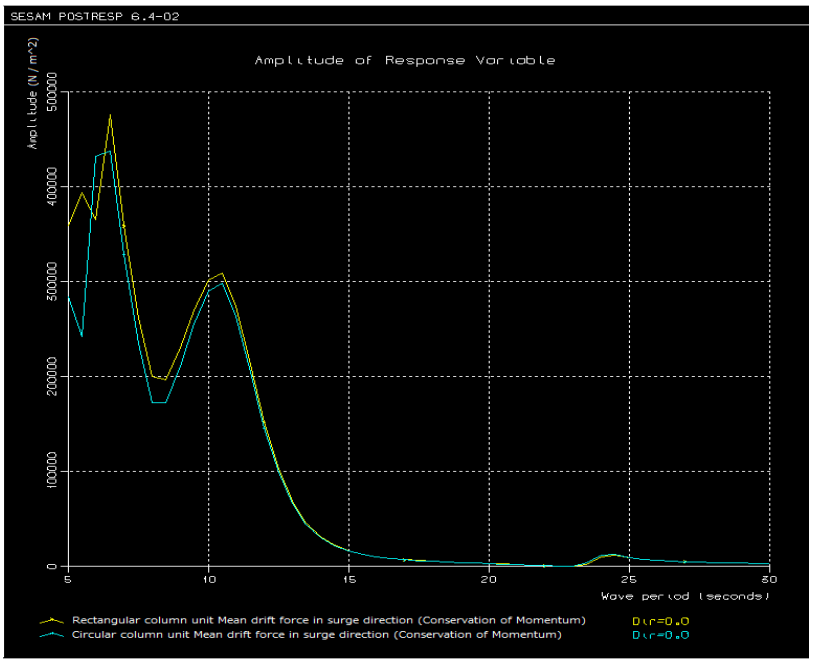

Figure 10.17 second order mean horizontal drift forces 0^{o} approach (surge direction)

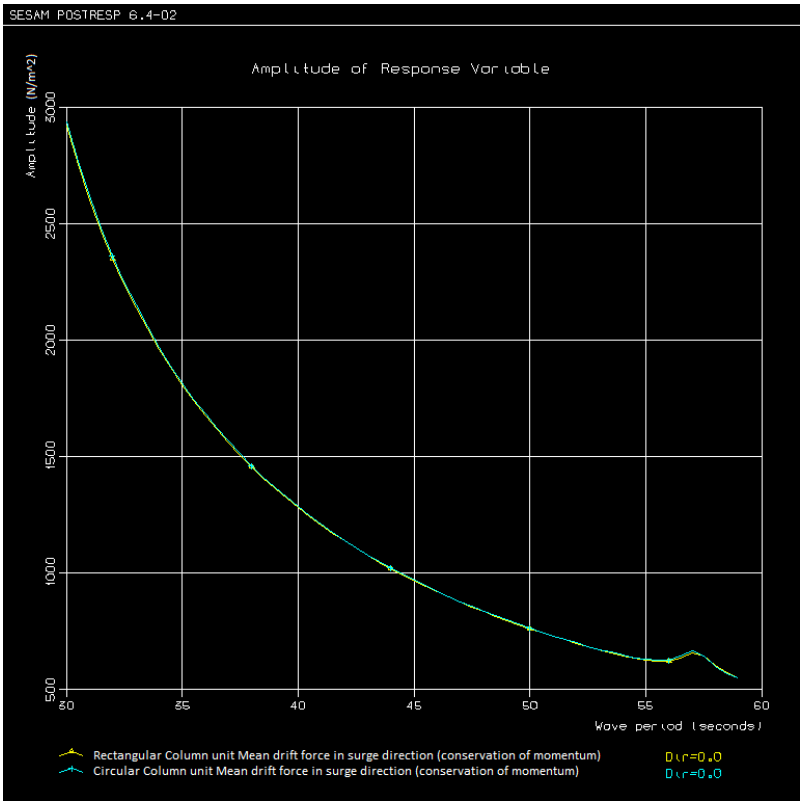

Figure 10.18 second order mean horizontal drift forces 0^{o} approach (surge direction)

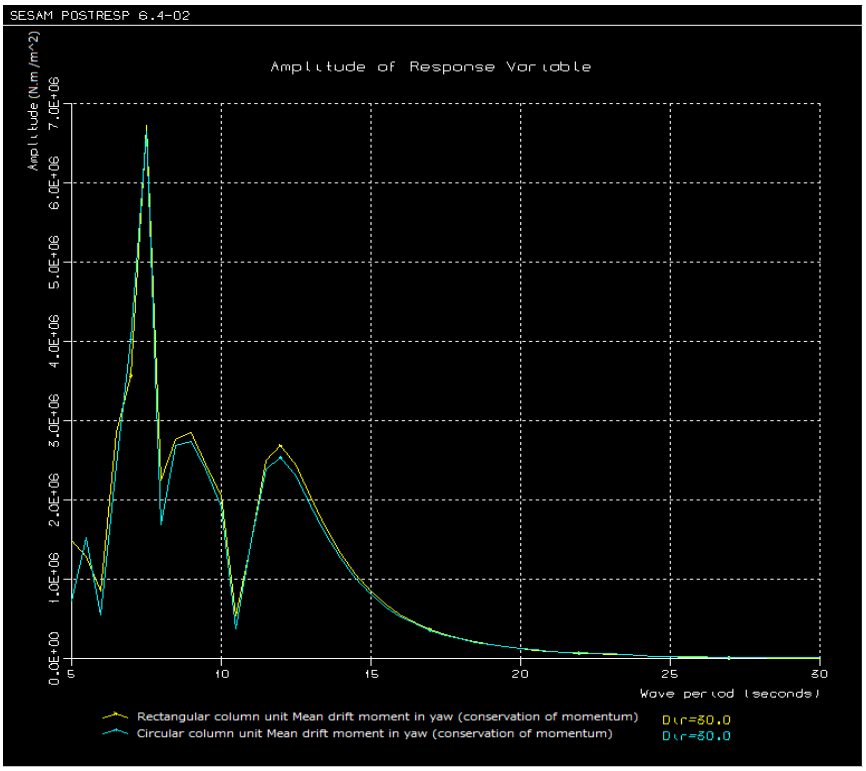

Figure 10.19 second order mean horizontal drift moment 30^{o} approach (yaw direction)

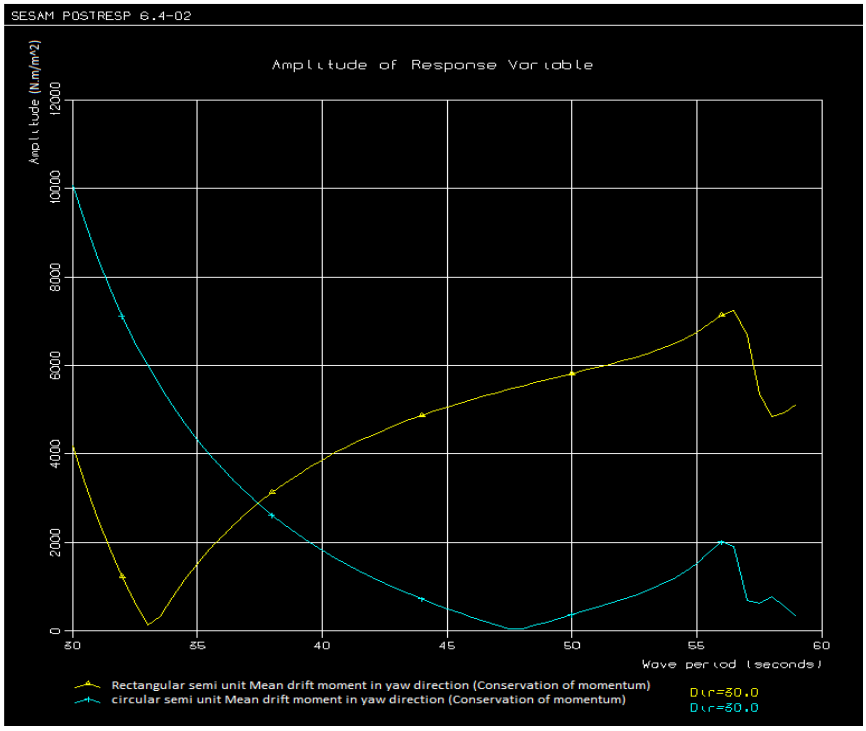

Figure 10.20 second order mean horizontal drift moment 30^{o} approach (yaw direction)

In figures 10.17 and 10.18, it is seen that the rectangular column semisubmersible exhibits more wave reflective ability than the rectangular column semisubmersible unit, that the drift surge force is a almost 4% higher than the circular column semisubmersible for the low periods in the interval. But as the wave period increases, the rectangular columns ability to reflect the waves gets lower that, the drift force in figure 10.7 is seen to descend to zero. Just around at the heave natural period i.e. around 24.4sec, the drift surge force of both semisubmersible units is seen to rise to a little degree and again starts to drop. The reason for this is that, due to resonance, each structure is able to reflect the incoming wave. However, no difference can be spotted between the two semisubmersible units' mean drift surge forces afterwards.

Similarly the second order mean drift yaw moment is also presented in figure 10.19 for 30^{o} wave .There is only a marginal difference between the yaw drift moments of the rectangular column unit and the circular column unit. For high frequencies, the mean drift moment of the rectangular column unit seems to have slightly higher peal values than the circular column semi unit. However, it can be seen from figure 18.20 that, as the wave frequency decreases (for longer waves), the difference between the mean drift yaw moment of the two units become negligible.

12. Conclusion

In this work, first order global motion analysis of two large semisubmersible units that have the same displacement but different column geometry has been carried out. One of the units is a four legged rectangular column, ring pontoon unit while the other is a four legged circular column semisubmersible unit. The analysis is performed at an operational depth. No mooring line and riser effect has been included. First order global motion transfer functions for the six rigid body degrees of freedom are obtained from the analysis.

Comparison has been carried out in terms of the global motion transfer functions of the two semisubmersible units. Combining the global motion transfer functions with few selected sea states from a hundred year return period environmental contour line, global short term extreme responses have been determined. Short term minimum air gap responses and extreme slamming loads from breaking waves have also been compared. Finally, second order mean horizontal drift force transfer functions obtained from linear global motion analysis are compared. The analysis described in this work leads to the following conclusions:

- There are marginal differences between the global motion transfer functions of the two units
- The circular unit exhibits slightly lower hundred year return, 3-hr maximum responses in all the rigid body degrees of freedom , except for surge and sway directions
- The circular column unit has a slightly better air gap response behavior
- No significant difference has been observed regarding extreme slamming impact load results. This is because the surge motion response of the circular column semisubmersible unit has more or less similar behavior with the rectangular unit's surge response
- For short wave periods, the second order mean drift horizontal loads experienced by the rectangular column unit are marginally higher, than that of the mean drift loads experienced by the circular column semisubmersible unit. This makes the expected second order drift motions of the rectangular column unit a slightly higher.

References:

1. DNV (2010). *DNV-RP-C205 "Environmental Conditions and Environmental Loads"*. Det Norske Veritas AS.
2. DNV (2010). *DNV-RP-F205 "Global performance analysis of deepwater floating structures"*. Det Norske Veritas AS
3. DNV (2010). *DNV-RP-C103 "column stabilized units"*. Det Norske Veritas AS
4. NORSOK N003 (2007) *"actions and effects"*
5. Faltinsen, O. M. (1990). *Sea Loads on Ships and Offshore Structures*. Cambridge Ocean Technology Series. Cambridge University Press.
6. Subrata Chakrabarti, 2005. *Handbook of offshore structures.*
7. krish thaigaragan, Subrata Chakrabart (2005). *Handbook of offshore structures* Page 437-442
8. Ship Stability for Masters and Mates (Bryan Barrass) pages 134-135
9. Adrian Brian & Ruben Lopn Pulido. 2014. *Ship Hydrostatics and Stability*, 2nd edition. Pages 50 – 51
10. James G Speight,2015,(Handbook of offshore oil and gas operations) Pages 78-79
11. N.D.P.Barltrop and A.J.Adams *Dynamics of fixed marine structures* Pages 293-296
12. Thor I. Fossen (2011) *Handbook of Marine Craft Hydrodynamics and Motion Control pages*.122-125
13. Madjid Karimirad (2012) " *Offshore Energy Structures: For Wind Power, Wave Energy and Hybrid Marine Platforms"* pp 213-220
14. Haver, S. and Winterstein, S.R., "Environmental Contour Lines: A Method for Estimating Long Term Extremes by a Short Term Analysis," Transactions, Society of Naval Architects and Marine Engineers, Vol. 116, 2009, pp. 116-127
15. Junbo.jia ,*Essentials of Applied Dynamic Analysis*, 2014 pp137-139
16. Alexander babanin .2011. *Breaking and Dissipation of Ocean Surface Waves* pp 423-424
17. Lynne E. Frostick, Stuart J. McLelland, T.G. Mercer.2011 *Users Guide to Physical Modelling and Experimentation*. pp 48-49
18. (A.Paco, N.Fonseca and C.Soares,2012) Edited by (Carlos Guedes Soares, Y. Garbatov, S. Sutulo, T.A. Santos) Maritime Engineering and Technology P 214
19. Chan, E.-S., Tan, B.-C., & Cheong, H.-F. (1991, June 1). Variability Of Plunging Wave Pressures On Vertical Cylinders. International Society of Offshore and Polar Engineers.
20. Zhou, D., E.S. Chan, and W.K.Melville. (1991). "Wave impact pressures on vertical cylinders,"
21. Applied Ocean Research , Vol. 13, No. 5.
22. Extreme Loads due to Wave Breaking Against Platform Column,

23. Kirsty McConnell, William Allsop, Ian Cruickshank, "Piers, Jetties and Related Structures Exposed to Waves: Guidelines for Hydraulic Loadings", 2004. Pp 35-36
24. Yoshimi Goda, 2010 *Random Seas and Design of Maritime Structures*, , third edition , pp 180-182
25. A.Haver and Abdillah Suyuthi. 2009. *Extreme Loads due to Wave Breaking Against Platform Column*
26. Leo Holthuijsen .*2007. Waves in Oceanic and Coastal Waters*. pp 123-124
27. R.W.Lweis, Perumal Nithiarasu, kankanhalli seetharamu. *2008 Fundamentals of the Finite Element Method for Heat and Fluid Flow*

Appendix A

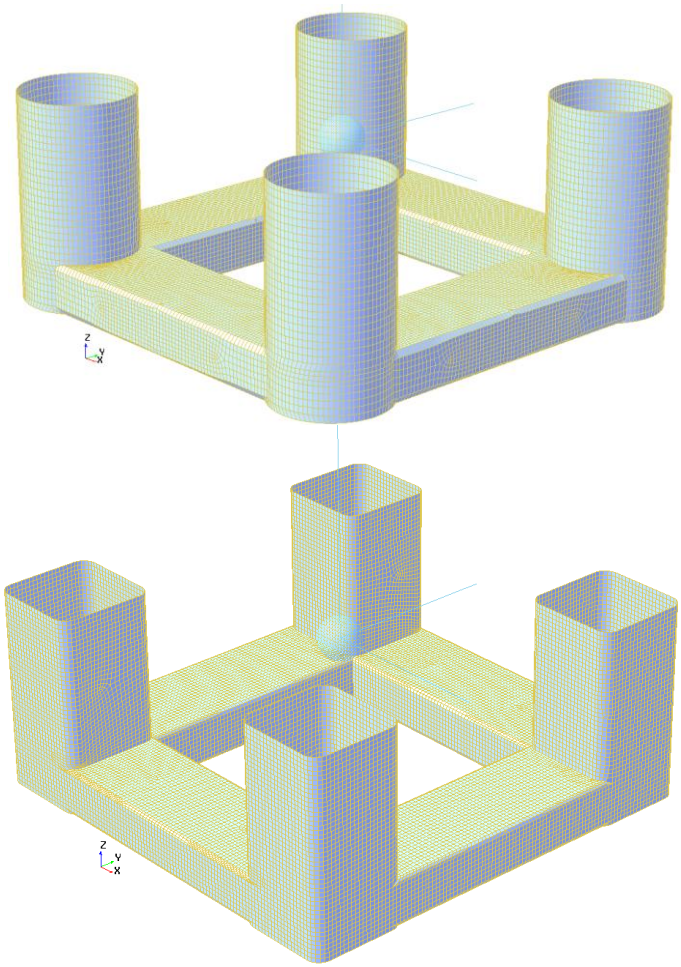

APPENDIX B

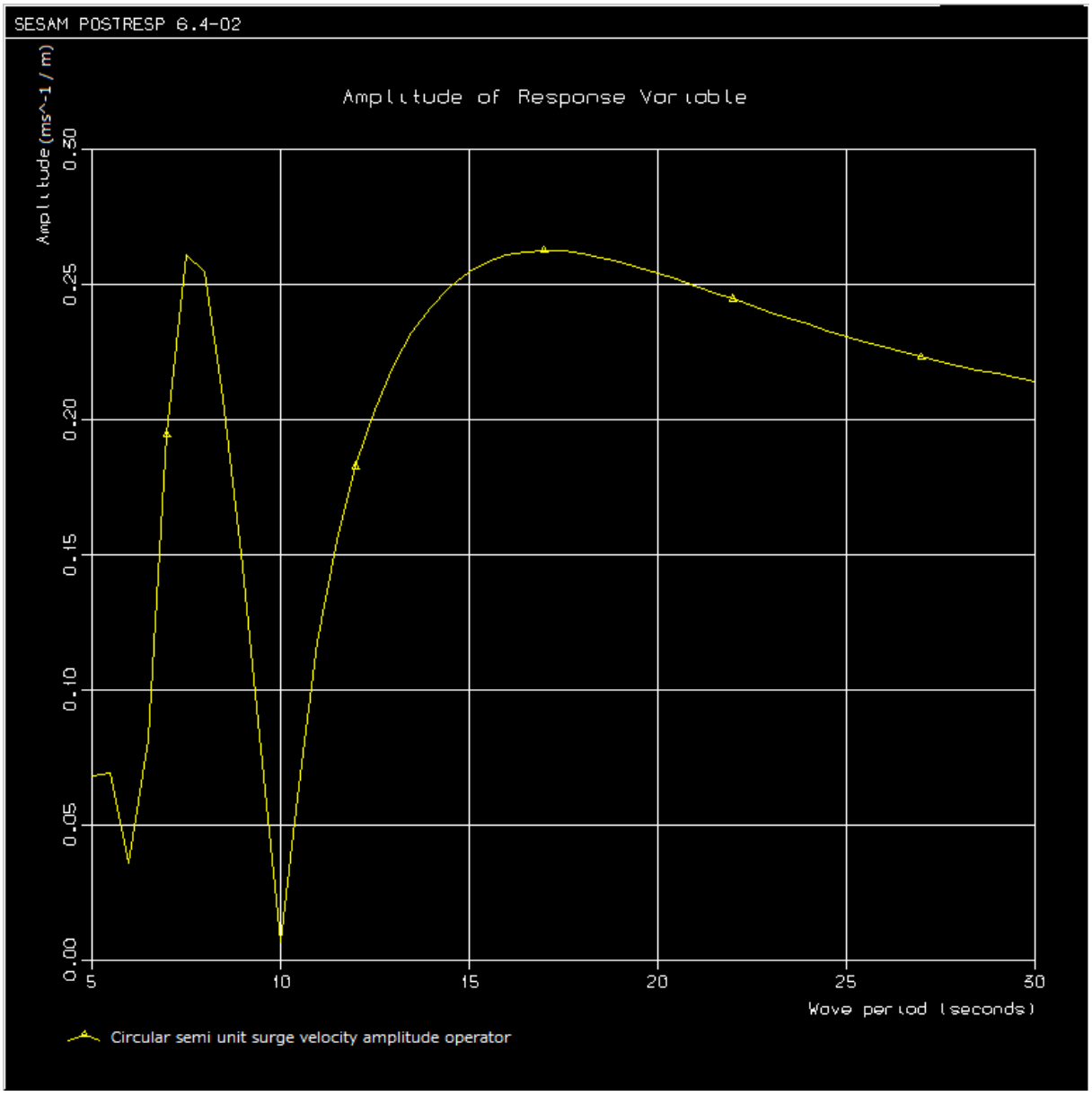

Circular column units surge velocity profile

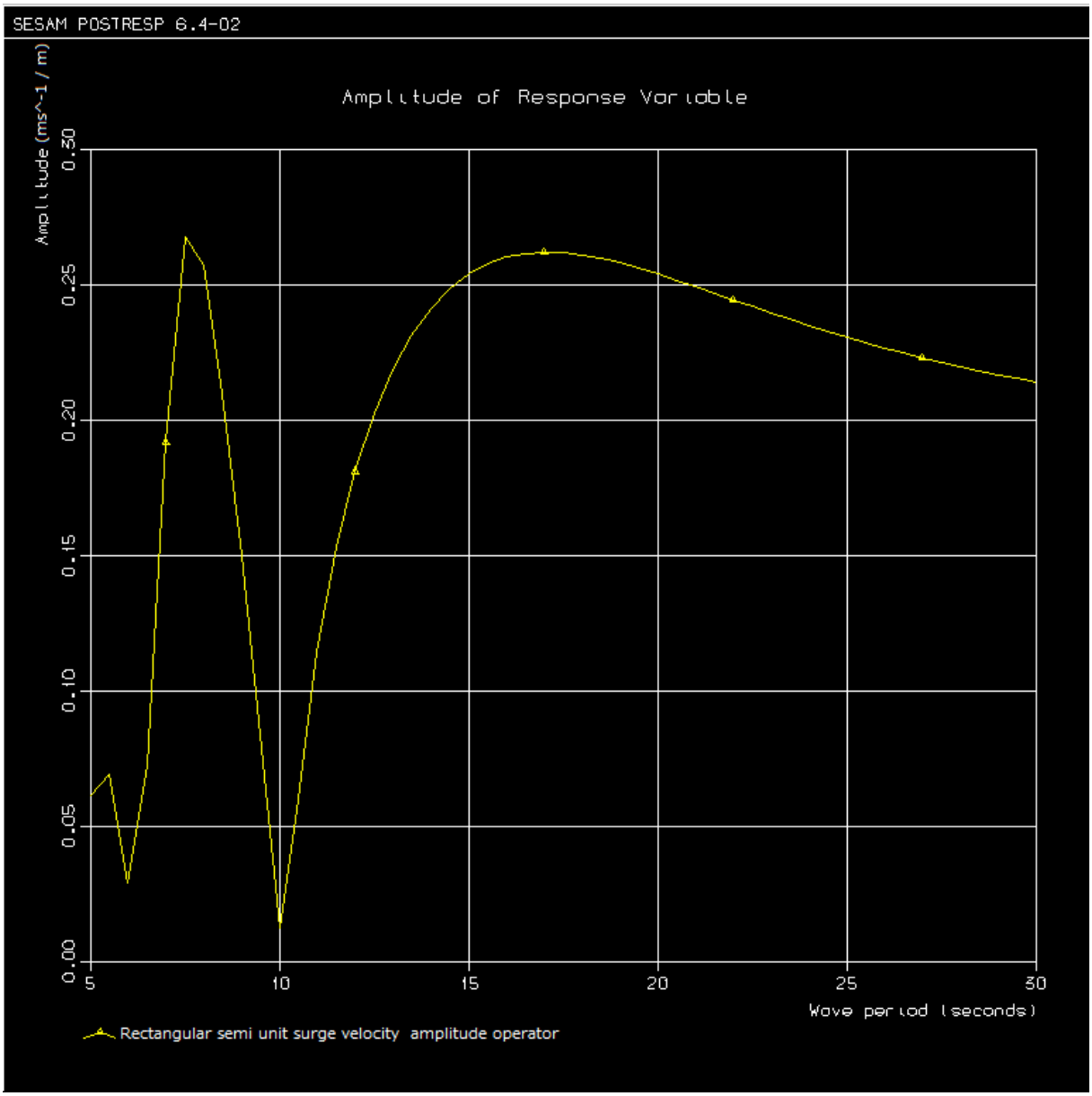

Rectangular Column Units surge velocity porifle